
Electronic Thesis and Dissertation Repository

2-2-2015 12:00 AM

Rotor Position Identification for Brushless DC motor

Muhammad Ikhlas

The University of Western Ontario

Supervisor

Dr. Lyndon J. Brown

The University of Western Ontario

Graduate Program in Electrical and Computer Engineering

A thesis submitted in partial fulfillment of the requirements for the degree in Master of Engineering Science

© Muhammad Ikhlas 2015

Follow this and additional works at: <https://ir.lib.uwo.ca/etd>



Part of the [Controls and Control Theory Commons](#)

Recommended Citation

Ikhlas, Muhammad, "Rotor Position Identification for Brushless DC motor" (2015). *Electronic Thesis and Dissertation Repository*. 2676.

<https://ir.lib.uwo.ca/etd/2676>

This Dissertation/Thesis is brought to you for free and open access by Scholarship@Western. It has been accepted for inclusion in Electronic Thesis and Dissertation Repository by an authorized administrator of Scholarship@Western. For more information, please contact wlsadmin@uwo.ca.

ROTOR POSITION IDENTIFICATIN FOR BRUSHLESS DC MOTORS
(Thesis format: Monograph)

by

Muhammad Ikhlas

Graduate Program in Electrical and Computer Engineering

A thesis submitted in partial fulfillment
of the requirements for the degree of
Masters of Engineering Science

The School of Graduate and Postdoctoral Studies
The University of Western Ontario
London, Ontario, Canada

© Muhammad Ikhlas 2015

Abstract

Permanent magnet BLDC motors are characterized by a central magnetic core, called the rotor, and fixed electric coils (usually six) equally spaced in a ring around the core, called the stator. Motor movement is controlled by alternately energizing and de-energizing the stator coils to create a rotating magnetic field that propels the rotor. In order for this process to work correctly, BLDC motors required a technology called electronic commutation, in which the coil currents must be very carefully synchronized to rotor position to ensure that the rotating field is correctly aligned with the permanent magnetic field in the rotor. Usually rotor position is measured by external sensors such as Hall-effect sensors and optical encoders and these external sensors increase the system cost and reduces reliability. In order to control the price and make it more reliable this thesis propose to infer the rotor position from voltage and current measurement of motor.

The most common approaches to sensorless control are based on the measurement of the electromotive force (back-EMF), that is induced by the rotor motion. As the back-EMF is nearly zero at very low speed and at stationary position, and can not be measured. Therefore a separate algorithm is required for start-up and control at low speed. The other method of sensorless control involves the inference of rotor position from the variation in inductance caused by rotor position. This thesis presents a prototype system for sensorless control of BLDC motors over the entire speed range of the motor, including stall (zero speed) conditions using the voltage and current signals from the motor.

Keywords: Rotor Position, Sensorless Control of BLDC motor, Rotor Position identification, BLDC motor position

Acknowledgment

I would like to express my deepest appreciation and gratitude to my Supervisor, Dr. Lyndon J. Brown, Assistant Professor, Department of Electrical and Computer Engineering, Western University, for his support, advice, guidance and encouragement throughout my study duration and research work. It has been an honor for me to work under a mentor with such graciousness.

I acknowledge the support of technicians in the Engineering workshop and my lab mates for their great help during my work.

I would like to thank for the love, moral support and encouragement from my family and friends throughout my life. From you, I will always find an unwavering source of support to strive forward.

Above all, I would like to thank ALLAH Almighty for having given me the courage, patience, and the intellectual power to overcome all difficulties that I have faced during my graduate studies.

Contents

Abstract	ii
List of Figures	viii
List of Tables	xi
List of Appendices	xii
List of Acronyms	xiii
List of Symbols	xiv
1 Introduction	1
1.1 Introduction	1
1.2 Background	2
1.3 Comparison between Brushed and Brushless motors	3
1.4 Comparison between BLDC and SRM	5
1.5 Structural Review	5
1.5.1 BLDC motor structure	7
1.5.1.1 Electrical and Mechanical Angles	8
1.5.1.2 Rotor Structure	9
1.5.1.3 Stator Structure	9
1.5.2 Switched Reluctance Motors (SRM) Structural Review	10
1.6 Typical Applications of BLDC	12

1.7	Problem Statement	13
1.7.1	Proposed Work	14
1.8	Thesis Organization	14
2	Literature Review	15
2.1	Introduction	15
2.2	Principle of operation of BLDC motor	16
2.2.1	Faraday's Law	17
2.2.2	Ampere's Law	17
2.2.3	Lenz's Law	18
2.3	BLDC Control Review	18
2.3.1	Six step Commutation	19
2.3.2	Sinusoidal Commutation	21
2.3.3	Field Oriented Control	23
2.3.4	Direct Torque Control	25
2.4	Rotor Position Estimation	27
2.4.1	Sensored Approach	27
2.4.1.1	Hall Effect Sensors	28
2.4.1.2	Variable reluctance (VR) sensors	29
2.4.1.3	Optical Encoders (Magnetic Encoders)	30
2.4.2	Sensorless Approach	31
2.4.2.1	Back-EMF Sensing Techniques	31
2.4.2.2	Inductance Variation	34
2.4.2.3	Extended Kalman Filter	34
2.4.2.4	Sliding Mode Observer	36
2.5	Switched Reluctance Motor Control Review	36
2.5.1	Principle of Operation of SRM	37
2.5.2	Sensorless Control of SRM	38
2.5.2.1	Sensorless control of SRM using Phase Inductance	39

2.6	Summary	40
3	Modeling of BLDC motor	41
3.1	Introduction	41
3.2	Magnetic model	42
3.2.1	Basic concepts	42
3.2.2	Magnetic Materials	43
3.2.3	BLDC Magnetic Model with Equivalent Electrical Circuit	43
3.3	Electrical Model	45
3.3.1	Flux Linkage	46
3.3.2	Per Phase Electrical Model	47
3.4	Mathematical Model	49
3.5	Torque in BLDC	50
3.5.1	Ideal Torque	51
3.5.2	Torque Ripple	51
3.5.3	Torque and Multiple pole pairs in BLDC Motors	52
3.6	Back-EMF in BLDC	53
3.7	General Electro-Mechanical Model	54
3.8	Summary	55
4	Measurements and Analysis	56
4.1	Introduction	56
4.2	Inductance measurements	56
4.2.1	Variable Inductance	57
4.2.2	Inductance Readings using LCR meter	58
4.3	Voltage measurement	59
4.3.1	Measured Voltage	60
4.3.2	Filtered Voltages	62
4.4	Current measurement	63

4.4.1	Hall-Effect based Current Sensor Readings	64
4.4.2	Filtered Current	65
4.5	Inductance from Voltage and Current Signals	66
4.5.1	Wye-Configuration	67
4.5.1.1	Conclusion	69
4.5.1.2	Wye Configuration With with back-EMF	70
4.5.2	Delta Configuration	71
4.5.2.1	Frequency Domain Analysis	71
4.5.2.2	Delta Model For Inductance Information	72
4.5.2.3	Conclusion	75
4.6	Electrical Time constant Analysis	77
4.6.1	BLDC motor Analysis	77
4.6.1.1	At Maximum Inductance	78
4.6.1.2	At Minimum Inductance	78
4.6.1.3	Comparison of Voltages and Currents at two positions	79
4.7	Summary	81
5	Conclusion	83
5.1	Summary	83
5.2	Problems Faced	85
5.3	Future Work	85
	Bibliography	88
	A Torque for Multiple Pole-Pairs	95
	B Inductance Variation of BLDC motor	98
	Curriculum Vitae	103

List of Figures

1.1	Comparison between Radial and Axial Flux motors	6
1.2	Comparison between Inner Rotor and Outer Rotor motors	7
1.3	Three phase BLDC motor with circuit diagram	8
1.4	4-pole and 8-pole permanent magnet rotor	10
1.5	slotted and slotless stator motors	11
1.6	One phase cross-section of 8/6 SR machine	12
2.1	Block diagram of basic BLDC motor system	17
2.2	Six Step Commutation, Microcontrollers Sol Inc.	19
2.3	BLDC motor with six transistors power bridge	20
2.4	Sinusoidal commutation with Hall sensor output	21
2.5	Comparison between Six-step and sinusoidal commutation	22
2.6	Direct (d) and Orthogonal (q) components	23
2.7	Clarke's transformation	24
2.8	Park's transformation	25
2.9	Block diagram of generic FOC control drive	25
2.10	Inverter voltage vectors and stator flux vectors	26
2.11	3-phase Hall sensor chart with 120degree angle separation	28
2.12	Variable Reluctance sensor	29
2.13	Single ended Optical encoder	30
2.14	Back-EMF zero crossing detection circuit model with PWM On-time	32
2.15	Zero crossing points of the back-EMF	33
2.16	Block diagram for EKF system for rotor and speed estimation of a BLDC motor	35

2.17	Aligned and Unaligned positions in SRM	37
2.18	Per phase self inductance curve for SRM	39
3.1	Cross sectional view of inner roto motor	45
3.2	magnetic circuit of simple BLDC motor	46
3.3	Simplified magnetic circuit of simple BLDC motor	46
3.4	Simplified Electrical Model of BLDC motor	48
3.5	Sinusoidal and Trapezoidal torque	51
3.6	Ideal Torque and Current Shape for BLDC motor	52
3.7	Sinusoidal and Trapezoidal Back-EMF of the motor	54
3.8	Electro-Mechanical model of BLDC motor	54
4.1	BLDC Motor Under testing	57
4.2	Closed look of magnets for motor under testing	58
4.3	Measured Inductance of 1 phase	59
4.4	Measured Inductance of all three phases	59
4.5	Dotted Points Showing reading of all three phases for $0^\circ - 90^\circ$	60
4.6	Lab setup to measure the Voltage and Current	61
4.7	1 Phase to Phase Voltage of Motor	62
4.8	Two Phase to Phase Voltages of Motor	62
4.9	Pulses generated by PWM in Voltage signal	63
4.10	Filtered Voltages	64
4.11	Two Phase Currents	65
4.12	Noise in Current and its Filtered wave	66
4.13	Raw Voltage data with External Voltage Present	67
4.14	Raw Voltage data with no External Voltage	67
4.15	Wye model for our setup	68
4.16	Current Mean Values and Slopes with no Voltage	69
4.17	Ratio of Inductance and Resistance when no Voltage present	70

4.18	FFT of window for Current of Phase A	71
4.19	FFT of window for Current of Phase B	72
4.20	FFT of a window for Phase AB Voltage	72
4.21	FFT of a window for Phase BC Voltage	73
4.22	Delta Configuration for Pure Resistive case	73
4.23	Inductance Variation for Phase A	74
4.24	Inductance Variation for Phase B	74
4.25	Inductance Variation for Phase C	75
4.26	Resistance Variation for Phase A	75
4.27	Resistance Variation for Phase B	76
4.28	Resistance Variation for Phase C	76
4.29	Lab Setup for Step Input Response	78
4.30	2 Phase to Phase Voltages for Both Tests	79
4.31	Current A Response for Both Tests	80
4.32	Current B Responses for Both Tests	80
4.33	Comparison of Phase A Current	81
4.34	Comparison of Phase B Current	82
4.35	Comparison of Phase C Current	82
5.1	\tan Inverse of Slope and Mean values of Current	86

List of Tables

1.1 Comparison Between Brushed and Brushless Motors	4
---	---

List of Appendices

Appendix A Torque for Multiple Pole-Pairs	95
Appendix B Inductance Variation of BLDC motor	98

List of Acronyms

ADC: Analogue to digital convertor
AFPM: Axial flux permanent magnet
APFM: Axial flux permanent magnet
BACM: Brushless AC motor
BDCM: Brushless DC motor
BLDC: Brushless direct current motor
BLSM: Brushless servo motor
DTC: Direct torque control
ECBM: Electronically commuted brushless motor
ECDCM: Electronically commuted DC motor
EMF: Electromotive force
FOC: Field oriented control
FFT: Fast Fourier transform
MMF: Magnetomotive force
PMBDC: Permanent magnet brushless DC motor
PMSM: Permanent magnet synchronous motor
PWM: Pulse width modulation
RPM: Revolutions per minute
SMO: Sliding mode observer
SPMSM: Surface PM synchronous motor
SRM: Switched reluctance motor

List of Symbols

ε : EMF induced (V)

ϕ : Flux (Wb)

B: Magnetic field density (Wb/ m^2)

B_s : Stator magnetic field (Wb/ m^2)

B_r : Permanent magnets field in rotor (Wb/ m^2)

H: Magnetic field strength (A/m)

T: Torque (N.m)

ψ : Flux linkage (Wb(.turn))

μ_o : Permeability of free space (H/m)

μ_r : Permeability of material relative to free space (H/m)

λ_s : Stator flux linkage (Wb(.turn))

ω : Angular frequency

θ_e : Electrical angle (rad)

θ_m : Mechanical angle (rad)

θ_r : Rotor angle (rad)

dq: d-q coordinates

$\alpha\beta$: $\alpha\beta$ coordinates

Chapter 1

Introduction

1.1 Introduction

The basic purpose of motors are to convert electrical energy to mechanical energy. Looking at the world around us and considering the importance of devices which uses this mechanism, we cannot just simply neglect the electrical motors and their working. Brushless DC motors also known as Permanent Magnet direct current Synchronous motors are becoming very popular and useful because of their high power density (the amount of power per unit volume), long life, high efficiency and reliable operation. Brushless DC motors as opposed to brushed DC motors do not require any mechanical brushes for its commutation system. Removal of brushes for commutation reduces the electric spark which results in reduction of the Electromagnetic interference(EMI). Initially, Brushless DC (BLDC) motors were mostly used in high-end military applications but due to the high efficiency and long life these motors became more common in daily life applications. Recently, these motors are well preferred in many electrical equipments which includes both high-end military applications and low price household appliances and toys. The main reason for their widespread applications becoming reality after recent reduction in cost of these motors. Ideally, BLDC motors can be used any area where traditional motors (Brushed and induction motors) are being used as consumers now demands for the lower energy costs, better performance and reduced acoustic

noise which cannot be achieved using the traditional technologies.

A typical BLDC motor consist of permanent magnets in rotor, and fixed electric coils equally spaced in stator. As the rotor magnets (rare-earth magnets) which are used in BLDC motors typically have high magnetic flux density and high electrical conductance making rotor losses small which results in the higher efficiency.

1.2 Background

Historically, the electric motors were described in three categories: 1) Brushed Commutator DC motors, 2) Synchronous motors and 3) Induction motors. From start the variable speed machines were desirable but this was not possible with the synchronous machines. With time as the desire of variable speed machines has progressed, so did the types of the machines. There were many variations of machines which were developed and one of these variations is Brushless Permanent Magnet machine. There were many steps and paths included in the development of these machines as mentioned by Jahns [1]. Initially a line-start permanent magnet machine was introduced and later in addition to that an electronically commutated (brushless) permanent magnet machine was devised. With more advancements in machine designs, eventually the concept of sinusoidal permanent magnet machine was introduced in combination with the inverter to provide an adjustable speed machine without brushes which can give servo like performance.

Although the brushless DC motors were devised but these early motors were not able to generate a great deal of power but when the permanent magnet materials became readily available in the 1980s, the use of BLDC motors to generate higher power looked possible. If not more, using permanent magnets combined with high voltage transistors, enabled brushless DC motors to generate as much power as the old brush DC motors. Near the end of the 1980s, Robert E. Lordo of the POWERTEC Industrial Corporation unveiled the first large brushless DC motor, which had at least ten times the power of the earlier brushless DC motors.

There are number of Acronyms associated with Brushless DC motors. A few of them are mentioned below:

- BACM: brushless AC motor
- BDCM: brushless DC motor
- BLSM: brushless servo motor
- ECBM: electronically commuted brushless motor
- ECDCM: electronically commuted DC motor
- PMBDC: permanent magnet brushless DC motor
- PMSM: permanent magnet synchronous motor
- SPMSM: surface PM synchronous motor

Although there is inconsistency in literature for specifying the name of motors but in this thesis we will use BLDC motor (brushless DC motor) for trapezoidal back-EMF and PMSM (permanent magnet synchronous motor) for sinusoidal back-EMF.

1.3 Comparison between Brushed and Brushless motors

The main difference between Brushed and Brushless motor is the elimination of Carbon Brushes which were used in Brushed motors to control the motor speed. The elimination of Brushes gives many advantages to Brushless motors over Brushed motors which make them suitable for different applications. The basic Comparison between Brushed and Brushless motors is described in Table 1.1.

Table 1.1: Comparison Between Brushed and Brushless Motors

Brushed Motors	Brushless Motors
Low efficiency	High efficiency (no voltage drop across brushes)
Shorter Life	Longer Life (less losses)
Moderate Speed Range	High Speed Range (No mechanical limitation due to brushes)
High electrical noise (due to brushes)	Low electrical noise
Low construction cost	Higher construction cost
Simple and inexpensive control	Complex and expensive control
Low output power to size ratio	High output power to size ratio
Periodic maintenance required	Less maintenance due to absence of brushes
Less efficient heat dissipation	Good heat dissipation

1.4 Comparison between BLDC and SRM

Switched reluctance motor (SRM) is a type of motor which is different from Brushless DC motor in torque production mechanism. In the case of BLDC motors, torque is produced by interaction of magnetic flux of windings and permanent magnets, whereas the SRM works on the principle of variable reluctance [2]. These motors generate torque without any permanent magnets and with no concentrated windings on their shaft. The SRM drive system first became available in early 1980's as a result of work done in Leeds and Nottingham universities [3] - [4]. The main difference between a BLDC motor and SRM motor is the assemblies of rotor and stator and the materials used. SRM motors also need the sensors and an electronic commutation controller similar to BLDC motors. The main advantages of using SRM are given below:

1. SRM is inexpensive to manufacture as it is made up of simple laminated steel and has no rotor windings.
2. As there are no rotor windings in SRM, they mainly get heated up in stator where the machine is easily cooled.
3. SRM can work on high speed in intense environments because of their simplicity and ruggedness.
4. The SRM requires unipolar currents only, allowing the design of an inexpensive converter with one controllable power switch per phase.

1.5 Structural Review

To understand how Brushless DC motors are more effective and better to use, it is really important to have a good understanding of how the Brushless DC motors are made up and how they work. Any Brushless DC motor is made up of two main components i.e. 1) a physical member which is stationary called the **Stator** and 2) a physical member which rotates called

the **Rotor**. There are basically two configurations of DC motors on basis of the structure of stator and rotor.

1. Axial Flux
2. Radial Flux

Axial flux motors [5] are also an active area of research but these type of motors are not that common in servo application as compared to radial flux motors. These type of motors have special applications such as floppy disk spindle drives. The primary reason for less use of these motors is the stator construction. As the flux flows axially in these motors, the stator must be laminated circumferentially. This construction orients slots at ever increasing distances from one another. As a result, this significantly increases stator manufacturing time and cost. The Axial flux motors are further divided into single sided AFPM machines and double sided AFPM machines [5]. The difference between radial and axial flux motors is explained in Figure 1.1

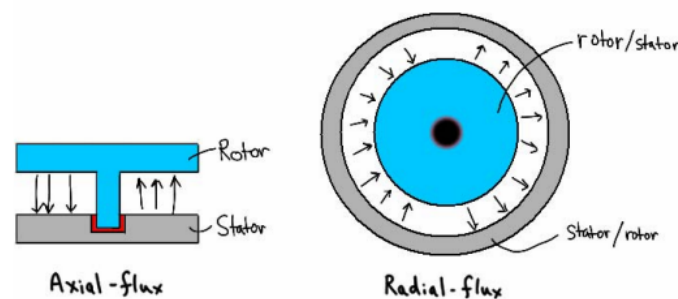


Figure 1.1: Comparison between Radial and Axial Flux motors

The radial flux motors are further divided into two categories. 1) Inner Rotor motors, 2) Outer Rotor motors. **Inner Rotor** motors provide a smaller diameter, lower motor inertia because of the smaller size and better heat dissipation. On the other hand the **Outer Rotor** motors may provide the larger overall motor diameter and can provide larger inertia which is mostly

desired in constant speed applications. Although for outer rotor motors, individual magnets can be used but the more common practice is to use a single bonded magnet ring inside the rotor. This motor is also easy to wind as the teeth of the stator points outward. The main difference between inner and outer rotor motors is explained in Figure 1.2

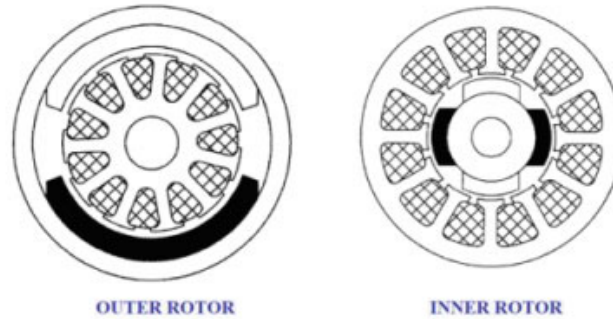


Figure 1.2: Comparison between Inner Rotor and Outer Rotor motors [6]

1.5.1 BLDC motor structure

All of the electrical and mechanical issues because of the brushes with the brushed technology are eliminated in brushless DC motors. In BLDC motors the brushes are replaced with an electronic controller which control the speed of the motors. The current carrying coils/winding are stationary and energized sequentially to cause the Permanent Magnet rotor to turn. BLDC motor is usually constructed in single-phase, two-phase and three phase configurations, where the three phase configuration is the most commonly available for BLDC motors. BLDC motors with more than three phases can also be manufactured but they are not common and they hugely increases the manufacturing cost [7]. A typical three phase BLDC motor with its circuit diagram is shown in Figure 1.3.

Since BLDC is a synchronous motor, the stator and the rotor fields rotate at the same frequency. This means that there is no slip between stator and rotor in the case of BLDC motors. The three phase BLDC motor is driven by applying the positive current to one of the motor

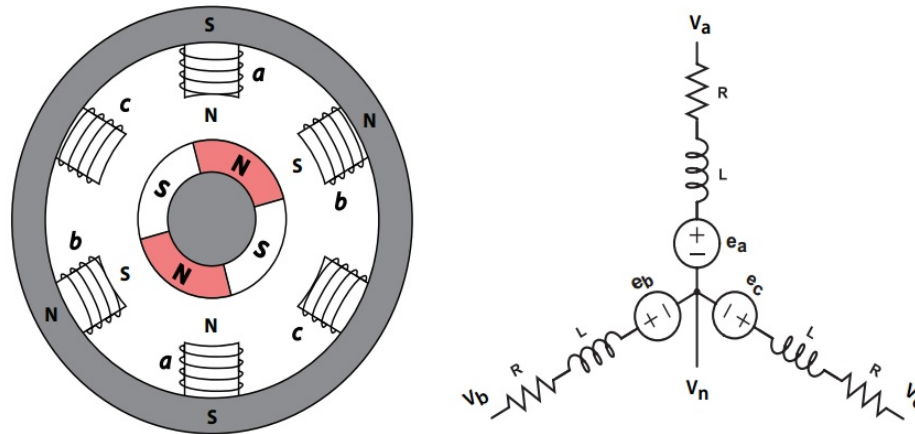


Figure 1.3: Three phase BLDC motor with circuit diagram

phases and a negative current to another while leaving no current going into the third phase. The interaction between the field generated in the stator due to current and by the permanent magnets on the rotor, generates the torque in the motor and as a result the motor starts to rotate. To keep the motor rotating, the current in the stator which generate the magnetic field needs to be commutated in a specific pattern. This current commutation is controlled and switched in specific commutation steps for each electrical rotation.

1.5.1.1 Electrical and Mechanical Angles

It is same in any type of electrical motor to define two related terms of speed and position. The position is the mechanical position of the motor and the speed of the motor is the speed by which the rotor rotates. When the rotor rotates one complete revolution, it follows a complete 360 degrees mechanical path. Once it traverses the complete path, the rotor is back to its original position. This motion is described by the mechanical angle of the motor, while electrical angle is defined as "An angle that specifies a particular instant in an alternating-current cycle or expresses the phase difference between two alternating quantities". Electrical angle is usually expressed in electrical degrees. The number of magnetic poles on rotor plays

the main role in determining the relationship between electrical and mechanical positions of the motor. For a motor which has single pole pair, the electrical and mechanical revolution are equal and hence the electrical and mechanical angle are also equal. But in case of more than one pole pair, the number of electrical and mechanical revolutions are not equal and hence their angles. The relationship between the electrical angle and mechanical angle can be expressed using Equation 1.1, which shows that as the number of pole pairs increases the electrical revolutions in one mechanical revolution also increases.

$$Polepairs = \frac{Electrical\ angle}{Mechanical\ angle} \quad (1.1)$$

1.5.1.2 Rotor Structure

Generally, permanent magnets are used to build the Rotor of a brushless DC motor. The number of magnets in the rotor defines the number of rotor poles. Depending on the requirements, we can have BLDC motor with different number of poles. By increasing the number of poles in the rotor we can increase the torque but it reduces the maximum speed of the motor. The greater number of magnet poles does generate greater torque but more magnet poles implies having less room for each pole. Eventually the maximum point is reached where the gap between rotor magnet poles becomes significant percentage of the total space on the rotor, and the torque no longer increases. The optimum number of magnetic poles mainly depends on the motor geometry and the material properties which is being used in the motor. The torque generated depends on the material used for the construction of the permanent magnet as the torque depends on the flux density of the material. The higher the flux density of material used the higher the torque generated. 4-poles and 8-poles rotors are shown in Figure 1.4

1.5.1.3 Stator Structure

The stator of the BLDC motor is made up of laminated steel with windings placed in the slots. Traditionally, the stator of BLDC motor resembles the stator of an induction AC motor.



Figure 1.4: 4-pole and 8-pole permanent magnet rotor [8]

Windings in the stator can be arranged in both star and delta pattern. The star configuration at low RPM gives high torque while the delta configuration gives low torque at low RPM. Each winding is constructed with numerous coils interconnected with each other and these windings are distributed over the stator to generate the required number of poles. We can also divide BLDC motors in two types according to the stator windings variant i.e. trapezoidal motors and sinusoidal motors. This difference is created on the basis of the interconnection of the coils in the windings to give different type of back EMF. Sinusoidal motors are smooth rotating motors which make them popular for applications which require quiet operation and low vibration but these type of motors need additional cost of windings and also the complicated algorithm to control. The lamination in stator can be slotted or slotless as shown in the Figure 1.5. A slotted core has high inductance which reduces the speed range of the BLDC motor. Therefore slotless core is more suitable for high speed requirements but they increase the cost as slotless core needs more winding to compensate for the air gap.

1.5.2 Switched Reluctance Motors (SRM) Structural Review

SRM machine is a brushless machine which has doubly salient geometry i.e. it has salient poles on both rotor and stator. In SRM the rotor is made up of stack of laminated steel which is cut to get the desired number of poles in the rotor. The stator is also made up of steel laminations and cut to yield the required number of stator poles. The stator pole in SRM

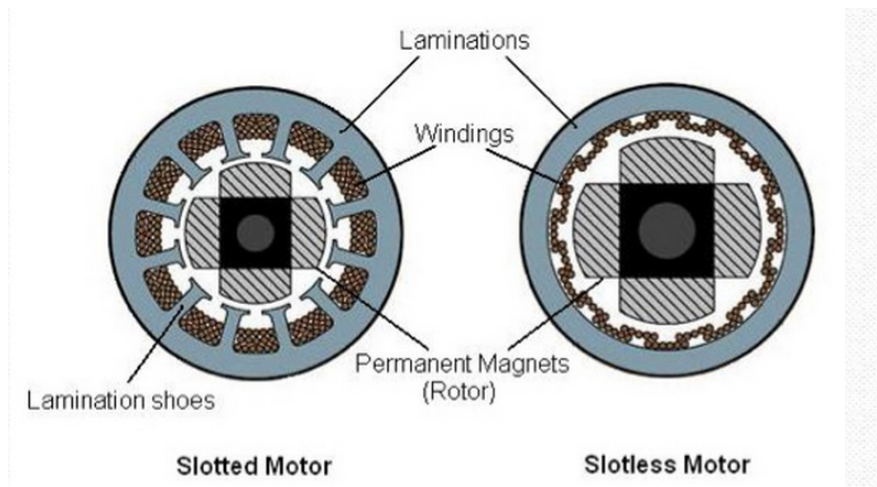


Figure 1.5: slotted and slotless stator motors [9]

has a simple concentrated winding and there are no conductors of any type on the rotor. These simple windings on the stator pole are connected in diametrically opposite pairs and are independently connected to a remote switching circuit for its commutation. Commonly, the rotor and stator are assembled from steel lamination of the same grade and thickness. The construction of SRM is very simple, reliable and rugged which gives it few advantages over the conventional brushless machines [10]. A cross-sectional overview of a typical 8 stator and 6 rotor poles machine is shown in Figure 1.6.

Though SRM is the simplest machine in design as compared to other electrical machines but they are difficult to control. The double saliency of the SRM causes strong non-linear magnetic characteristics which results in complicating the control analysis of the machine. SR machines have higher torque ripple and they do tend to be more noisy as compared to other electrical machines i.e. BLDC machine. However, this torque ripple and noise can be significantly reduced by using a better SRM mechanical design and algorithm which can compensate for these problems. Generally, increasing the number of phases in SRM reduces the ripple in torque, but it results in increasing the overall motor costs due to the need of more electronics to operate the SRM.

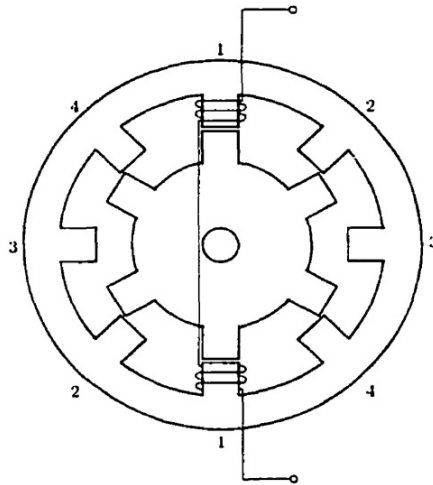


Figure 1.6: One phase cross-section of 8/6 SR machine

1.6 Typical Applications of BLDC

Regardless of the need of a complex motor controller for BLDC motors, BLDC motors offers several inherent advantages which are not available by using brushed DC motors in terms of high torque and wide speed range. Better heat dissipation, improved efficiency and greater power density for BLDC motors make them more suitable and advantageous in many applications. The research presented in [11] -[12] shows that the permanent magnet machines could become more important than induction motors for servo applications. The major applications for BLDC motors are given below:

1. Battery Powered Applications

- (a) Electric and Hybrid vehicles
- (b) Electric scooters and bicycles
- (c) Low Voltage Drives

2. Home and Building Applications

- (a) Blenders and hand power tools and fans

- (b) Fans in cooker hoods
- (c) Washing machines
- (d) Air Conditioners and refrigerators [13]

3. Industrial Applications

BLDC motors are primarily useful in actuation, servo and variable speed applications where position control and stable operations are required. BLDC motors are commonly used as:

- (a) Linear motors
- (b) Servomotors
- (c) Extruder drive motors
- (d) Actuators for industrial robots
- (e) Automotive HVAC(Heating Venting and Air-Conditioning)

1.7 Problem Statement

Typically rotor position in BLDC motors is measured using external sensors i.e. Optical sensors and Hall-effect sensors which increases the cost of the system and reduce its reliability and life span. In order to make them more efficient with more reduced cost the external sensors for position and speed should be eliminated. The approaches used to measure the rotor position without sensors are generally known as sensorless control and are mainly dependent on the measurement of the electromotive force (EMF), which is induced by the rotor. As the back-EMF is almost zero at standstill and near to zero speed, and can not be measured accurately, another mechanism is required which can handle the control of BLDC motors at near zero speed increasing the cost.

1.7.1 Proposed Work

Keeping the cost and durability of BLDC motors in mind this thesis propose to infer the rotor position of the motor from voltage and current signal measurements by solving these voltage and current signals to find the inductance of each phase. This inference of rotor position can be used to generate a proper sequence for commutation of motor.

1.8 Thesis Organization

The thesis is organized in the following manner.

Chapter 1 provides a basic introduction of Brushless Direct Current Motors (BLDC motors).

Chapter 2 gives the detailed background of BLDC motor control in two portions covering both sensed control and sensorless control. Also some aspect of Switched Reluctance motors control are described.

Chapter 3 presents the BLDC model for one phase covering its both magnetic part and electric part along with the description of mathematical model. At the end of the chapter the motor part is combined with the mechanical part and explains the three phase model.

Chapter 4 deals with the experimental work and the analysis of the data obtained from the experiments. It also covers the results obtained for both delta and wye models.

Chapter 5 covers the conclusion, including a general description of the experiments which were done, their results and the future work on them.

Chapter 2

Literature Review

2.1 Introduction

The Brushless DC motor has become very important in most of the small-scale electric vehicles from low performance application to high end applications [14]. The BLDC motor is inherently efficient, has a very high power to weight ratio and the removal of brushes makes them best choice for such applications. However the current state of electrical controllers available in industry restricts these motors capabilities and offer only limited controllability. This performance issue related to commercial controllers available in industry is basically because of the simple control techniques that are invariably used. Most of the controller use six step control strategy which results in poor dynamic performance of the motor and high torque ripple leading to greater vibrations and shorter motor life. Also these controllers are not capable of working on low speed range and limit the performance of the BLDC motors.

This chapter explains the motor structure and the existing control algorithms used in industry. To begin with, the basic principle of operation of BLDC motor is presented. This section also covers the torque and back emf generation and the similarities and differences between three-phase sinusoidal and trapezoidal motors. The second section describes the BLDC motor control technologies covering both the sensed and sensorless approach. A few of the

major approaches adopted are discussed for both sensed and sensorless control for motor drives. The third section covers the main part of the BLDC motor control i.e. the rotor position calculation which is the most important step in most of the sensorless control methods. The last section of this chapter presents the overview of switched reluctance motors and the sensorless approach used to control the SR motors.

2.2 Principle of operation of BLDC motor

A brushless DC motor is generally described as a permanent magnet synchronous machine which is fed with rotor position. The BLDC motors are mostly controlled using 3-phase power inverter bridge. The motor needs the position of rotor for starting and providing the proper commutation sequence so that the power devices in the inverter bridge are turned high (on) accordingly and the motor can rotate. Once the sensor determines the rotor position, the power devices are commutated sequentially. In case of brushed motor the current is commutated using brushes but for BLDC motors this is done electronically without brushes and therefore are known as electronic motors. The problems associated with brushes are eliminated in BLDC motors making it more rugged as compare to a brushed DC motor. The basic Brushless DC motor system consists of mainly four parts, power devices, BLDC motor, sensors and the control algorithm as shown in Figure 2.1. The power devices transmits power from the source to the Brushless DC motor which is then transformed into mechanical energy in the second block. The main feature of BLDC motor is the detection of rotor position of BLDC motor which is done by sensors/sensorless and this calculated position is transmitted to the control algorithm used which make the decision on the basis of the position detected. The controller sends commands to the power devices to turn on or off the specific devices.

The working of rotational electric machines are basically combination of different physics laws mainly Faraday's law, Ampere's law and Lenz's law. These physics laws are briefly explained below. These laws will be further used in Chapter 3 for explaining the flux linkage

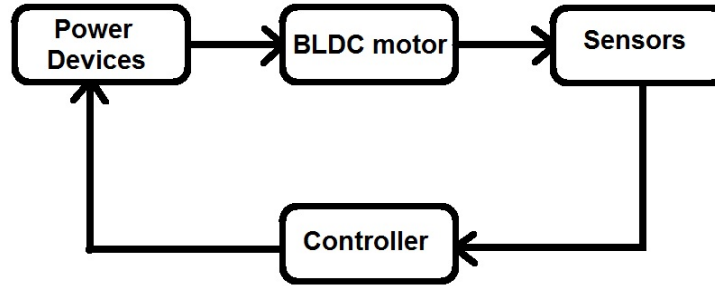


Figure 2.1: Block diagram of basic BLDC motor system

and voltage induced in case of BLDC motors.

2.2.1 Faraday's Law

Faraday's law of induction was presented by Michael Faraday (1791-1867), which describes the voltage induced in a coil of wire in following two different forms:

1. "A moving conductor cutting the lines of force (flux) of a magnetic field has a voltage induced in it".
2. "A changing magnetic flux inside a loop which is made from a conducting material will induce a voltage in the loop".

Mathematically the Faraday's law is explained in Equation 2.1 where φ represents the total flux through the loop of wire in a plane perpendicular to the flux and ε represents the voltage induced.

$$\varepsilon = \frac{d\varphi}{dt} \quad (2.1)$$

2.2.2 Ampere's Law

Ampere's law was discovered by Andre-Marie Ampere in 1826 and states that:

“The integral around a closed path of the component of the magnetic field tangent to the direction of the path equals μ_o times the current intercepted by the area within the path”.

Mathematically Ampere’s law is expressed as in Equation 2.2 below:

$$\oint B.ds = \mu_o.I \quad (2.2)$$

Ampere’s law is very useful when magnetic field is calculated for a current distribution with a high degree of symmetry. Only the currents crossing the area inside the path are taken into account and only these currents contribute to the generation of magnetic field [15].

2.2.3 Lenz’s Law

Lenz’s law is named after Heinrich Lenz and it states that:

“An Induced voltage is produced by a change in magnetic flux. The polarity of the induced voltage is such that it produces a current whose magnetic field opposes the change which produces it”.

Mathematically it is expressed same as Faraday’s law but with the opposite sign as this voltage is induced in the opposite direction against the change which produces it.

$$\varepsilon = -\frac{d\varphi}{dt} \quad (2.3)$$

2.3 BLDC Control Review

A typical Brushless DC motor is driven by voltage pulses to specific phase of the stator in accordance to the position of the rotor. To generate the maximum torque in the brushless DC motor, these voltage pulses should be applied properly to the active phases of the three-phase winding system so that the angle between the rotor flux and the stator flux is kept close

to 90 degrees. Therefore, special controllers are required which control the voltage on the basis of rotor position detected. Once the rotor position is detected, the controller works appropriately to generate a proper commutation sequence of the voltage strokes so that the BLDC motor keep on rotating. The BLDC motor is supplied with the three-phase inverter and the commutation sequence can be simply used to trigger the switching actions of the inverter. There are different control techniques available in industry for brushless DC motors and are explained below.

2.3.1 Six step Commutation

The six step commutation also know as trapezoidal commutation is the simplest form of the commutation which is available in the market to control the BLDC motor. Figure 2.2 shows the six step commutation for brushless DC motors.

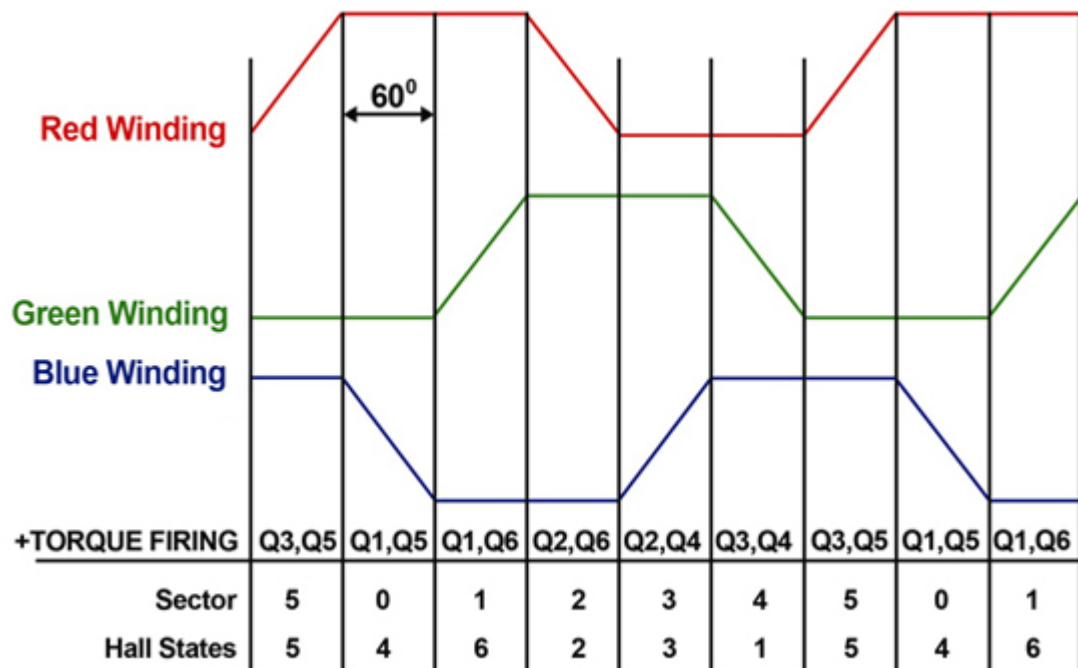


Figure 2.2: Six Step Commutation, Microcontrollers Sol Inc.

The trapezoidal commutation requires the digital Hall devices to detect the position of the rotor aligned 30 degree electrically from the zero crossing point of the phase. As soon the Hall signal transition takes place, the sequence is changed for the phase current, thus the commutation of the motor occurs and if this commutation keeps working, the BLDC motor will rotate continuously. The three-phases of the BLDC motor are energized in 120 degree sequences and each phase winding's voltage is high for 120 degrees. The current is conducted through two of the three phase windings at anytime with one phase winding held at a high electrical potential and the other at low electrical potential. The third phase winding is kept off during this interval. This gives the six possible commutation steps per one complete revolution as shown in Figure 2.2 [13].

Figure 2.3 shows the BLDC motor with transistors bridge which generates the six-step commutation sequence shown in Figure 2.2 [13].

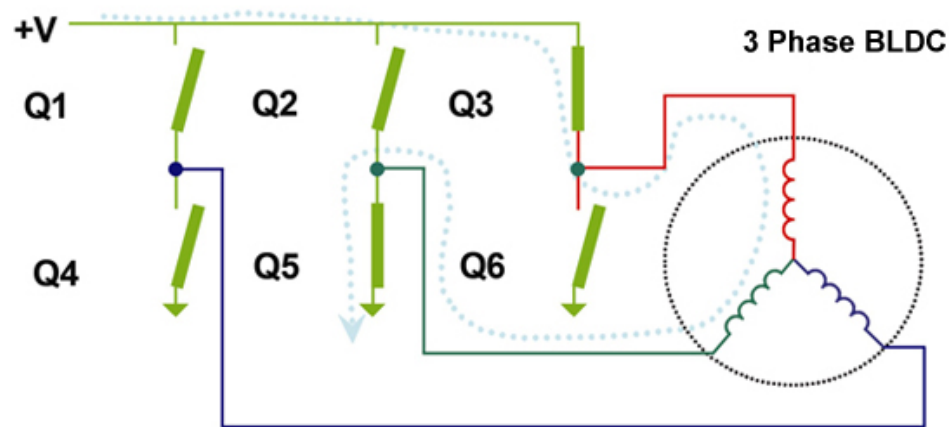


Figure 2.3: BLDC motor with six transistors power bridge

The trapezoidal commutation is the cheapest commutation way of controlling a brushless motor. It is suitable for high speed applications where the motor mechanics will eliminate the torque ripple that is produced because of the switching current from one phase to the next. The increased torque ripple results in larger vibration, noise and subsequently shorter motor

lifespan.

2.3.2 Sinusoidal Commutation

The ideal approach to drive the sinusoidal brushless motor is to use the sinusoidal commutation technique. By using the sinusoidal commutation, the flat peaks of six-step commutation are replaced with sinusoids. There are two possible ways by which sinusoidal commutation is achieved. As analog Hall effect devices can generate a sinusoidal signal when the motor rotor passes over the sensor magnetic poles. The signals, which are correct for commutation of the motor are combined with the demand signals to generate the sinusoidal commutation for the motor. This method is the cheaper one of the two but using this method can generate more noise and affect the commutation sequence resulting in poor performance of the motor. Figure 2.4 shows the sinusoidal commutation with respect to the Hall sensor output.

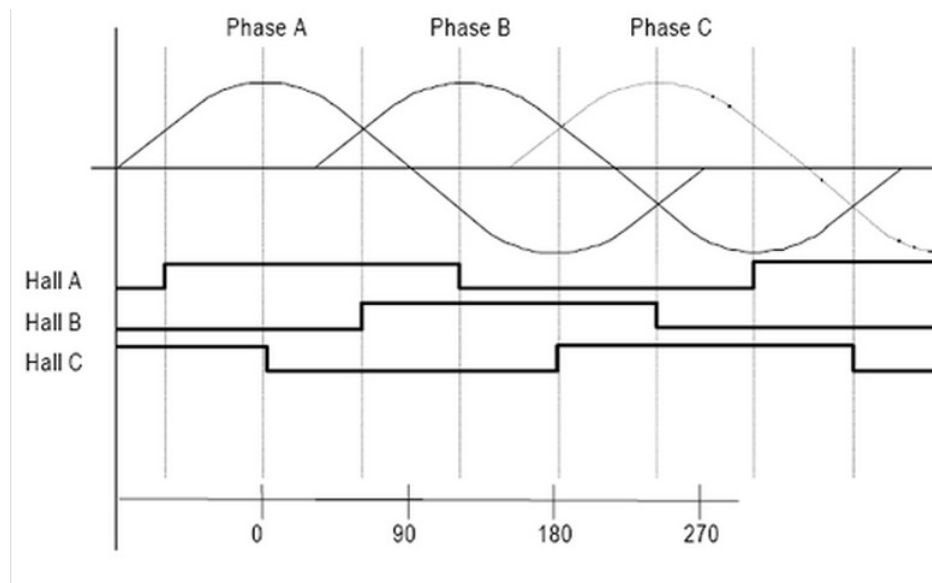


Figure 2.4: Sinusoidal commutation with Hall sensor output [16]

The second method to generate the sinusoidal commutation uses the encoders. This method

of commutation gives the best result of the two approaches, but adding the encoders increases the overall cost of the motor. The commutation is done in the second approach by generating a $\sin(\theta)$ phase A command signal and 120 degrees shifted $\sin(\theta+120)$ phase B command signal and multiplying this by the current command. The nature of the sinusoidal back-EMF needs the commutation phases to be overlapped and because of this overlap the torque ripple is reduced and more precise control of the motor is achieved. The comparison between six-step and sinusoidal commutation is shown in Figure 2.5 [17].

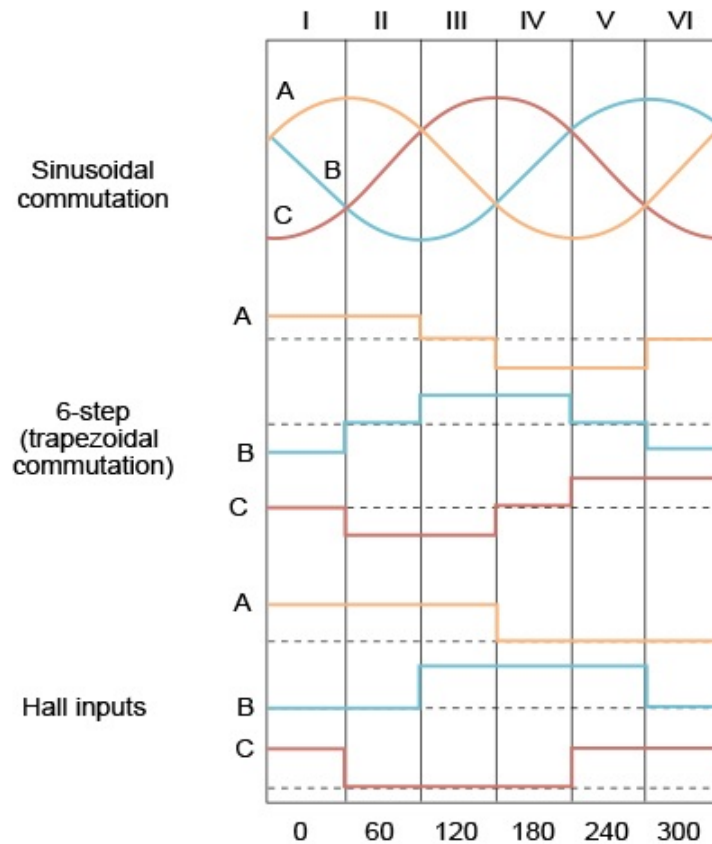


Figure 2.5: Comparison between Six-step and sinusoidal commutation [17]

2.3.3 Field Oriented Control

The Field Oriented Control (FOC) also called Vector Control for BLDC motors is a process to achieve torque control by controlling the space vectors of voltage and current directly in a new reference frame known as the d-q reference frame. In this process the flux linkage state vector is decomposed into two discrete components, the first component is flux(d) and the second component torque(q). During this process a three-phase system is transformed into a two co-ordinate (d-q) system. This transformation is computationally intense mathematics as it demands a lot of computer based computation and simplification, and is known as Park's and Clarke's transformation. This method is computationally so complex that it needs high processing power DSPs, micro-controllers or FPGAs in controlling the motor. Figure 2.6 shows the graphical representation of the the d-q components. The q-d components are intrinsically orthogonal to each other [18].

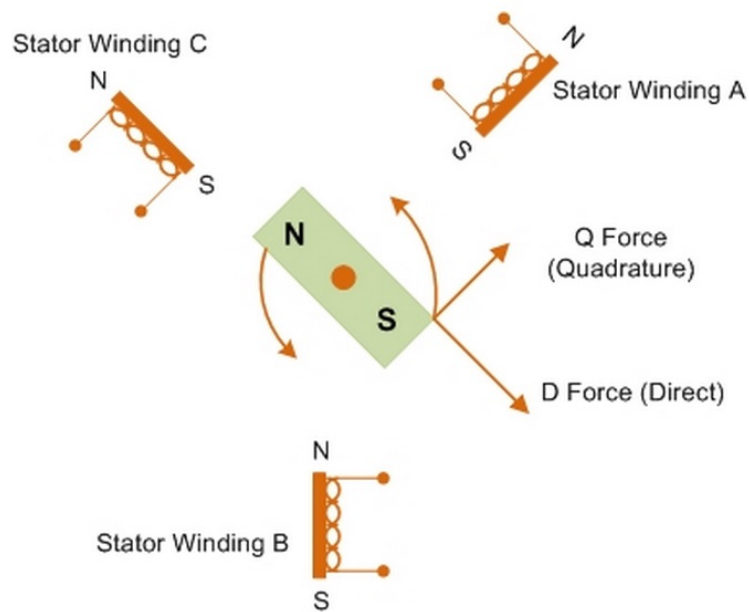


Figure 2.6: Direct (d) and Orthogonal (q) components [19]

The first step for the FOC is the Clarkes transformation which takes the 3-phase stator cur-

rents and transforms it to a two-dimensional orthogonal variables mostly denoted by α and β [20]. Figure 2.7 shows the graphical representation of the Clarke's transformation. Once the three phase system is transformed into two phase (α & β) stationary system, it is necessary to transform them into a system that is rotating along with the rotor flux. This step is done using Park's transformation [21]. Figure 2.8 shows the graphical representation of the Park's transformation. After Clark's and Park's transformations the stator current is now in two-phase system aligned with the rotor flux. The direct component does not provide any useful torque generation information and can be neglected. The quadrature component is mainly responsible for the actual torque generation of the motor. These two components are processed and then converted back to stator referenced two-phase system to generate the pulse width modulation (PWM) to drive the motor appropriately.

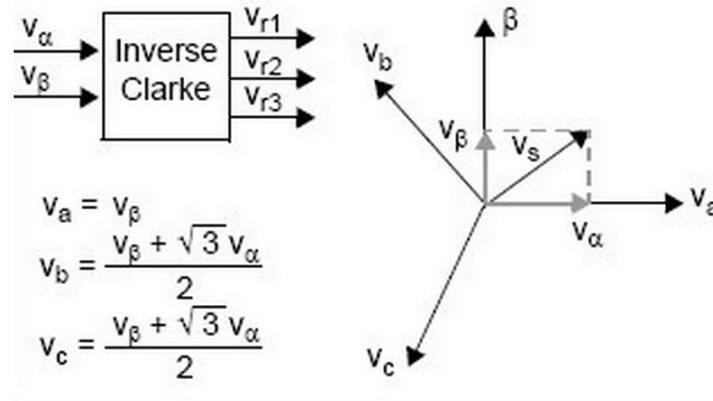


Figure 2.7: Clarke's transformation [20]

Using FOC provides the precise motor control over the large speed ranges and because of its nature the FOC has been successfully implemented for BLDC motors as well as PMSM motors in past two decades. The overall operational behavior of FOC is explained in Figure 2.9 [22].

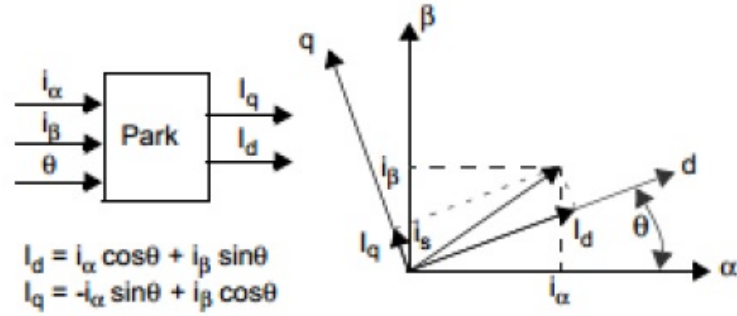


Figure 2.8: Park's transformation [20]

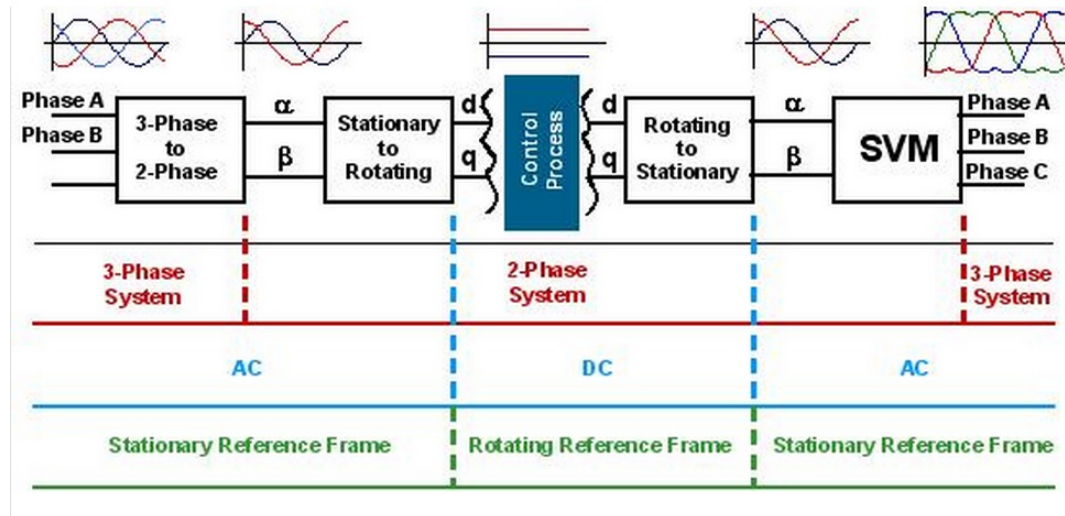


Figure 2.9: Block diagram of generic FOC control drive [22]

2.3.4 Direct Torque Control

Direct Torque Control (DTC), as expressed by its name is a method which directly controls the electromagnetic torque and flux linkage by rapidly manipulating the stator flux. It was originally developed for controlling the induction machines [23] - [24]. After getting great performance success in induction machines this approach was introduced in BLDC motors as well [25] - [26]. DTC operates by comparing the reference values of the stator torque and flux with the actual observed values. The flux and torque which are derived directly from the stator flux linkage are the only required feedback parameters for DTC process. Therefore, to

apply DTC method an estimator is needed to estimate the torque and flux of the stator. Along with an estimator, a look-up table and hysteresis comparators are also needed to complete the process [27]. In DTC method the stator currents and the DC-bus voltage are sampled at each interval and using the manufacturer provided data and these measured values of current and voltage for the stator resistance, the flux of stator is calculated in α - β reference frame. During DTC process the stator flux rotation is divided into six possible discrete inverter voltage vectors as explained in Figure 2.10.

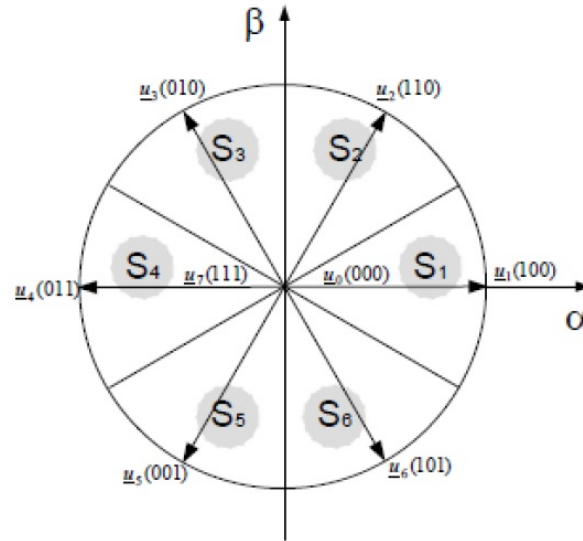


Figure 2.10: Inverter voltage vectors and stator flux vectors [27]

After determining the current flux vector located in sectors S1-S6, the magnitude of the stator torque and flux is determined and then compared with the reference values in relative hysteresis comparators. The output taken from these comparators is then fed to a lookup table and the proper voltage vector is then selected from the lookup table using the rotor flux vector position and torque. Therefore, in case of DTC the PWM is replaced with a simple look-up table and is no longer needed [28]. DTC approach has many variations now available in industry and are used for both PMSM and BLDC motor drives. Mostly this method to control the motors is used for large machines commercially and was not available for small

motor drives. Unlike FOC, DTC method does not need any reference frame transformation and rotor position estimation which decreases the overall cost of the drives and also requires less development time. Cassadei [28] concluded that the DTC is preferred in high dynamic load applications but it results in a higher current and higher torque ripple comparing to FOC method.

Direct torque control method based on hysteresis controllers as mentioned above have some serious drawbacks such as larger amount of torque and flux pulsation and the variable frequency of the inverter. Also using DTC to control the BLDC motor needs a continuous observation on stator flux linkage and the accuracy of this observation is affected by stator resistance variation, electric and magnetic interference and measurement errors.

2.4 Rotor Position Estimation

The measurement/estimation of rotor position is the most critical step in controlling the BLDC motors. A small error in position estimation for BLDC motor can result in very poor performance and in some cases it may result in a complete motor failure. The estimation of the rotor position can be done by sensed and sensorless approaches. In sensed approach some type of external sensors are attached with the motor, while for sensorless there are no sensors attached to the motor itself.

2.4.1 Sensed Approach

Most of the existing control algorithm uses sensed position estimation which increases the total cost of the motor but these are the simplest and most commonly used techniques. For brushless DC motors, the only requirement per electrical cycle is the knowledge of six phase-commutation instants, therefore sensors with low cost are widely used in industry. In reality the motion sensor based on magnetic field detection principles stand out because of their many advantages and detection benefits.

2.4.1.1 Hall Effect Sensors

Hall Effect sensor is the most common sensor seen in rotating machines. Hall-effect theory states that “if an electric current carrying conductor is kept in magnetic field, the magnetic field exerts a transverse force on the moving charge carriers that tends to push them to one side of the conductor”. The presence of this transverse voltage is called the Hall-effect as it was first discovered by Edwin Hall in 1879. For rotor position estimation, mostly there are three hall effect sensors embedded into the stator. Whenever the rotor magnetic poles passes near these Hall-effect sensors they generate high or low signal showing the S or N poles of the rotor magnet. Hall sensors are embedded into the fixed part of the motor and this is done by a complex process as any misalignment in the sensors with respect to magnets in rotor will produce an error in the rotor position estimation.

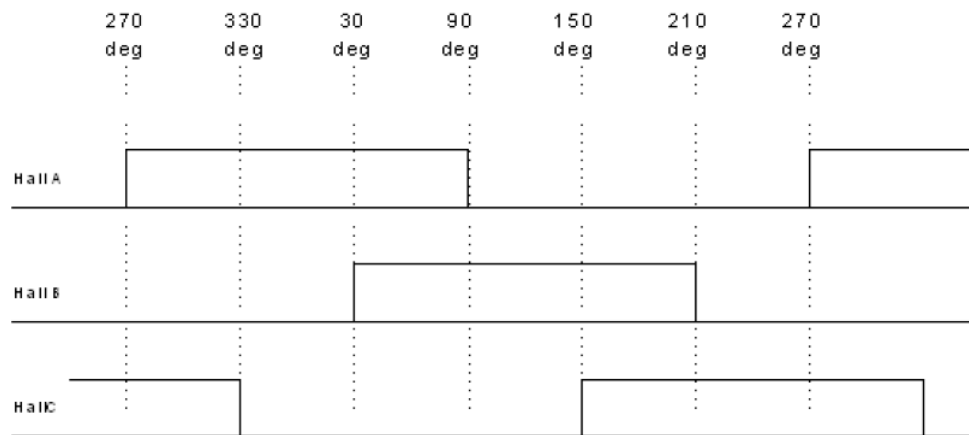


Figure 2.11: 3-phase Hall sensor chart with 120degree angle separation [29]

The main obvious drawback of using hall effect sensor is the increase in overall cost of the motor, as the hall effect sensors needs to be added by the manufactures because of the complex process required. This increase in the cost of the motor is almost negligible for the larger machines, but in small machines the cost of the sensors is greatly significant. Hall effect sensors also require some power for their operation which adds more wiring to the motors and adds up in the wiring cost of the motor. Big issue is that the addition for both sensing and

wiring reduce the reliability of the motor. The classical three hall effect sensor configuration just estimate the position of the rotor to an accuracy of 60 degrees only. Therefore, using the simple classical approach we can only get the position of the rotor with less accuracy.

2.4.1.2 Variable reluctance (VR) sensors

The variable reluctance sensors are used to detect the position and speed of the moving metal components and are also referred as a passive magnetic sensor as it does not need any power for itself to detect the signal. The VR sensor consists of a winding wound around a cylindrical magnetic material made up of ferrous. A magnet is attached behind the pole piece which creates a magnetic field through pole and windings. When these sensors are placed near a moving device, a simple technique for measuring the speed is created. The frequency of the signal is directly proportional to the speed of the device. The amplitude of the signal depends on the speed of rotation, the material being sensed and the the distance of the material from the sensor. It is usually very simple to implement and the physics behind its operation includes magnetic induction [30]. A basic mechanism of how variable reluctance sensors works is explained in Figure 2.12.

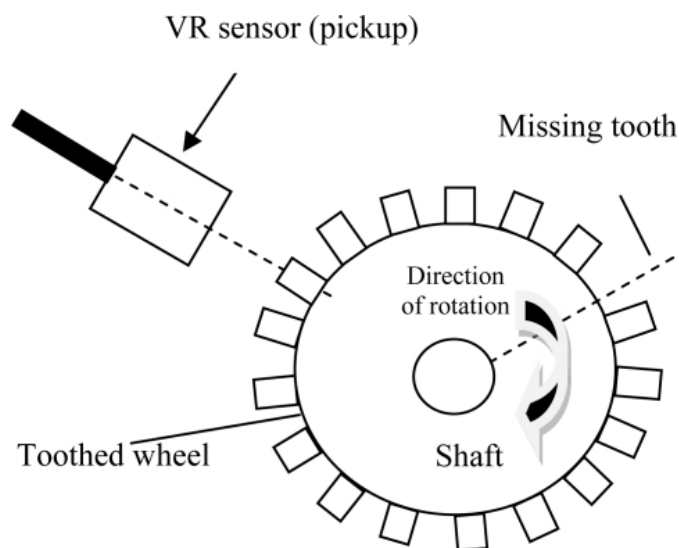


Figure 2.12: Variable Reluctance sensor [31]

The main advantage of using variable reluctance sensor is its low cost and simplicity. VR sensors are robust and can operate at higher temperature ranges and also these sensors are small in size so they can be embedded in places where other sensors may not fit. These sensors are resistant to high pressure and high temperature as well as chemical attacks [32]. These sensors need less wiring connections which enhance its reliability and reduces the wiring cost [31].

2.4.1.3 Optical Encoders (Magnetic Encoders)

The optical sensing technology is the most accurate and provide the highest resolution of the position estimation. As the name shows the optical encoders use light to identify the positions. The optical encoders consists of a light source, sensor, movable disk and a fixed mask. A photo detector is used in optical encoders to sense the alternating light beams and the encoder's electronics convert this pattern into an electrical signal which is then processed to find how far from original position the disc has rotated. The Optical Shaft Encoder uses an infrared light sensor to detect illumination from an infrared LED passing through slots cut in the circumference of a rotating wheel. A single optical encoder is shown in Figure 2.13.



Figure 2.13: Single ended Optical encoder [33]

Optical encoders are good choice in application where high resolution is required such as office equipment and medical equipment. Optical encoders are also able to perform in much tougher environments which needs both high resolution and durability like automated vehicle

guidance. There are many different considerations when determining what type of encoders to use in a specific application. Choosing a right optical encoder for a particular application is not a difficult process but its always good to ensure all the different application criteria are considered before selecting a specific encoder [34].

2.4.2 Sensorless Approach

The problems associated with the cost and reliability of sensors used to detect the rotor position have motivated research in the area of sensorless position detection for BLDC motor drives. In the last decade, many sensorless drive solution has been offered to eliminate the costly and fragile position sensors for BLDC motor. These solutions mainly depend on the back-EMF detection of the motor [13] - [35]. Many research efforts have been done for this area but none works well at all speeds without reliability, accuracy and complexity problems, especially at very low speed ranges. Therefore, mostly a separate starting algorithm is needed to start the BLDC drive and once a particular speed is achieved where back EMF is easily detected then the controller start working on the basis of back EMF detection. Also the position error from a phase shift in transient state deteriorates the performance of the BLDC motor drive [13] - [36]. Below are the main sensorless approaches for controlling the BLDC motors.

2.4.2.1 Back-EMF Sensing Techniques

The most common approaches to sensorless control, such as that used by Lu[37], are based on measurements of the electromotive force (back-EMF) that is induced by the rotor motion. When a brushless DC motor starts rotating, back-EMF is generated by each winding which opposes the supplied voltage to the windings in accordance with Lenz's law. The shape of this back-EMF in Brushless DC motor is trapezoidal [38]. The back-EMF generated in a motor is directly proportional to its speed, therefore the back-EMF at low speed or stand still position is negligible. Monitoring this back-EMF from the terminal voltages in the salient phase of motor, the zero crossing of the back-EMF can be detected. The zero crossing points

in current waveforms are shown in Figure 2.15. Since back-EMF is zero at stand still and low speed ranges, the measured terminal voltage cannot detect the zero crossing. The back-EMF zero crossing position estimation is more suited to two-phase conduction motors. The zero crossing can be found by feeding the voltage of the un-powered winding with respect to the virtual ground and half the DC bus voltage to comparator. At this state the comparator output changes showing that the zero crossing has occurred and the next sequence can be started [39]- [40]. Back-EMF zero crossing detection with winding flow is explained in Figure 2.14.

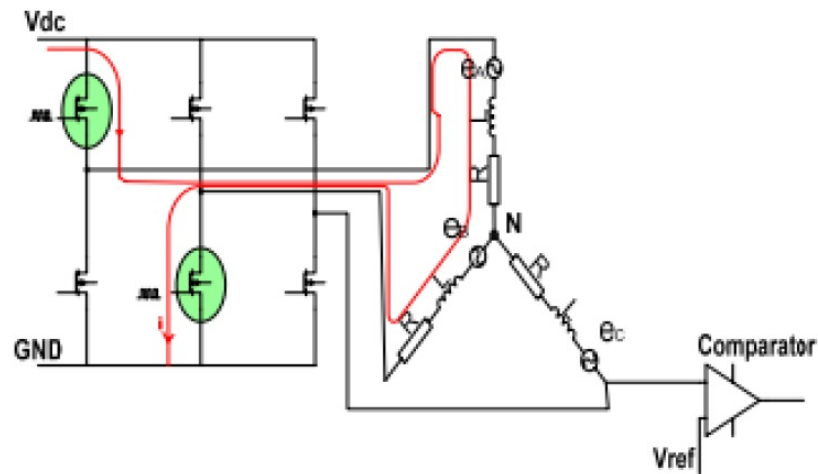


Figure 2.14: Back-EMF zero crossing detection circuit model with PWM On-time [39]

For typical BLDC motor, the back-EMF and the phase current should be aligned to generate a constant torque. To generate the maximum torque, the inverter should be commutated every 60 degree by detecting the zero crossing of the back-EMF and the floating coil of the motor so that the current is in phase with the back-EMF of the motor [42] - [43].

Back-EMF zero crossing detection does overcome lot of problems which are associated with conventional sensor base approach for position estimation as it does not need any phys-

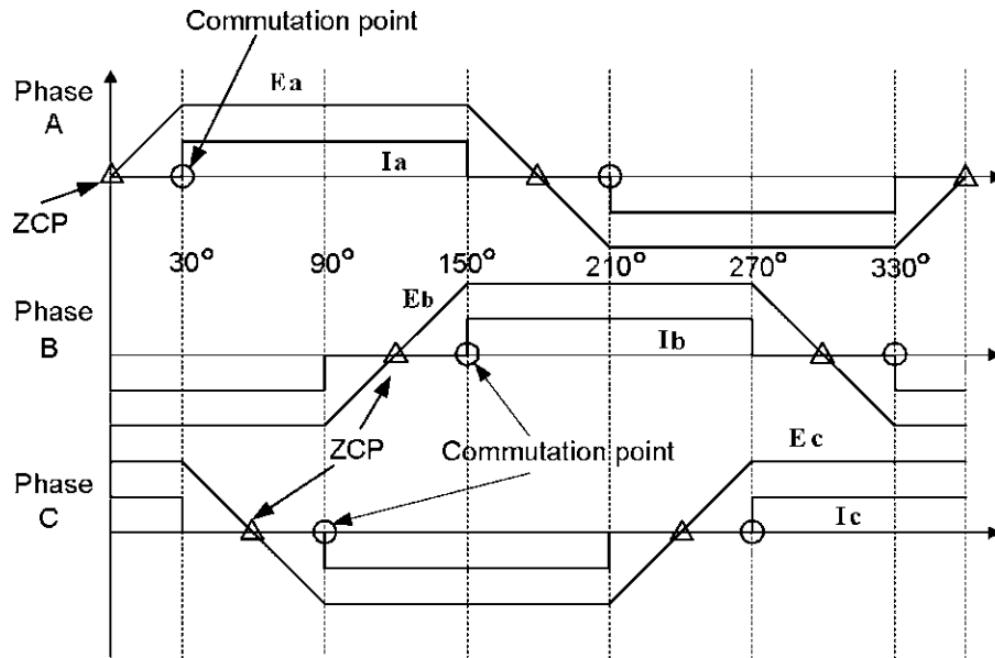


Figure 2.15: Zero crossing points of the back-EMF [41]

ical sensors to be mounted in or on the surface of the motor. There are also some drawbacks of using this sensorless approach for the position estimation as mentioned below:

1. The back-EMF is directly proportional to the speed of the motor. This means that there is no back-EMF when the rotor is at stationary state and also very low at low speed. Therefore, the back-EMF sensing approach is not applicable at all speed ranges and need a separate mechanism to control the BLDC motor at stand still and low speed ranges.
2. The back-EMF sensing method requires one phase to be non-current carrying in order to detect the back-EMF which means that only two phases are available for the conduction which results in the trapezoidal back-EMF which reduces the efficiency performance of the motors.
3. The estimated commutation points have some position error during the transient period when the speed of the motor is accelerated or decelerated rapidly.

4. By using the back-EMF sensing approach, the rotor position of the BLDC motor can be detected typically from 20% of the rated speed [13].

2.4.2.2 Inductance Variation

One of the method of sensorless control that is at least theoretically possible, involves the inference of rotor position from the variation in inductance caused by rotor position. This effect has been exploited by Jang et al [44] to develop pulse-based start-up algorithms, in which the variable response times to current changes at different rotor positions are used to detect rotor position. In this approach the variation of inductance on the relative position of rotor and stator is utilized. Cassat et al.[45] detected the position of rotor at stand still by comparing the rise time of the currents due to the inductance variation after a current pulse was injected into all six segments of any electrical cycle. As compared to the conventional back-EMF, the method presented by Jang et al. [44] based on inductance calculation can drive the brushless DC motor to a normal speed smoothly without showing any time delay or vibration in startup.

2.4.2.3 Extended Kalman Filter

The Extended Kalman filter (EKF) algorithm is an optimal recursive estimation process for non-linear systems if the measurement and the state transition model are both linear as in that case it will be identical to a regular kalman filter. This approach is based on the extension of R.E. Kalman's recursive solution to discrete-data linear filtering problems which was published in 1960. In this extension the basic Kalman filter is applied to a non-linear state space systems. Using EKF approach we can get the accurate estimate of the future state of the variables despite errors or noise in the variables measured [46]. A common EKF used for estimating the rotor position of a BLDC motor is presented by Terzic and Jadric [47]. EKF system is computationally intensive and requires an efficient formulation which covers all aspects of implementation such as processing time and storage memory, etc. instead of straight forward implementation [48].

The extended Kalman filter approach can be used to determine the position and speed of the motor. In this method the motor state variables are estimated in both transient and steady states [49]. The block diagram for the EKF system used for the speed and position estimation for rotor in BLDC motor is shown in Figure 2.16 [47]. In this system the measured speed (ω_k), phase currents (i_k) and the estimated rotor position ($\hat{\theta}_{k/k}$) are used as a feedback signals. The rest of the parameters are calculated and measured to find out the estimation of next state of the rotor position and speed.

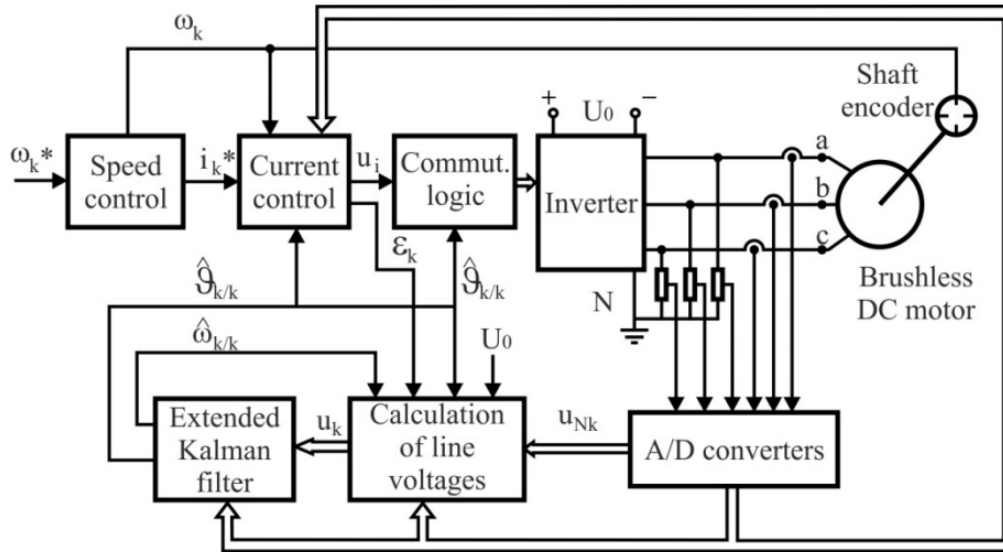


Figure 2.16: Block diagram for EKF system for rotor and speed estimation of a BLDC motor [47]

Though EKF system gives an accurate estimation of the rotor position and speed in BLDC motors but this approach is very complicated and computationally very intense. Also some specific problems need to be solved related to voltages and current waveforms for BLDC motor before applying the EKF approach [47]. EKF approach at very low speed is also not accurate and the rotor position estimation error becomes too large and the sensorless approach using EKF is no longer applicable to control the BLDC motor [47].

2.4.2.4 Sliding Mode Observer

Sliding mode observer (SMO) is a special kind of a non-linear control of the motor which is different from the conventional control methods. The approaches discussed above for sensorless control are motor observers. In this approach a sliding motion is generated on the error between the output of the observer and the actual measured system output [50]. This sliding movement to move a system along a certain path to do small, high frequency upper and lower movement under certain conditions makes this method a variable structure control. There are different approaches being adopted to design a sliding mode observer. One of the approaches is based on the equivalent control technique in which the system equations are converted to two suitable sub-systems. An appropriate sliding plane is then selected and a full state observer for the reduced order is designed. The other approach is designing a full state observer instead of reduced order and then sliding mode techniques are applied to stabilize the resulting error system [51].

Using sliding mode observer method for controlling BLDC motor drives gives a good overall performance as it gives much accurate rotor position. Also by using the estimated values as a feedback in closed-loop control, the real speed response of motor drives can be enhanced. Many researches are undergoing on different methods for designing SMO for better performance. This goes to show the broad nature of SMO theory and the requirement of a significant design for the successful implementation of any observer [52].

2.5 Switched Reluctance Motor Control Review

In the last two decades Switched Reluctance Motors has been investigated in details and these motors have become a strong contender for many applications in industrial, aerospace, automotive, robotics and domestic applications because of their simple construction and low cost. SRM provides many attractive performance features for the applications which are based on position detection [53] -[54].

2.5.1 Principle of Operation of SRM

SRM like BLDC machine is an energy converter which takes the energy from the magnetic fields created by the phase windings and exchange this energy between the electrical and mechanical subsystems. In a magnetic circuit, analogous to resistance there exists a magnetic reluctance which depends on the magnetic permeability of the material which is used for magnetic structure. In SRM the reluctance in the air gap between the rotor and stator poles is very large as compared to the reluctance of the steel lamination used. Therefore, the reluctance of the SRM is mostly considered to be because of the air gap. SRM is a doubly salient machine and when it start rotating the distance between the rotor and stator poles changes resulting in the change in the reluctance. There are two main positions which are of great interests in SRM known as "aligned position and unaligned position". In Aligned position the rotor pole is exactly aligned with the stator pole of the phase and hence the reluctance is minimum at this position. When the rotor pole and the stator pole is exactly unaligned the reluctance is maximum and this is known as unaligned position of SRM. These two positions for SRM are shown in Figure 2.17.

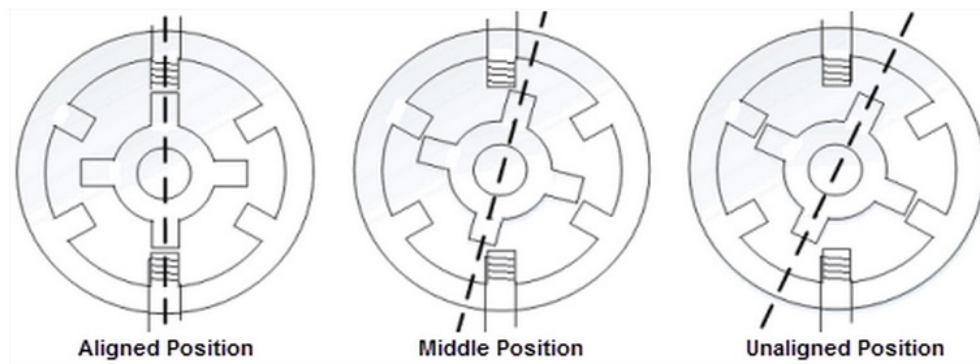


Figure 2.17: Aligned and Unaligned positions in SRM

In the Aligned position the rotor and stator are aligned and hence the reluctance is at minimum, there is no torque produced in the machine. This position is also known as the stable equilibrium position of the machine. Similarly, there is no torque produced in an unaligned

position as the reluctance is at its maximum and this position is also its equilibrium position but an unstable one. However, as soon as the rotor moves to any side of the equilibrium position, a torque is generated and this torque displaces the rotor further and attracts it to the next equilibrium position. As the rotor poles are identical throughout, the torque generated in SRM is periodic. The period of this torque is called the rotor pole-pitch (τ) and given by Equation 2.4, where N_r is the number of rotor poles.

$$\tau = \frac{2\pi}{N_r} \quad (2.4)$$

If the phases of the SRM is energized successfully in a proper sequence, a continuous torque is produced. For this successful commutation, the rotor position of the motor is required similar to BLDC motors. As the inductance of the stator coil varies with the rotation of the rotor from its minimum to maximum value, the SRM commutation needs rotor position continuously. Therefore, the performance of the SRM also depends on the accuracy of the position detection method used. As we have discussed different methods to detect the rotor position for the BLDC motors, they can also be used for SRM as well. Some researches has been done on the different rotor position detection methods for SRM including optical encoders [55], impedance measurement approach [56] and rotor position estimation from stator voltage and currents [57].

2.5.2 Sensorless Control of SRM

Similar to BLDC motors, position estimation is really important for better control of the switched reluctance motors, therefor these motors need special approach to detect the positions accurately. Using position sensors, however increase the size of the system, lower the reliability of the system and also impose some limitations for applications. Therefore, position estimation without using any sensor is the mainstream in SRM as well.

2.5.2.1 Sensorless control of SRM using Phase Inductance

In switched reluctance motors the inductance of the stator phase and the slope of inductance for the same phase, changes periodically with the position of the rotor and also the instantaneous current of the phase due to the magnetic saturation. The self inductance characteristic curves for SRM is shown in Figure 2.18. There have been many research efforts in the recent years on sensorless control of SRM on basis of the flux linkage and phase inductance [58]. Cai [58] presented a sensorless approach based on phase inductance of the SRM to control the motor. The phase inductance and flux linkage is related with each other according to Equation 2.5.

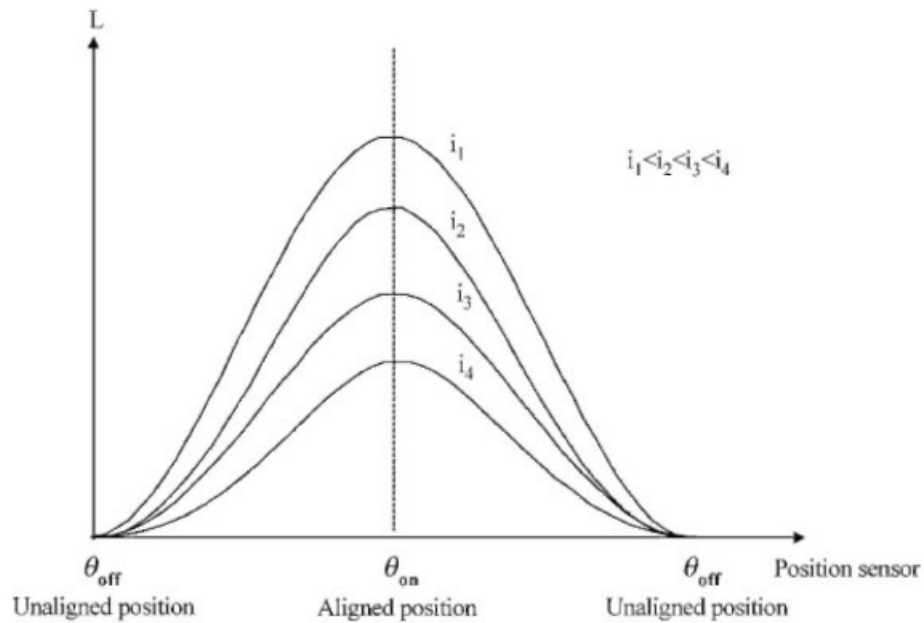


Figure 2.18: Per phase self inductance curve for SRM

$$L(i, \theta) = \frac{\psi(\theta, i)}{i} \quad (2.5)$$

Where L is the phase inductance, θ is the position of the rotor. The Equation 2.5 simply shows that the phase inductance can be easily calculated if we have the values of phase current and voltages but this is not the case when the motor phase is turned off as the current

goes to zero in that situation and ultimately the inductance at that state can not be calculated.

The approach taken by Cai is limited and less accurate as just using the inductance values of aligned and unaligned positions and set the value of the phase inductance to zero when current is decaying to zero in off state. By doing so the method is simplified but it leads to the problems and error in estimation of the rotor position. Also his approach is suitable for high speed operation as at low speed the error in position estimation is a problem and he proposed to use pulse injection methods to start and run the motor at low speed.

2.6 Summary

This chapter discussed the basic concepts of BLDC motors, starting with the design of the motor. The basic principle of operation was briefly discussed and basic laws were briefly presented. The third section covered the summary of the BLDC motor control and the commonly available approaches for controlling the BLDC motor were explained. As the rotor position identification is very important for the control strategies of the motor, both sensed and sensorless techniques which are available these days to find the rotor position in BLDC were discussed. In the last section of the chapter, the switch reluctance motors were introduced and discussed the principle of operation for SRM and then we looked into the sensorless control approach based on the phase inductance for SRM. The sensorless approach using inductance variance to control SR motors was of our interest to get some information of implementing the approach of inductance variation for BLDC motors.

Chapter 3

Modeling of BLDC motor

3.1 Introduction

As it is obvious that motors are used to convert electrical energy into mechanical energy. The brushless permanent magnet motor relies on the conversion of electrical energy to magnetic energy which is then converted into the mechanical energy. In this chapter the BLDC motor will be explained in individual parts i.e. Electrical part and magnetic part. In first section of the chapter we will discuss the magnetic model and flux linkage of the BLDC motors. In the second section of the chapter, we will look into the electrical model of the BLDC, also the per phase electrical circuit of the BLDC motors. In the third section of the chapter a brief mathematical model will be discussed and with the help of electrical, magnetic and mathematical models discussed, we will look into the torque and back emf generation for BLDC motors in the fourth section of the chapter. At the end of the chapter a general electro-mechanical model for motor will be discussed briefly.

3.2 Magnetic model

3.2.1 Basic concepts

There are two main sources of magnetic fields in BLDC motors, one being the permanent magnets and the other being a current flowing in windings. The magnetic field generated because of the current in stator windings is given by the Ampere's law as explained in section 2.2. The magnetic field of the permanent magnets is generally described by Equation 3.1, where B is the flux density of the magnetic field flowing through a given area of the material, μ is the permeability of the material used and the field intensity H is the resulting change in the intensity of the magnetic field due to the interaction of flux density (B) with the material.

$$B = \mu H \quad (3.1)$$

Magnetic circuit analysis is generally based on the assumptions of the linearity of the material and the collinearity of flux density (B) and field intensity (H). The two fundamental equations which leads to the magnetic circuit analysis are given below. Equation 3.2 relates the flux density to flux, where ϕ is flux, A is the cross sectional area and B is the flux density. Equation 3.3 relates field intensity to electromotive force, where F shows the electromotive force and H is the field intensity.

$$\phi = BA \quad (3.2)$$

$$F = Hl \quad (3.3)$$

Combining above two equation gives a relation which is analogous to Ohm's law for electric circuits and is explained in Equation 3.4 where μ is the permeability of the material.

$$F = \frac{\phi l}{\mu A} \quad (3.4)$$

3.2.2 Magnetic Materials

The magnetic properties of the material is generally referred in term of the permeability of the material and commonly expressed with respect to the permeability of the free space as shown in Equation 3.5, where μ_o is the air permeability and has the value of $4\pi \cdot 10^{-7}$ (H/m).

$$\mu_r = \frac{\mu}{\mu_o} \quad (3.5)$$

Commonly the materials having the permeability close to one are called non-magnetic materials while the materials with very high permeability are known as magnetic materials. The most common material used in the construction of the motors is steel which has a non linear permeability and that means the flux density through the material is not unique for a given field intensity. Recently different types of permanent magnet materials are available including alnico, ferrite, samarium-cobalt and neodymium-iron-boron. The ferrite type magnetic materials are inexpensive and are preferred in motor constructions. On the other hand the rare earth type materials e.g. samarium-cobalt offer the highest performance but they are highly expensive materials. Each of these magnetic materials have different properties and leads to different constraints and performance levels in BLDC motors. Usually the magnets are compared by the maximum energy product BH_{max} which is defined as the product of the flux density and the field intensity along the magnet demagnetization curve. Though, operating at maximum energy product is most efficient in terms of magnet volumetric energy density, magnets in BLDC are almost never operated at BH_{max} because of the possible irreversible demagnetization with increasing temperature in motors [7].

3.2.3 BLDC Magnetic Model with Equivalent Electrical Circuit

Flux in permanent magnetic motors generally travels through the rotor, across the air gap, through the stator, then again across the opposite air gap and finally back to the point where it started. Therefore, the flux passes through different media such as steel, permanent magnet materials, non magnetic materials (copper and insulation) and the air. For the simplification,

all of the media other than steel in the route of flux are considered to have the permeability of free space (μ_o). The steel in the motor construction used has a very high permeability and this is the only permeability which is taken under consideration for analysis of motor, which simplifies the analysis as reluctance of the steel is negligible as compared to air gap. The MMF generated by the stator winding drives magnetizing flux through the air gap and the steel. Since for basic analysis the reluctance of the steel is taken as negligible, therefore, the MMF developed across the steel is ignored and also the field strength is ignored [59].

The general cross section view of inner rotor is shown in Figure 3.1. The motor shown in the figure has four magnet poles, 2 pole-pairs. This motor has a factor of two in between electrical and mechanical angle. For simplification purposes the stator is shown without slots and windings. The flux leaving the north pole of the magnet travels through the air gap and enters into the stator where it divides into two parts. The flux flow is shown in the figure with arrows. In addition to the main flux flow as mentioned, some of the flux jumps directly from one magnet to the other without going through the air gap and stator as illustrated in the figure. This flux is known as the magnet leakage flux. The flux pattern shown in Figure 3.1 is same for every half pole pair and it is enough to just look into the one pair to understand and develop the magnetic model of BLDC motors. In this figure the two half magnets are modeled as flux source ϕ_r and their magnet reluctance as R_m . With the help of this magnetic structure, the magnetic circuit can be schematically modeled as shown in Figure 3.2 [7]. Where R_s , R_r and R_g shows the reluctance of the stator, rotor and the air gap respectively. The ϕ , ϕ_g and ϕ_l shows the magnet flux because of the permanent magnet, air gap flux and leakage flux respectively.

This circuit can be more simplified as shown in Figure 3.3 [60], where both magnets and air gaps are combined. As we discussed above that all the reluctances other than steel are ignored in the basic analysis of the motor, therefore only showing the reluctance of the steel in simplified circuit as below. The flux (ϕ_t) linking the turns of the coil is the combination of

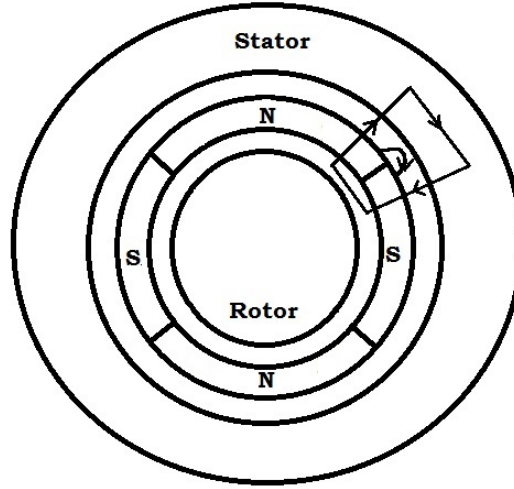


Figure 3.1: Cross sectional view of inner roto motor

two flux sources i.e. the coil (ϕ_c) and the permanent magnet (ϕ_m). The total flux is given by Equation 3.6.

$$\phi_t = \phi_c + \phi_m \quad (3.6)$$

Using the Equation 3.6 we can further divide this circuit in two parts by replacing total flux with coil flux in one part and magnetic flux in other. This circuit model is very basic and it is enough to understand the magnetic behavior of BLDC motors.

3.3 Electrical Model

Once we have discussed and modeled the magnetic circuit of BLDC motor, we can look into the electrical model. It is good to design an electric model of the motor with as less mechanical dependencies as possible. Instead of discussing all the three phases of the motor, we can look into the one winding for simplification and that can be enhanced for other windings as well. Before developing electrical circuit model for BLDC we need to explain the flux linkage first.

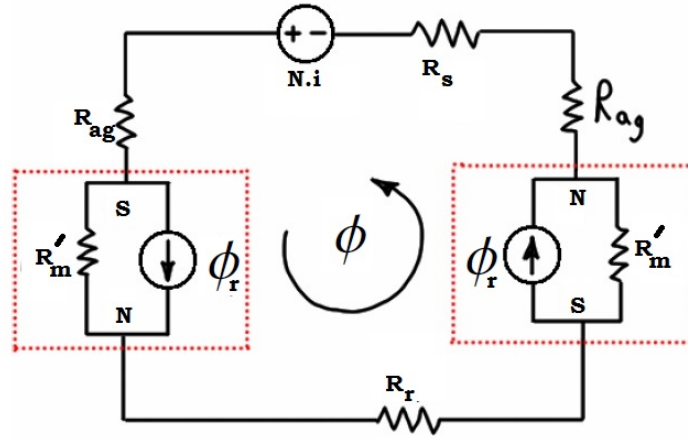


Figure 3.2: magnetic circuit of simple BLDC motor [60]

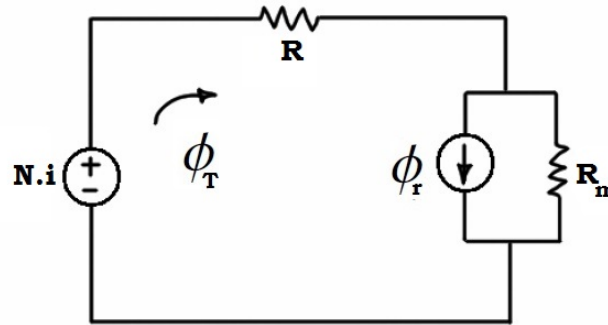


Figure 3.3: Simplified magnetic circuit of simple BLDC motor

3.3.1 Flux Linkage

The flux linkage in motors describes the total flux linked to the winding of the motor. The expression of the flux linkage depends on the current of the winding itself and all the variables that shows the external sources of flux. For example the flux linkage of a simple inductor only depends on the flux generated by the current which is passing through itself. For a BLDC motor the flux linkage expression of a winding of motor will consists of the part showing the flux linkage generated by the magnets of the rotor, a part for the flux which is being generated by the winding itself and a part for each additional windings which are present in the motor. Mathematically, the flux linkage for one winding of a BLDC motor is given in Equation 3.7.

Where λ_s shows the flux linkage of the stator winding.

$$\lambda_s = N.\phi_t = \frac{N^2 i}{R + R_m} + N.\phi_m \quad (3.7)$$

In this equation we can introduce the term for inductance in place of the term shown in the fraction as the inductance can be expressed as the function of the total reluctance as MMF source of the coil sees it in the given circuit. Therefore, Equation 3.8 gives the inductance as:

$$L = \frac{N^2 i}{R + R_m} \quad (3.8)$$

Using the above equation in the flux linkage equation defined by Equation 3.7, we get the flux linkage expression in term of inductance as given in Equation 3.9. Where the first term shows the flux linkage of winding itself and the second term shows the flux linkage generated because of the rotor.

$$\lambda_s = L.i + N.\phi_m \quad (3.9)$$

Though we have defined the inductance as a constant for this simplified case but in real machines like the one for our experiments the inductance of the motor can be a function of the rotor position. Therefore, we can represent the inductance of the motor in term of the rotor position as given in Equation 3.10.

$$\lambda_s = L(\theta_r).i + N.\phi_m \quad (3.10)$$

3.3.2 Per Phase Electrical Model

To develop a simplified circuit model for the BLDC motor phase, we can ignore the dependencies of the inductance and flux linkage on the rotor. If we ignore all the dependencies in the second part of the flux linkage expression, and replace it with a new variable ψ_r , we get the simplified expression of the flux linkage as given by Equation 3.11.

$$\lambda_s = L \cdot i + \psi_r \quad (3.11)$$

Now, to complete the development of simplified circuit model for the BLDC motor, Faraday's law can be applied to Equation 3.11 to get the induced voltage of the coil as given below:

$$\varepsilon = \frac{d\lambda}{dt} \quad (3.12)$$

$$\varepsilon = L \frac{di}{dt} + \frac{d\psi_r}{dt} \quad (3.13)$$

The above Equation 3.13 shows that the voltage induced in the case of the BLDC motor winding is depending on two terms, first is the inductor and the second one shows the flux of the motor. This expression can be modeled in terms of electric circuit as in Figure 3.4 showing the voltage induced in the winding of the motor.

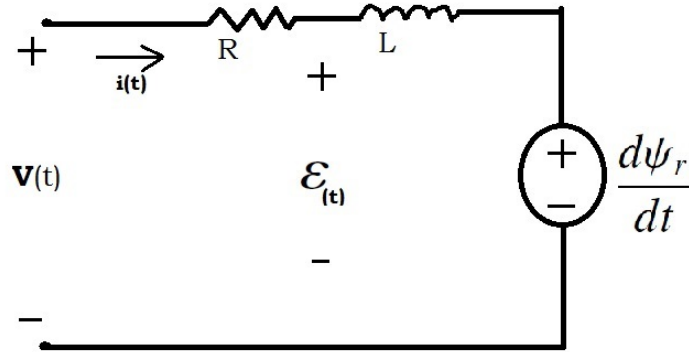


Figure 3.4: Simplified Electrical Model of BLDC motor

The figure above shows the simplified circuit model of a BLDC motor with neglecting the effects of the additional windings which exists in case of real motors. This model is good enough to understand the basic structure of the BLDC model and the flux generated in it.

3.4 Mathematical Model

Figure 3.4 shows a simple electrical model of a phase of the BLDC motor. If we solve the circuit for Voltage (V) and Torque (T), we get the following equations. Where J , T_L and k_f shows the rotor inertia, mechanical load and friction constant respectively.

$$V = Ri + L \frac{di}{dt} + \varepsilon \quad (3.14)$$

$$T = k_f \omega_r + J \frac{d\omega_r}{dt} + T_L \quad (3.15)$$

Rearranging the equations 3.14 and 3.15 to create a state space representation gives:

$$\frac{di}{dt} = -\frac{R}{L}i - \frac{k_e}{L}\omega_r + \frac{1}{L}V \quad (3.16)$$

$$\frac{d\omega_r}{dt} = \frac{k_t}{J}i - \frac{k_f}{J}\omega_r - \frac{1}{J}T_L \quad (3.17)$$

Using the Equations 3.14 and 3.15, the state space representation can be given as: [61]

$$\begin{pmatrix} \dot{i} \\ \dot{\omega}_r \\ \dot{\theta}_r \end{pmatrix} = \begin{pmatrix} -\frac{R}{L} & -\frac{k_e}{L} & 0 \\ \frac{k_t}{J} & -\frac{k_f}{J} & 0 \\ 0 & 1 & 0 \end{pmatrix} * \begin{pmatrix} i \\ \omega_r \\ \theta_r \end{pmatrix} + \begin{pmatrix} \frac{1}{L} & 0 \\ 0 & -\frac{1}{J} \\ 0 & 0 \end{pmatrix} * \begin{pmatrix} V \\ T_L \end{pmatrix} \quad (3.18)$$

and

$$\begin{pmatrix} i \\ \omega_r \\ \theta_r \\ T_e \end{pmatrix} = \begin{pmatrix} 1 & 0 & 0 \\ 0 & 1 & 0 \\ 0 & 0 & 1 \\ k_t & 0 & 0 \end{pmatrix} * \begin{pmatrix} i \\ \omega_r \\ \theta_r \end{pmatrix} \quad (3.19)$$

3.5 Torque in BLDC

As the torque and back-EMF generated by a phase winding in a motor is a function of the rotor position and are not likely to exactly work according to the mechanism of the basic laws discussed, but these are good to get the understanding of how torque and back-EMF are generated in motors. As discussed previously that each winding of motor phase consists of a resistive part (R), Inductive part (L) and back-EMF as shown in Figure 3.4. When the current flows in the phase winding as mentioned in the figure, the resistance creates Ohmic losses or heat losses, the inductor creates the magnetic field and stores the energy in it and the back-EMF part absorbs the power representing the power converted to mechanical power represented by the torque times the angular velocity. This power is then converted into mechanical power and results in the torque (T) produced in the motors. For real motors, as there are multiple phase windings, so the total torque generated is the sum of the torque generated by individual windings. Generally torque generated in case of BLDC motors is given by Equation 3.19, where k is called the torque constant of the motor.

$$T(t) = k.i(t) \quad (3.20)$$

The torque generated in case of BLDC and PMSM motors is shown in Figure 3.5. The trapezoidal torque shows the torque generated for BLDC motor and the sinusoidal torque shows the torque generated for PMSM. From Equation 3.20 and Figure 3.5, it is obvious that the torque generated in motors is mainly determined by the shape of the current in phase of the motor. Ideally, the torque generated by the motor should not depend on the position of the rotor to get the linear torque varying with magnitude of the current. But in case of real life, the motors torque varies with the rotor position resulting in the form of torque ripple which causes the rapid change in the motor load when the torque of the motor changes.

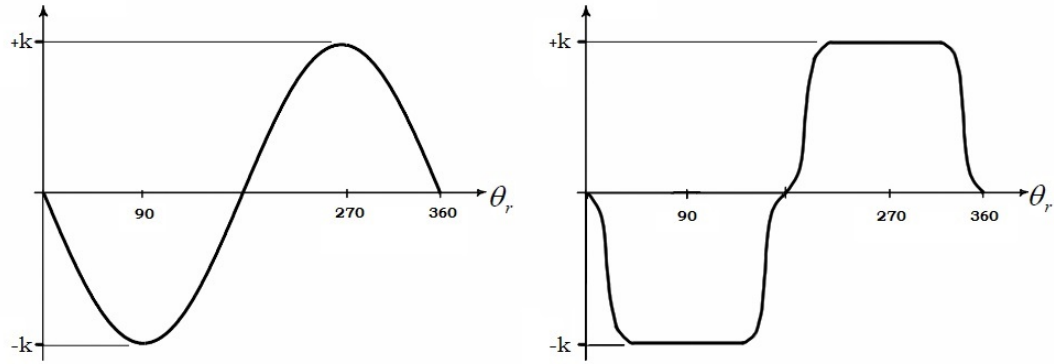


Figure 3.5: Sinusoidal and Trapezoidal torque

3.5.1 Ideal Torque

As discussed earlier the torque generated in case of BLDC motors is trapezoidal in shape and this shape is mainly dependent on the shape of the current. Also the torque produced in ideal case is constant and it is proportional to the amplitude of the current. Generally we can conclude the torque as a product of the phase current amplitude and the torque constant of the motor. Figure 3.6 shows the ideal torque generated for three phases along with the shape of the current of the phases.

3.5.2 Torque Ripple

The ideal torque for BLDC motor as discussed is not actually available in real motors. The main disadvantage of BLDC motors is that the torque produced in these motors is not close to ideal. As shown in the Figure 3.6 the current changes and make transition instantly, but in reality, the transition in the current waveform takes some time. As a result of this delay in transition time, a ripple is produced in torque of BLDC motor. This is known as the "Torque Ripple" or "Commutation Torque Ripple". There can be some other practical reasons in real motors such as magnetic material non-uniformity and the issues in the design of the motor.

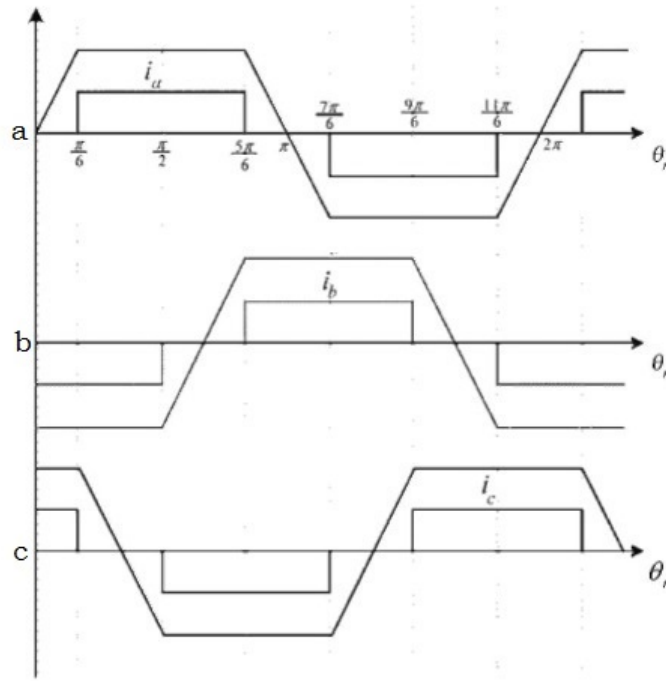


Figure 3.6: Ideal Torque and Current Shape for BLDC motor

This torque ripple reduces the overall efficiency of the motor by generating the noise and vibration in the system. This torque ripple can be reduced by improving the motor design and using the more efficient control mechanism to control the BLDC motor.

3.5.3 Torque and Multiple pole pairs in BLDC Motors

As we have discussed previously, there are two magnetic fields available in BLDC motors i.e. first because of the permanent magnets and the second because of the stator current. In case of BLDC motors the torque is generated only when the poles of the permanent magnets and the stator are equal. If the number of poles of magnets (p) is not equal to the number of the poles created by the current in stator (q), the total torque is equal to zero. The magnetic fields in terms of magnetic poles and stator poles is given by Equation 3.21 and Equation 3.22 respectively.

$$B_s(\theta) = B_s \cos\left(\frac{p}{2}\theta\right) \quad (3.21)$$

$$B_r(\theta) = B_r \cos\left(\frac{q}{2}(\theta - \alpha)\right) \quad (3.22)$$

For the case when $p=q$, the torque is given by Equation 3.23, while the torque is equal to zero when $p \neq q$. See appendix A for details.

$$T = \frac{\pi g r l p B_s B_r}{2\mu_o} \sin\frac{p}{2}\alpha \quad (3.23)$$

3.6 Back-EMF in BLDC

According to the Faraday's law of induction, an EMF is produced in a conductor placed in a magnetic field. Similarly, in case of BLDC motor, as a result of the torque produced in motor, an EMF is induced known as back-EMF. This is called back-EMF because it opposes the torque being generated by the motor. This induced EMF in motors is directly proportional to the magnetic field strength in the motor and its rotor speed. As it is directly proportional to the speed, when the motor is first started, there is no induced EMF and the maximum current flows which results in the maximum motor torque. The back-EMF increases with the speed and the torque produced by the motor is reduced and at the normal operation of the motor, the torque generated by the motor will be reduced as the back-EMF will be at its maximum. Mathematically the back-EMF of the BLDC motor is given by Equation 3.24, where k is the motor constant. For BLDC motors the back-EMF shape is trapezoidal and for PMSM the back-EMF is in sinusoidal shape as shown in Figure 3.7.

$$\varepsilon(\theta_r) = k(\theta_r)\omega(t) \quad (3.24)$$

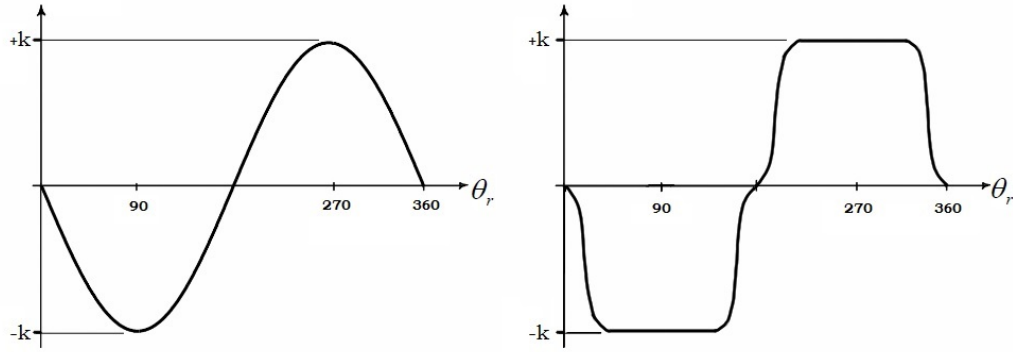


Figure 3.7: Sinusoidal and Trapezoidal Back-EMF of the motor

3.7 General Electro-Mechanical Model

As the main purpose of motors is to convert the electrical energy into mechanical energy. As discussed before, for BLDC motors the electrical energy is first converted into magnetic energy which is then forwarded to mechanical loads connected with BLDC motors. The Figure 3.8 shows the electric, magnetic and mechanical portions associated with BLDC motors. In the figure the inertia of the load is shown as J and the friction is shown as b .

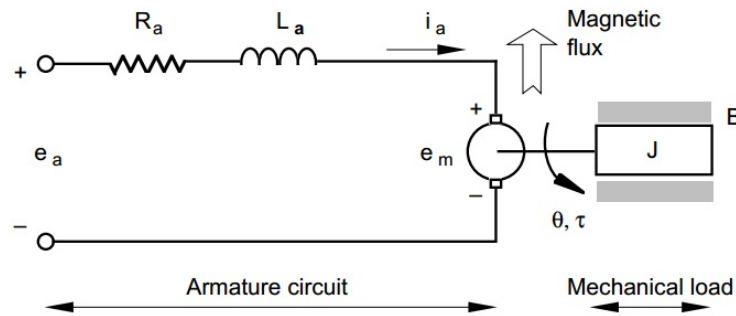


Figure 3.8: Electro-Mechanical model of BLDC motor

The figure above shows the electro-mechanical model of a single phase of BLDC motor. For real motors, we can combine three of these models to show the model of the three phase BLDC motor, which is often called the "phase-variable model". The total torque and back-EMF in case of three phase BLDC motor is the vector sum of the torque and back-EMF of individual phases and can not be investigated unless all the three phases of the motor are considered.

3.8 Summary

In this chapter the basic concepts of electrical and magnetic model of BLDC were discussed. Starting with magnetic model of the motor, we discussed the basic concepts of permeability, flux, MMF for the magnetic materials and then looked into a simple magnetic model and its equivalent electric circuit for BLDC motor. Then we developed the flux relationship and discussed the electric circuit model of one phase winding in motors. With the help of the simplified electric circuit for the one phase winding, state space model was discussed which can be used in MATLAB to define BLDC motor. Once the electric and magnetic models were discussed, we looked into the torque and back-EMF generated and its trapezoidal and sinusoidal shapes. This whole discussion was done with the help of a simplified model for one phase winding, then in the last section of the chapter, the general electro-mechanical model was described and extended to the three phases.

Chapter 4

Measurements and Analysis

4.1 Introduction

This chapter describes the experimental setup of the BLDC motor in lab to collect the required voltage and current data. The BLDC motor discussed here is outer rotor motor with 46 magnets (23 pole-pairs). The magnets are placed with equal spacing on the inner side of the rotor. There are 51 slots on the stator of the motor. The windings and rotor magnets of the motor used are shown in Figure 4.1. As shown in Figure, the BLDC motor has three phase wires coming out and also the hall effect sensing cable. For our case we have not used hall effect sensors to collect the position signals from the motor.

4.2 Inductance measurements

The inductance of the material is its property by which it produces an induced voltage due to the change of the current flowing through itself. The inductance of a material denoted by L is measured in SI units as Henry (H), named in honor of Joseph Henry who discovered it. Typically, the coil of wire in a circuit gives inductance and is known as inductor. The relationship of the inductance to voltage is given as in Equation 4.1.

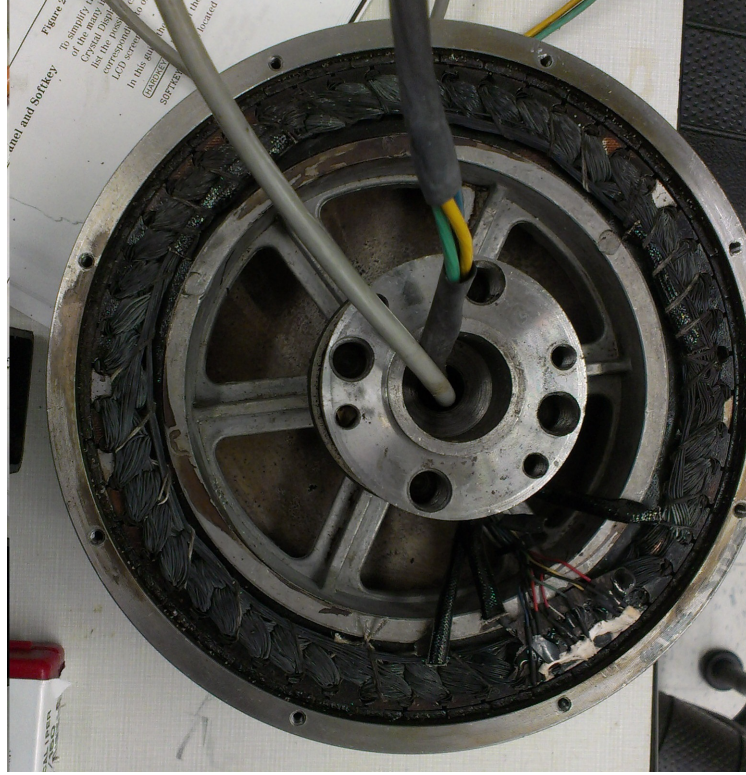


Figure 4.1: BLDC Motor Under testing

$$V(t) = L \frac{di}{dt} \quad (4.1)$$

4.2.1 Variable Inductance

In general all electrical circuits have inductance, which may result beneficial or could also add noise to the circuit. As discussed in previous chapter, for real BLDC motors the inductance is not a constant value and changes with respect to the rotor position. Therefore, the inductance becomes a function of rotor position and can be denoted as $L(\theta_r)$. For a time varying inductance the above equation changes to Equation 4.2.

$$V(t) = L \frac{di}{dt} + i \frac{dL}{dt} \quad (4.2)$$

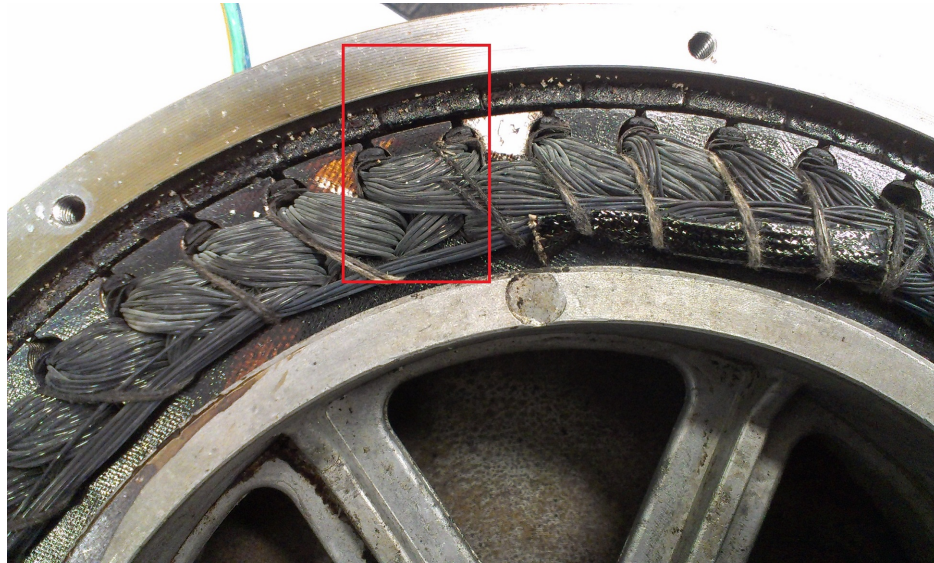


Figure 4.2: Closed look of magnets for motor under testing

4.2.2 Inductance Readings using LCR meter

To measure the variation of our BLDC motor, we used the Agilent 4285A Precision LCR meter and recorded the values of inductances of all three phases. The LCR meter was set to 75 KHz and 1 volt. The circumference of the motor was measured as 700mm, and we divided the circumference in 350 equal parts. Therefore, the inductance was measured for each phase at every 1.0286 degrees and recorded. See appendix B for detailed readings for each phase.

The readings were recorded and plotted in MATLAB which gives us the inductance variation of a phase in one complete revolution. As mentioned previously, the motor under testing had 46 magnets (23 pole-pairs). Therefore, the plot of the inductance variation of each phase gave us 46 peaks in one complete revolution as shown in Figure 4.3. The inductance for phase A was varying between $782 \mu\text{H}$ and $942 \mu\text{H}$ with approximately 18.5 % variation between peak and minimum values.

All three phases showed the same variation of inductance as shown in Figures 4.4 and 4.5. The Figure 4.4 shows the inductance variation of three phases for 0 to 180 degrees and other

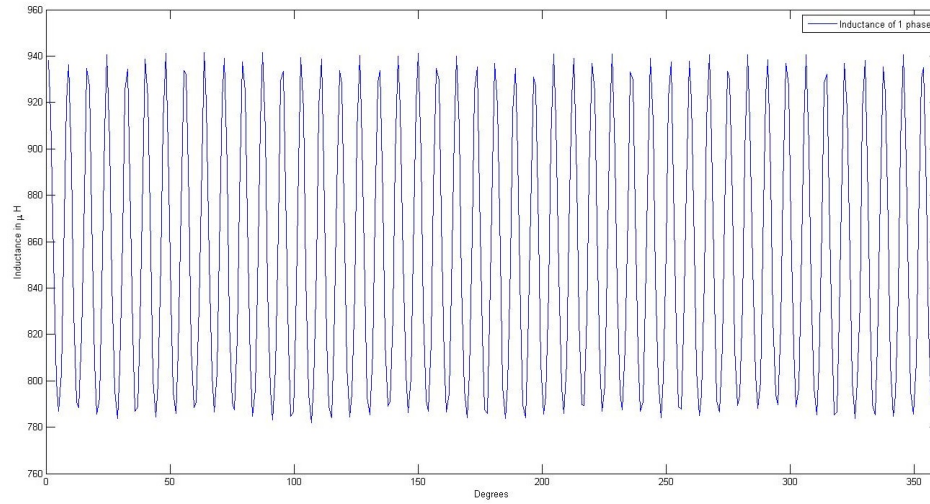


Figure 4.3: Measured Inductance of 1 phase

shows for 0 to 90 degrees.

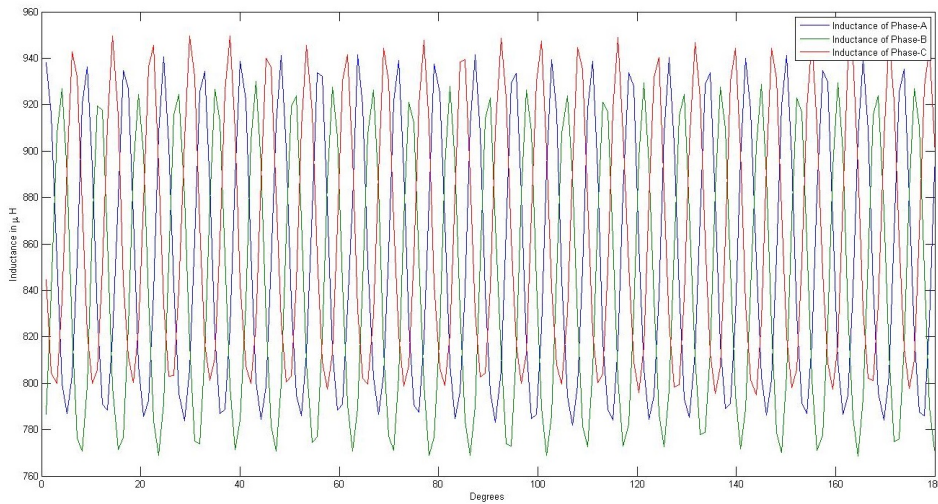


Figure 4.4: Measured Inductance of all three phases

4.3 Voltage measurement

The lab setup for the voltage measurement is shown in Figure 4.6. The 48V/25A power supply was used to run the motor with the help of ASI Bac350 controller. The voltage signals were

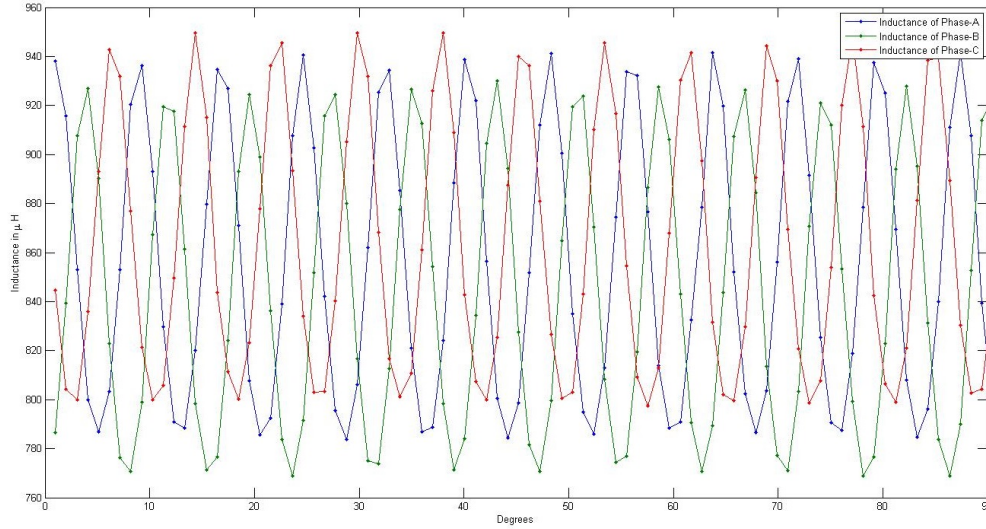


Figure 4.5: Dotted Points Showing reading of all three phases for $0^\circ - 90^\circ$

measured from the phases of the motor, giving the phase to phase voltage.

This phase to phase voltage was fed to a voltage divider to drop the voltage by 6 times as the voltage was varying between $\pm 48\text{V}$. This dropped voltage was then read with the National Instrument data card 6132. The data card has the differential input mode and connected with front end interface using National Instruments board SCB-68. The data card recommended input voltage was ± 10 , that is why we used the voltage divider to drop the voltage 6 times from 48V to 8V . First, we started with Signal express to get the data from the NI card but the signal express lite edition does not gave the required number of samples with higher sampling rate. The MATLAB was then used to collect the data from the motor using NI card.

4.3.1 Measured Voltage

The BAC 350 controller from ASI was used to control the motor. The controller operated as a variable frequency AC power supply without a filtering capacitor on the out put. Instead filtering was provided by the inductance of the motor. Thus the motor was operated as a standard synchronous motor. As the NI card being used had differential input mode, so the

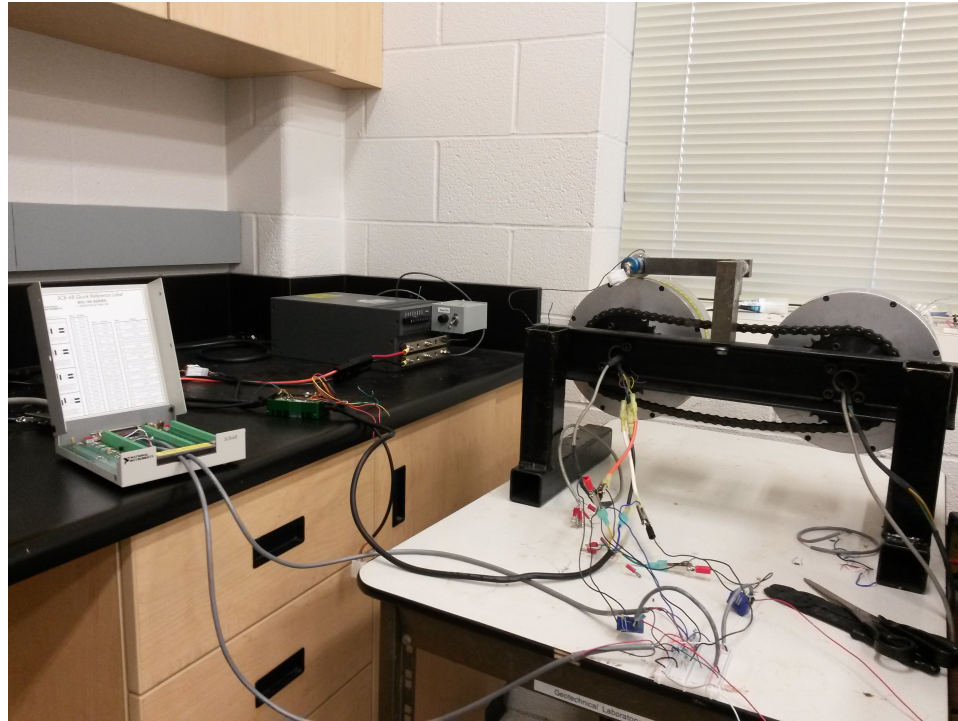


Figure 4.6: Lab setup to measure the Voltage and Current

two phases were connected to the positive and negative terminal of the card to get the motor voltage. The phase to phase voltage of the motor is shown in Figure 4.7.

The voltage signal is ranging between ± 8 volts, as the voltage supplied was dropped by six times. As the NI 6132 card has four input channels so we can read two voltages and two currents simultaneously. We can find the third phase to phase voltage by adding the other two phase to phase voltages. The Figure 4.8 shows the two phase to phase voltages being measured using the data card.

This voltage signal is composed of the pulses generated by PWM signal. The two main components of the PWM signal defines its behavior. The first component is its frequency at which the pulses are being generated, which in our case is 13 KHz. The second component is the duty cycle, which shows the duration in which the signal is high (on). Similarly, our

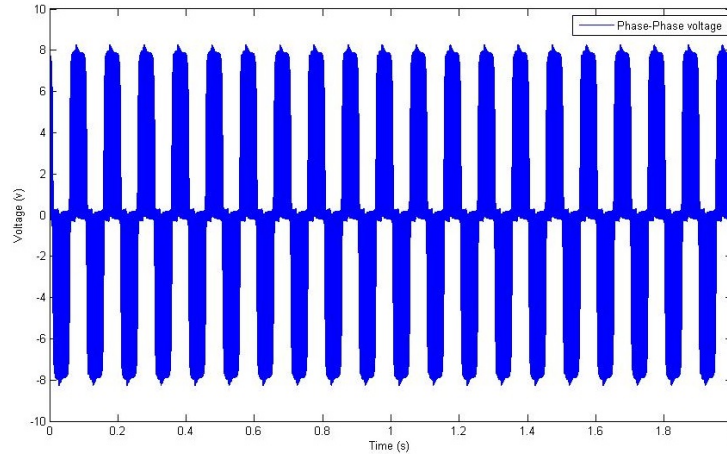


Figure 4.7: 1 Phase to Phase Voltage of Motor

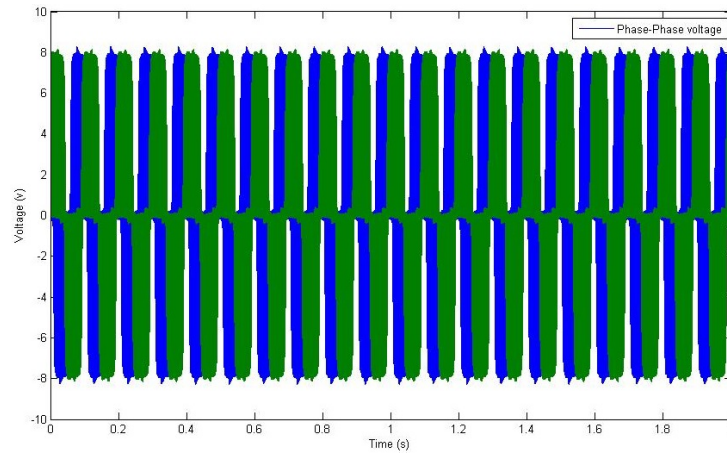


Figure 4.8: Two Phase to Phase Voltages of Motor

voltage signals measured are composed of the PWM signals of 13 KHz and the duty cycle of approximately 18%. The figure 4.9 shows the pulses of PWM in our voltage signal.

4.3.2 Filtered Voltages

The ASI controller (BAC350) used, which supports both sensed and sensorless commutation for BLDC motors, to run the motor from computer works with a Pulse Width Modulation (PWM) of 13 KHz. The voltage signal measured by data card was then filtered to get a sinusoidal waveform for all the three phases of the motor. The second order low pass filter was

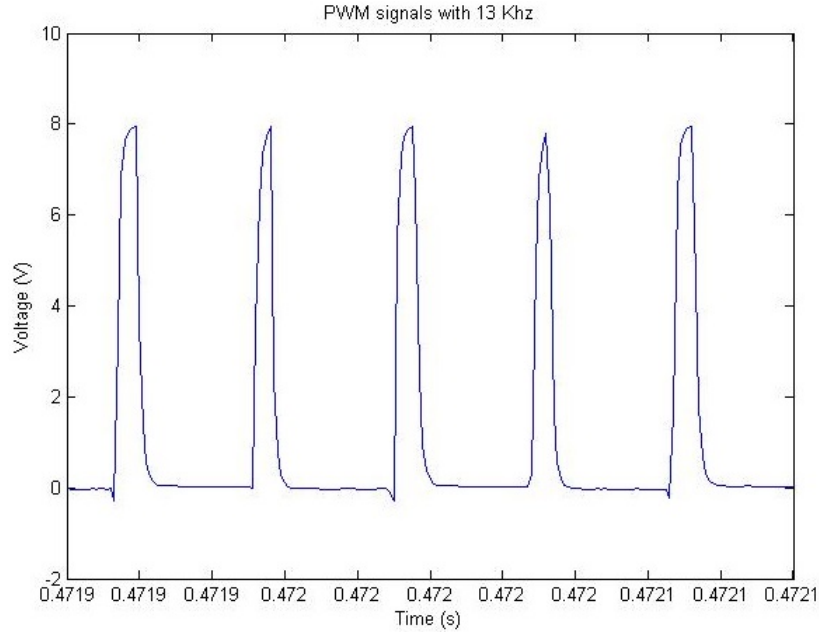


Figure 4.9: Pulses generated by PWM in Voltage signal

used in simulink to filter the voltage signals. The transfer function of the second order low pass filter is given by Equation 4.3.

$$H(s) = \frac{\omega_n^2}{s^2 + 2\omega_n s + \omega_n^2} \quad (4.3)$$

The Figure 4.10 shows the first half of the filtered voltages using the above mentioned filter with ω_n is 8 KHz for our case, as we wanted to remove the PWM frequency to see the voltage in motor phases.

4.4 Current measurement

To measure the current in the motor phases, we started with introducing a shunt resistance in series with one of the motor phase and measured the voltage drop across the shunt to find the current passing through that phase. We tried this experiment with different shunt resistances, but the inductive voltage drop across the shunts always dominated the measurements.

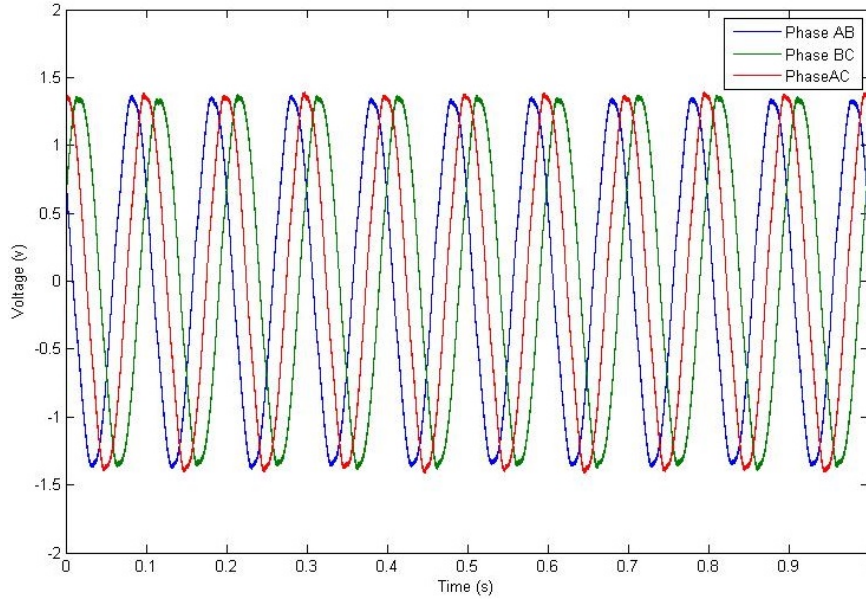


Figure 4.10: Filtered Voltages

4.4.1 Hall-Effect based Current Sensor Readings

Because of the issues discussed above with using shunt resistances for measuring current in phases, we decided to go with Hall-Effect based current sensors to measure the current of the motor. These current sensors were introduced in two of the phases as we used two channels of our data card for voltages. The current sensors from LEM (CASR-6np) were configured for three primary turns, tripling the resolution of the sensor. The sensors gave the output as V_{out} which is then used to find the amplitude of current by Equation 4.4. The current sensors need 5V input power to operate and the output of the current sensors have a nominal zero value at 2.5V. This offset was subtracted from the output collected and the current waveforms found after subtracting the offset are shown in Figure 4.11.

$$\text{voltage swing (Vs)} = \text{primary current (Ip)} * \text{gain (Gth)} \quad (4.4)$$

For $V_{swing} = 1.542$ V, the current I_p is calculated as:

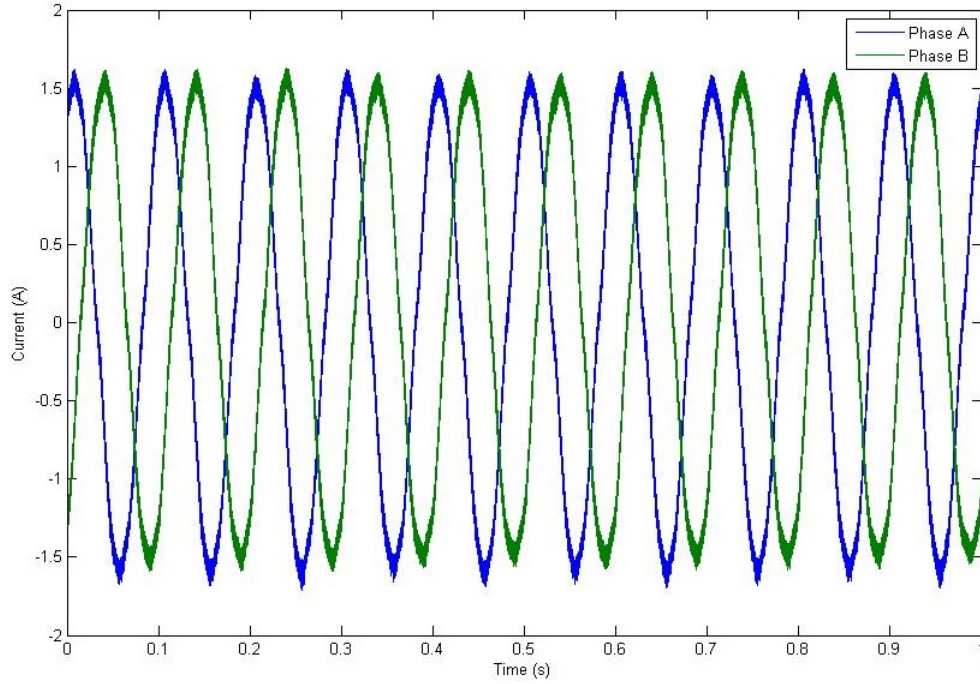


Figure 4.11: Two Phase Currents

$$I_p = (V_{swing}/G_{th}) * I_{pn}(for 3 - turns) \quad (4.5)$$

$$I_p = (1.542V/625mV/A) * 2A = (2.4672)(2A) = 4.9344A_{peak} \quad (4.6)$$

Figure 4.11 shows the current of two phases for half rotation of the motor. The current signal in Figure 4.11 shows the V_{out} of the current sensor, which corresponds to the 4.9344 A peak current as calculated above.

4.4.2 Filtered Current

The current measured using hall effect based current sensors were noisy. The current signals were filtered using FFT approach and filtering out the bin of the noise frequency to reduce the noise in the required data. The signals were transformed to the frequency domain us-

ing MATLAB and we found that the most of the noise in the decay waveform of current signal after each PWM on pulse was approximately at 430 KHz. After removing the noise in frequency domain the current signals were again transformed back to time domain for our further analysis. The Fig 4.12 shows the current decay with noise and after reducing the noise in frequency domain.

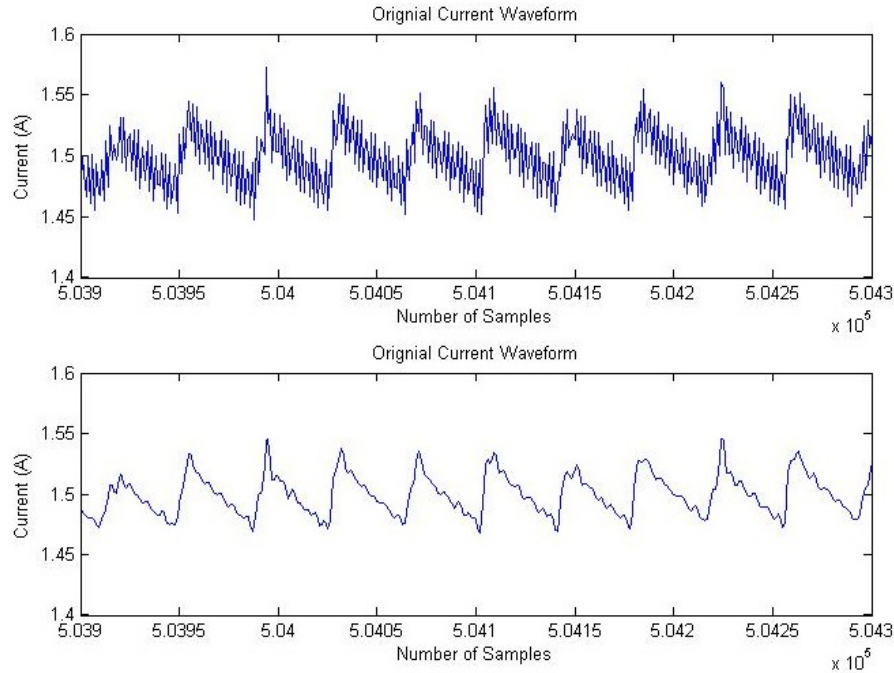


Figure 4.12: Noise in Current and its Filtered wave

4.5 Inductance from Voltage and Current Signals

To calculate different parameters in three phase circuits, we have two basic configurations to deal with. The first one is Wye configuration and the second is Delta configuration. For balance circuits we can transform easily from one configuration to the other. The acquired data was divided in two sets i.e. one where the external voltage was present and the second with no external voltage present. Figure 4.13 shows the data set where the external voltage was present. The solid lines shows the voltage AB and dotted lines shows the voltage BC for

first five indices. Similarly Figure 4.14 shows the dataset with no external voltage present. The solid lines shows the voltage AB and dotted lines shows the voltage BC for the same indices.

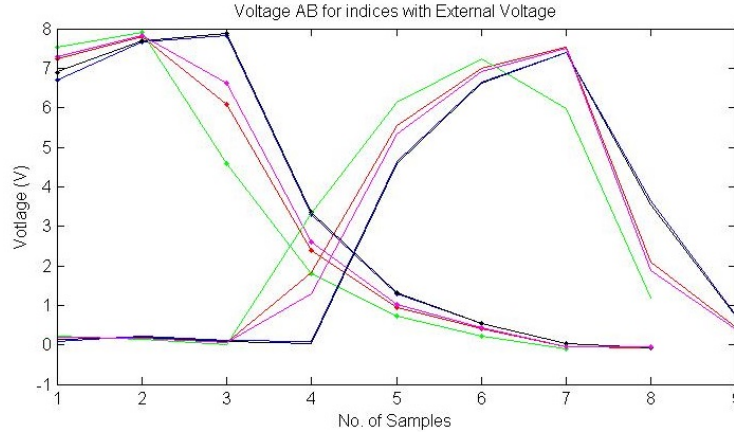


Figure 4.13: Raw Voltage data with External Voltage Present

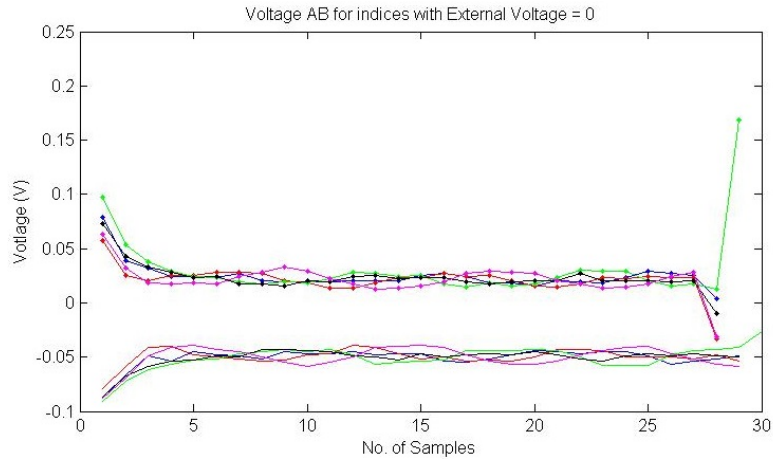


Figure 4.14: Raw Voltage data with no External Voltage

4.5.1 Wye-Configuration

Once we filtered our data, we started to work out the inductance and resistance information from the voltage and current signals. As the data measured is the phase voltages and line

currents. Taking Wye configuration to start with and assuming that the neutral point in Wye configuration as zero (0). The Wye model for our setup is shown in Figure 4.15. The data was divided in two different sets, one including the data of the indices where the voltage was present and the second having the data when there was no voltage present. The general Ohmic relation for one phase of the motor is given by Equation 4.7.

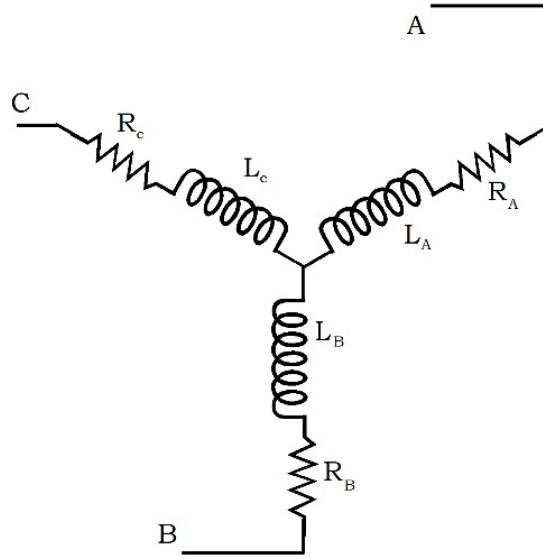


Figure 4.15: Wye model for our setup

$$V = IR + L \frac{dI}{dt} \quad (4.7)$$

For the case where we consider the neutral voltage is equal to zero, during the portion of the PWM cycle where the external voltage is zero, the above equation becomes equal to zero resulting in a ratio of inductance to resistance as give by Equation 4.9.

$$IR + L \frac{dI}{dt} = 0 \quad (4.8)$$

$$\frac{L}{R} = - \frac{I}{dI/dt} \quad (4.9)$$

Least squares degree one polynomial fit was applied to the acquired current data in order to get the mean values and the slopes of the current to find the L/R relation. Assuming resistance (R) as a constant and the ratio of inductance and resistance will give us the waveform of the inductance. Using Polynomial fitting, the mean current values and slope of the current for dataset where no external voltage is present is shown in Figure 4.16. The plot is scaled to show both mean values of current and slopes in one figure.

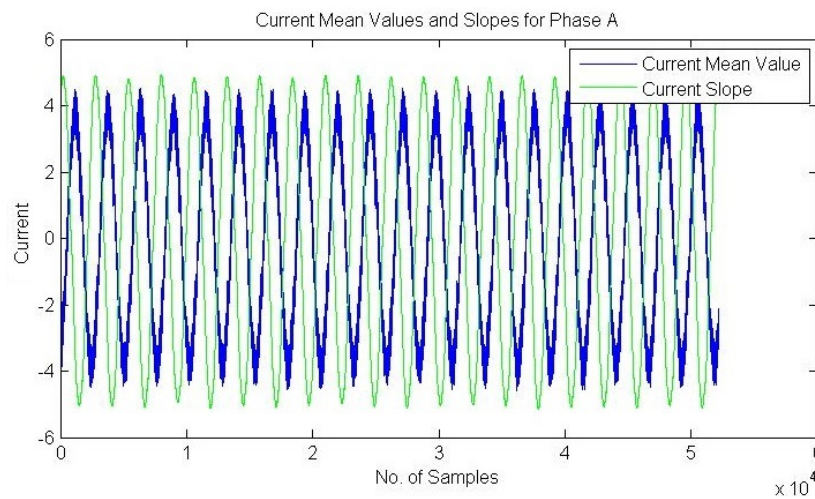


Figure 4.16: Current Mean Values and Slopes with no Voltage

The ratio of the inductance and resistance calculated using this approach shows the plot of a tan function. The Figure 4.17 shows the plot of the ratio of inductance and resistance when there is no voltage present.

4.5.1.1 Conclusion

The Figure 4.17 shows the ratio of the inductance and resistance resembles the function of tangent. Working on this result we can look into the atan function for slope and mean values to get the ratio of inductance and resistance, which can give us the position of the motor but at this point we can not infer the position of rotor from L/R ratio as we need more experiments

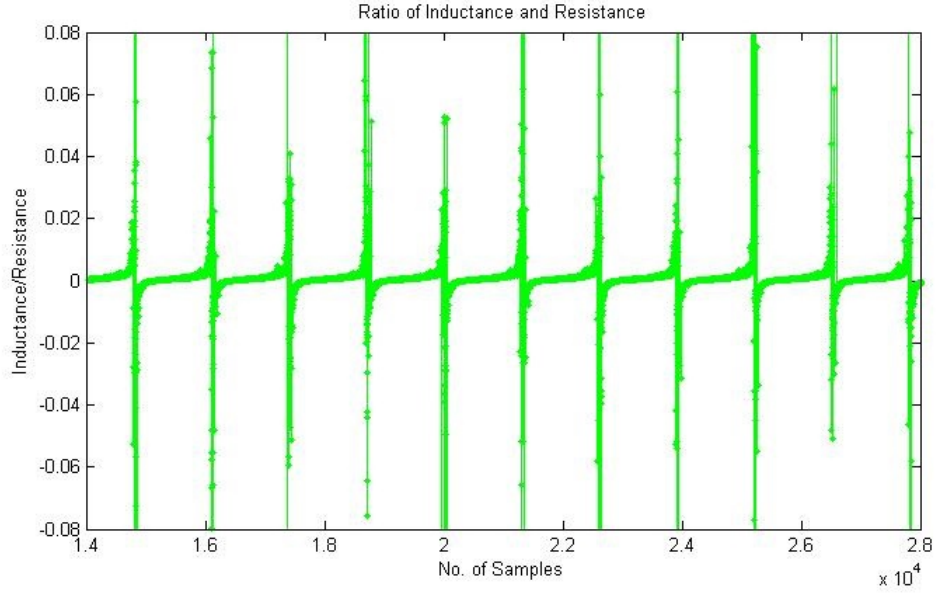


Figure 4.17: Ratio of Inductance and Resistance when no Voltage present

for the motor with varying speed to verify this.

4.5.1.2 Wye Configuration With with back-EMF

In the previous section we considered the indices with no voltage present and no back-EMF, which simplified the equation and resulted in ratio of inductance and resistance as given by Equation 4.13. If we include the back-EMF into account as well, then the voltage relation for indices with no input voltage present is given by Equation 4.10. Similarly if we look the voltage relation of one phase of motor with back-EMF and input voltage present, it is given by Equation 4.11. In these equations, ϵ shows the back-emf generated in motor phase. We cannot use this one equation to find the ratio of inductance to resistance as we have three unknowns present in this equation.

$$0 = I.R + L \frac{di}{dt} - \epsilon \quad (4.10)$$

$$V = I.R + L \frac{di}{dt} - \epsilon \quad (4.11)$$

4.5.2 Delta Configuration

4.5.2.1 Frequency Domain Analysis

For further analysis on calculation of inductance from the voltage and current signals, the data measured was transformed into frequency domain. The Fast Fourier Transform (FFT) is an approach to transform the data from time domain to frequency domain and vice versa. The whole data was divided in windows having twelve PWM pulses and then Fast Fourier Transform was applied on all the windows of data. The FFT transform works by decomposing the data sequence into different frequencies. Figures 4.18 and 4.19 shows the current of two phases in time domain with its transform in the frequency domain.

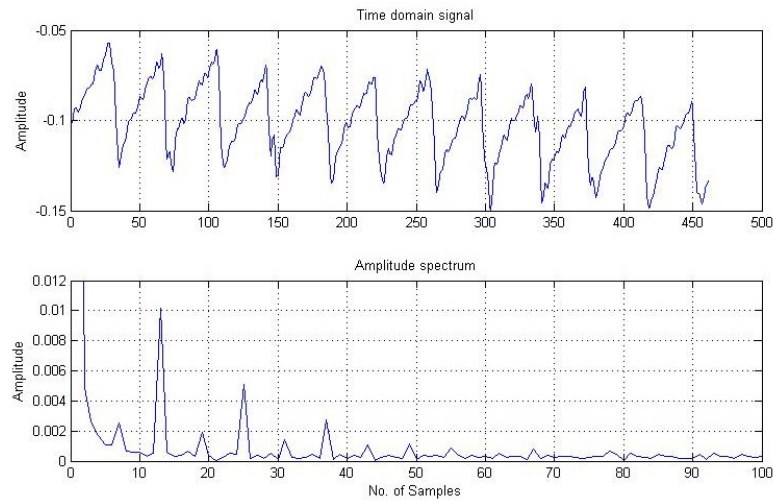


Figure 4.18: FFT of window for Current of Phase A

The frequency domain shows that there are three major harmonics available in current data. These harmonics are occurring at multiples of 13 KHz, which is our PWM switching frequency. Similarly the voltage signal was divided into same window length and transformed to frequency domain. The Figures 4.20 and 4.21 shows the voltage of the window selected and its transformed signal in frequency domain.

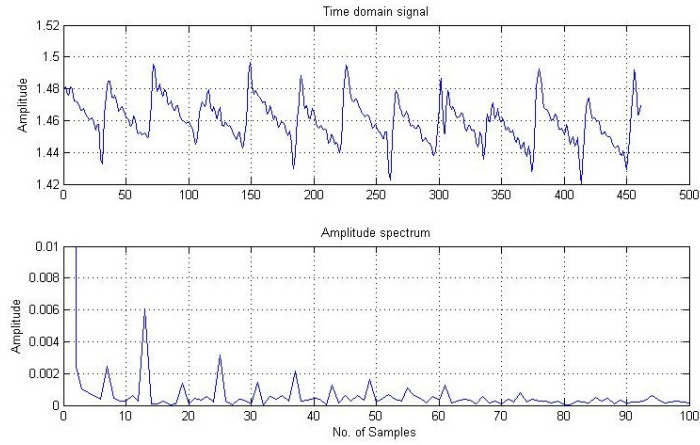


Figure 4.19: FFT of window for Current of Phase B

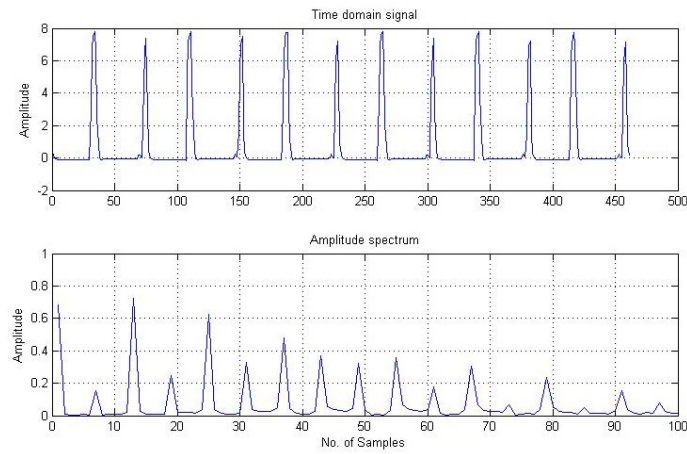


Figure 4.20: FFT of a window for Phase AB Voltage

4.5.2.2 Delta Model For Inductance Information

Once the data was transformed to frequency domain, the voltage and current analysis were applied using the Delta configuration of the motor. The amplitude and the angles of the first five harmonics were picked from frequency domain. These five harmonics were then used in three phase delta model. Figure 4.22 shows the delta model for only resistive case. The voltage equations for delta configuration are given by Equation 4.12 and Equation 4.13.

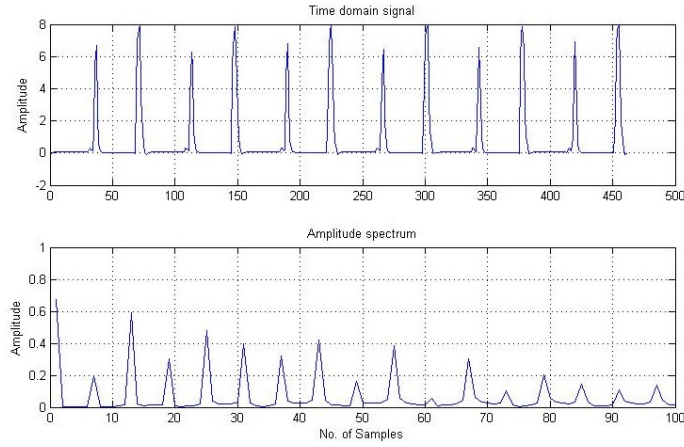


Figure 4.21: FFT of a window for Phase BC Voltage

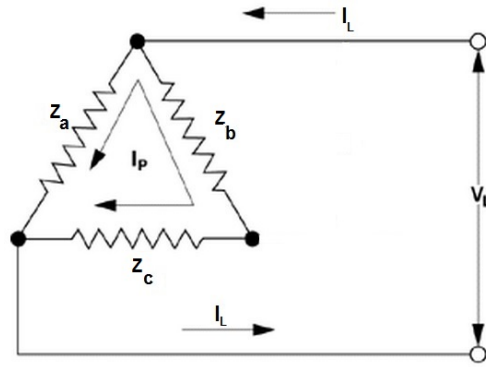


Figure 4.22: Delta Configuration for Pure Resistive case

$$V_{AB} = (R_A + j\omega L_A).I_A - (R_B + j\omega L_B).I_B \quad (4.12)$$

$$V_{BC} = (R_B + j\omega L_B).I_B - (R_C + j\omega L_C).I_C \quad (4.13)$$

Replacing ω with the values of frequencies for first five harmonics in Equation 4.12 and 4.13 gave us ten equations in total with six unknowns. These were solved in a least squares sense for all six unknowns.

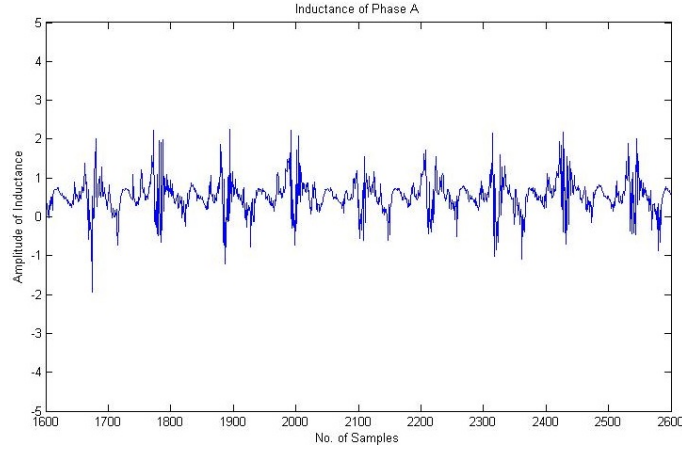


Figure 4.23: Inductance Variation for Phase A

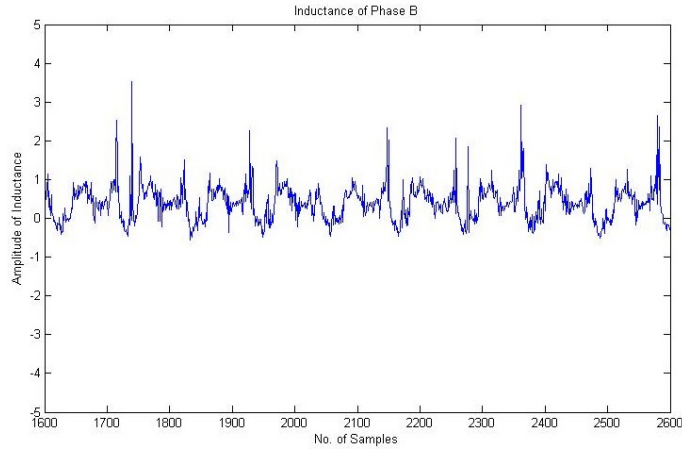


Figure 4.24: Inductance Variation for Phase B

Using all the equations generated by first five harmonics and solving it gave result in inductances and resistances for all the three phases. This approach was applied for all the FFT windows which were generated by dividing the whole data set. Therefore, the three inductances (L_A , L_B and L_C) and three resistances (R_A , R_B and R_C) were calculated for each window. Figures 4.23, 4.24 and 4.25 shows the inductance of phase A, Phase B and Phase C. Similarly the resistances calculated are shown in Figure 4.26 , 4.27 and 4.28.

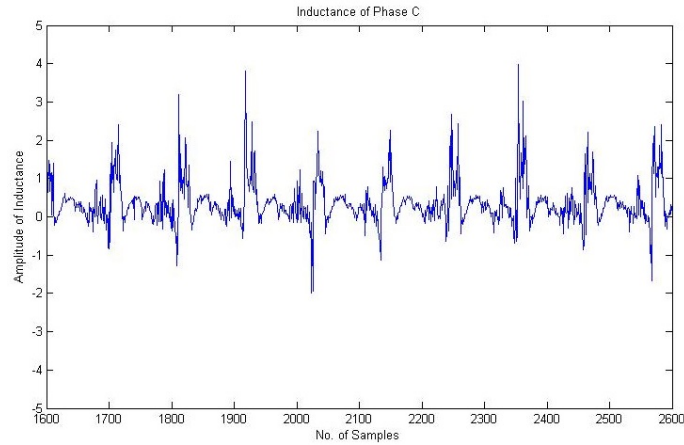


Figure 4.25: Inductance Variation for Phase C

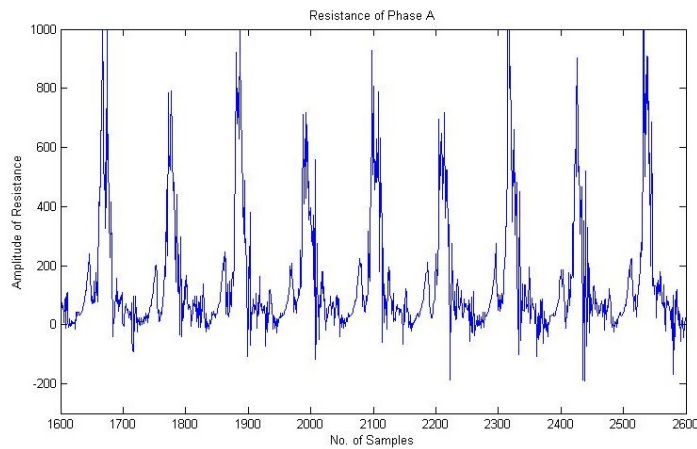


Figure 4.26: Resistance Variation for Phase A

4.5.2.3 Conclusion

The delta configuration model for motor was used to generate the inductance and resistance for each phase using the data obtained from frequency domain. The figures for inductances for each phase shows much noisy signals. Similarly for the resistances calculated, the Figures 4.26, 4.27 and 4.28 shows the noise in resistances for each phase as well. From these results we can not infer the position of the motor because of so much noise in them and also these plots for inductance does not show any traces of inductance variation at different frequencies.

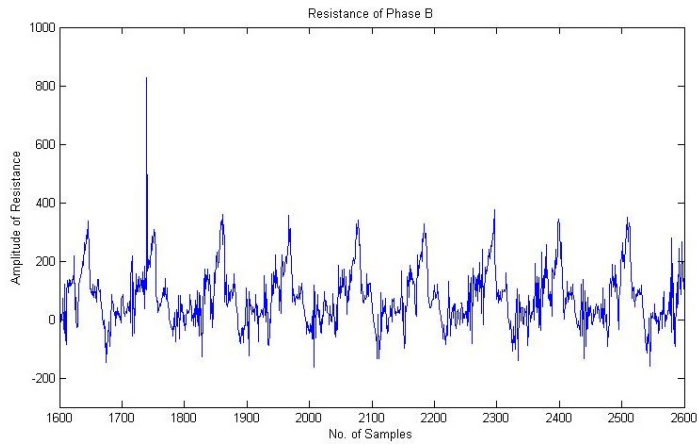


Figure 4.27: Resistance Variation for Phase B

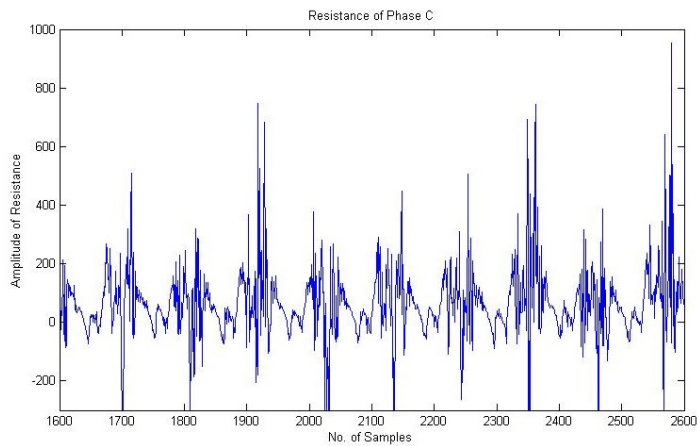


Figure 4.28: Resistance Variation for Phase C

The simple model of the motor as an inductance in series with a resistor is almost certainly wrong. Standard simple models of motor usually incorporate a model composed of a resistor (representing copper or conductive losses) in series with a parallel combination of inductor and resistor (representing eddy and hysteresis losses.) Proper modeling of the true frequency dependent nature of the load should be performed and these calculations should be repeated.

4.6 Electrical Time constant Analysis

At this point, after looking at both Delta and Wye models, we can not yet infer the position of the rotor from voltage and current signals. To verify whether the electrical signals do contains the information about the motor position, we decided to do the step response test for the motor at both the measured minimum and maximum inductance points. This response of the current can be characterized by the electrical time constant (τ). Physically, the time constant is the amount of time taken to reach the 63.2 % of the final steady state value from its starting point.

$$\text{For RC circuits } \tau = RC \text{ (Ohms X Farads)} \quad (4.14)$$

$$\text{For RL circuits } \tau = L/R \text{ (Henry/Ohms)} \quad (4.15)$$

The physcial value of time constant taken as 63.2 % comes from the Euler's constant. Mathematically, the value of 63.2% for first time constant is given in Equation 4.17. After five time constants the value reaches to 99.5 % from its initial value which is considered as the final steady state value.

$$\left(1 - \frac{1}{e}\right) .100 \% = 63.212\% \quad (4.16)$$

4.6.1 BLDC motor Analysis

For BLDC motors, the resistance of the phases are constant and hence the change in electrical time constant will be due to the change in inductance only. We made a frame for the motor front side so that the motor does not rotate when the voltage is applied to the motor. The setup to freeze the motor was for two different positions, first where the inductance of the phases is at maximum and second, where the inductance of the phases is at minimum. The lab setup is shown in Figure 4.29.

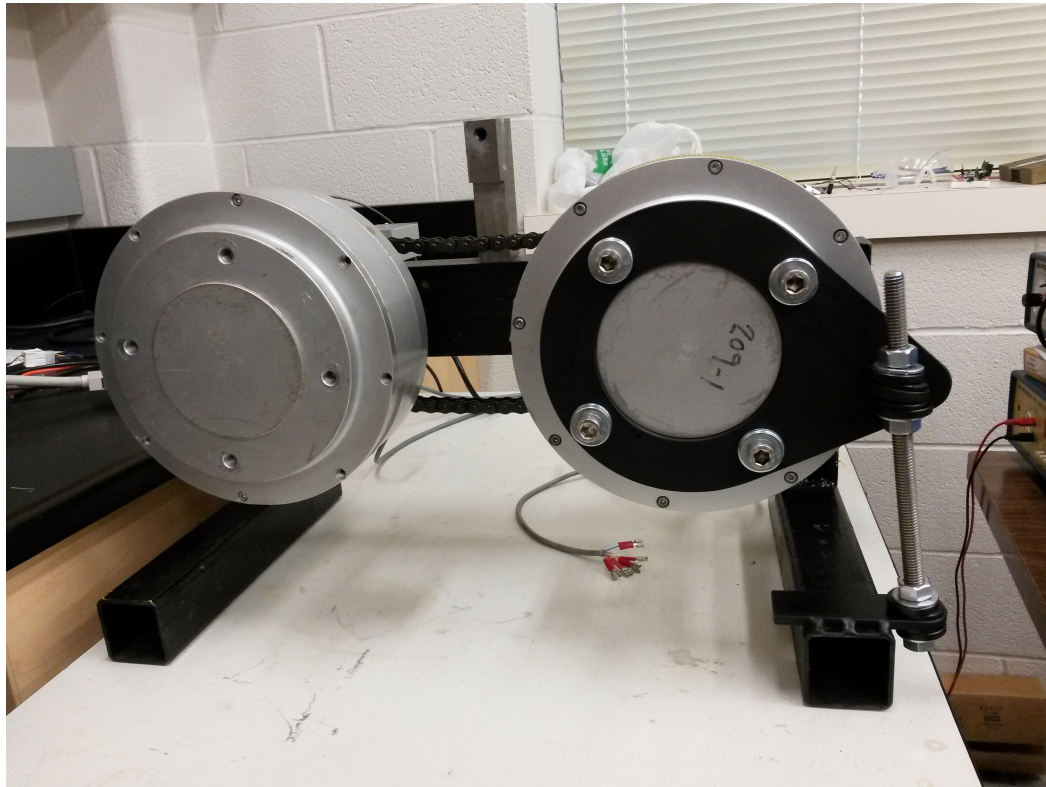


Figure 4.29: Lab Setup for Step Input Response

4.6.1.1 At Maximum Inductance

The motor was froze at a point where the inductance of phase A-B was at its maximum. The voltage was applied to motor for short interval of one second and the data was collected in MATLAB for currents and voltages of the phases.

4.6.1.2 At Minimum Inductance

Similarly, after collecting the data for the position where the motor inductance was at maximum, the motor was froze at the point where the inductance of phase A-B was minimum. Again same voltage was applied for one second and the data was collected.

4.6.1.3 Comparison of Voltages and Currents at two positions

To compare the data acquired from both tests, it is really important to verify that the input voltage provided for both tests is same. Figure 4.30 shows the input voltage for both tests. The dotted lines shows the two phase to phase input voltages AB and BC when the motor was froze at the point where inductance is minimum. Similarly, the solid red and magenta lines shows the two phase to phase voltages AB and BC when the motor was froze at point where the inductance was maximum.

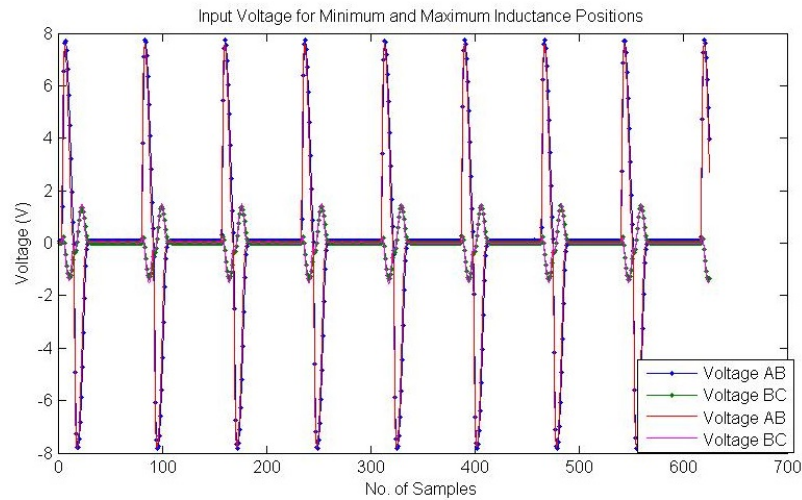


Figure 4.30: 2 Phase to Phase Voltages for Both Tests

Similarly, Figures 4.31 and 4.32 shows the two current responses for both tests. The dotted lines shows the response of two phase currents where the inductance was minimum and the solid lines shows the response of same phase currents where the inductance was minimum.

The acquired data for currents were noisy and we took the average of eight periods to reduce the noise. As given in Equation 4.17, the time constant depends on the value of resistance and inductance for RL circuits. Comparing the two datasets, we can see that the change in the current for all the phases are different for two positions as shown in Figures 4.33, 4.34 and 4.35. The difference in the rise in current for two positions with constant resistance and

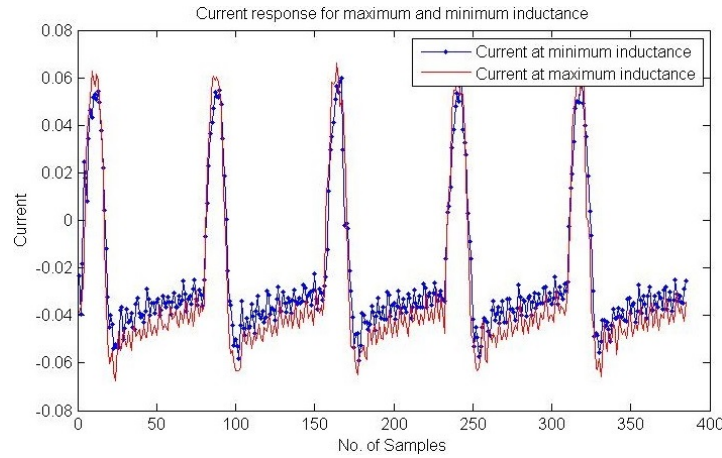


Figure 4.31: Current A Response for Both Tests

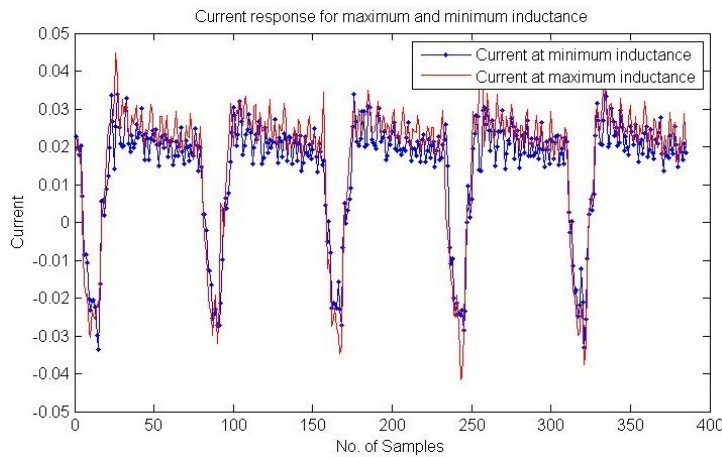


Figure 4.32: Current B Responses for Both Tests

same input voltage shows that the step response is different for currents at two different positions.

By looking the Figures 4.33, 4.34 and 4.35, we can conclude that the current behavior is different for two different positions i.e. the position with maximum inductance and the position with minimum inductance. With the help of these result we can conclude that the currents and voltages data collected for two different positions shows that the Inductance is different at these positions and ultimately we should be able to find the inductance of the

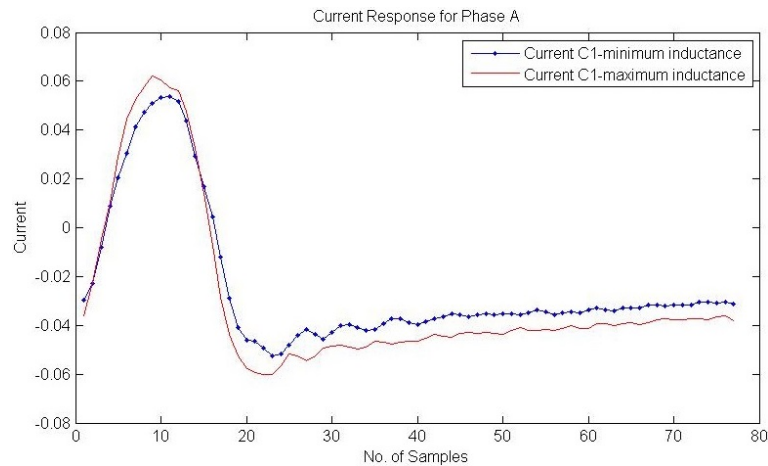


Figure 4.33: Comparison of Phase A Current

motor with the help of internal voltage and current signals.

4.7 Summary

This chapter covered the experiments performed to measure the required parameters for the BLDC motor used in lab. Starting with the variable inductance measurements which were taken by the 4285A LCR meter with no load and no power. These inductance values were taken by manually moving the motor by hands with much care. The voltage and current signals from the motor were collected using National Instrument data card 6132, when motor was running with Bac 350 controller. The data card (NI 6132) just have the differential input mode so the phase voltages were collected by connecting the data cards positive and negative wires with two phases of the motor. Hall effect based current sensor (CASR-6np) from LEM was connected in series with two phases to get the current measurement. Once we collected the required data, analysis was done both in time domain and frequency domain, on the data using MATLAB to see the current and inductance variation in complete revolution of the motor. In the last section of the chapter we discussed the step response of the motor at two different positions to verify whether or not the change in inductance comes up in the voltage and current signals of the motor.

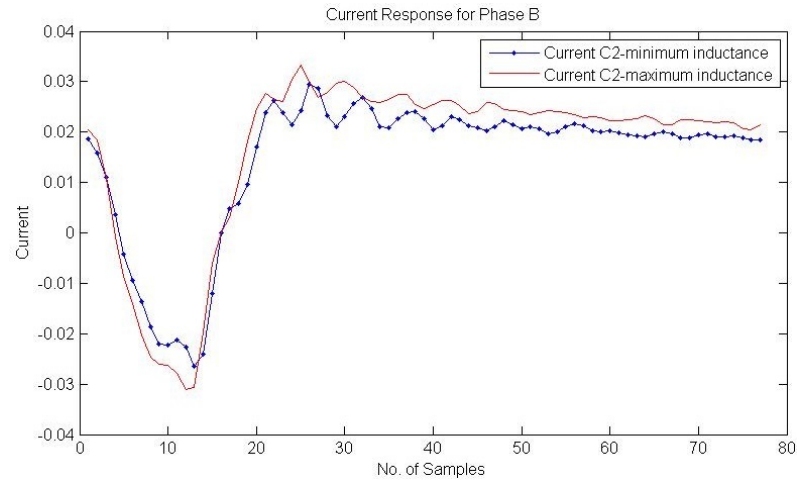


Figure 4.34: Comparison of Phase B Current

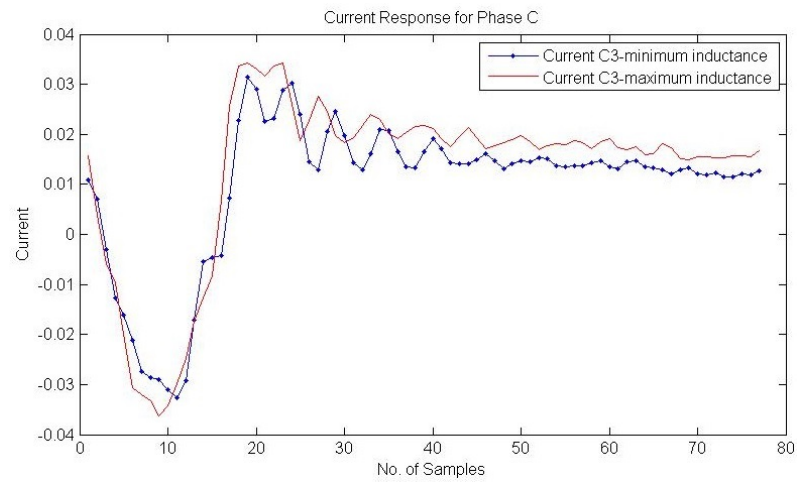


Figure 4.35: Comparison of Phase C Current

Chapter 5

Conclusion

5.1 Summary

In this thesis, a sensorless control approach for BLDC motor was investigated. The main purpose of the thesis was to look for an approach to control the BLDC motor for full range of speed. The proposed approach base on the identification of the rotor position in BLDC motors using the voltage and currents signals present in the motor and finding out the inductance of each of the phase to relate that with position of the rotor. The thesis was divided in two main parts. First part was covering the literature review and simple BLDC motor model. This first part discussed both sensed and sensorless approaches recently being used in industry. The second part covered experimental analysis for the sensorless approach proposed to control the BLDC motor.

At this point, it is still not possible to infer the rotor position from the voltage and current measurements. The voltage and current signals measured were used to find the inductance of the phases of motors considering both delta and wye configuration. Starting with wye configuration, we assumed that the neutral point in Wye setup is at zero voltage. The current and voltage data was divided in two sets, one set having all the portions of the data where the voltage was high(on) and the other set having all the portions where all the voltage were

low(off). For wye configuration we took the set where the voltage was low(off) and used the general equation of the phase model with zero voltage. Assuming the resistance to be constant and re-arranging the Equation 4.11 gave us the ratio of the inductance and resistance. Finding this ratio and analyzing the plots showed that the ratio calculated has a very high amplitude of noise and also not in fact proportional to the inductance, and thus could not be used to directly infer the position.

With no good results in Wye configuration, we considered the delta model for inferring the inductance. In case of delta model, we used the phase voltage and currents measured directly from the motor and transformed them to frequency domain to work on the harmonics as well. As explained in Chapter 4, we divided the whole data set in windows covering exactly twelve pulse width periods. FFT was applied on all of these windows to get the frequency components of both voltage and current signals. Equation 4.16 was used to develop the delta model for first five harmonics. Using both real and imaginary parts from the FFT, and solved them in MATLAB for each phase inductance(I_A , I_B and I_C) and resistance (R_A , R_B and R_C). The inductance calculated for each phase shows extremely noisy signals.

After working on both delta and Wye analysis the results showed no success for rotor position identification, and to verify whether the variation in inductance can be inferred from the voltage and current signals of the motor, the step response of the motor was performed. For this a front frame for motor was designed to freeze the motor at two different positions i.e. first where the inductance is maximum and the second where the inductance was at minimum. This frame as shown in Figure 4.29 gave the freedom of freezing the motor for different position within almost ten degrees, so that at least one point where the inductance was maximum and one point where the inductance was minimum should be available to select. The motor was applied with the same external input voltage for both tests and the data was collected in MATLAB for analysis. As in case of inductors, with applied input voltage the current does not raise to its maximum value instantly. This characteristic is often

expressed in terms of electrical time constant and is equal to the product of resistance in ohms and inductance in henry. As the resistance is constant for both tests, any difference between the current response of two tests is only dependent on the change in the inductance. The comparison between the two tests in Figures 4.33, 4.34 and 4.35 shows that the response of the current is different for both tests, indicating the inductances for two positions are different. This means that the voltage and current signals from the motor does have the information about the variation in inductance and inductance of each phase can be calculated using the voltage and current signals of the motor but the per phase basic impedance model used is not valid and both delta and Wye configurations does not show any good results for variation in inductance. Therefore, a new model should be selected for motor losses and the analysis need to be performed again with new model for inductance information.

5.2 Problems Faced

As mentioned in Chapter 4, the data card available in lab to collect the measurement has 4 input differential channels. Therefore, it was not possible to get all three phase to phase voltages and line currents simultaneously. So we measured two phase to phase voltages and two line currents, from which we calculated the third phase to phase voltage and current.

The other main issue was measuring the line currents by introducing the shunt resistance. We tried different shunt resistances but inductive voltage drop across shunts always dominated the measurements. Therefore we decided to use the hall effect based current sensors to measure the line current.

5.3 Future Work

Some of the suggestions for the future work related to this thesis are:

- If the inductance was a constant, then from Equation 4.2, we would get $L/R = \text{constant}$

as given in Equation 5.1. As discussed in section 4.5.1.1 the ratio actually appeared as a tan function implying that the inductance (L) is clearly not constant. In fact when L is not constant equation 5.1 should be replaced by Equation 5.2. We believe that we can show that when I and L are sinusoids, this will produce a ratio that appears of the form of a tan (theta) where theta represents the electrical angle. Thus the inverse tan of some scaled and shifted function of this ratio should give us rotor angle.

$$-\frac{I}{dI/dt} = L/R = \text{constant} \quad (5.1)$$

$$L \frac{dI}{dt} + I \frac{dL}{dt} + IR = 0 \quad (5.2)$$

The inverse tan of the ratio of slop and mean values of current for all the four quadrants is shown in Figure 5.1. This plot may give us the position of the motor, but for that it needs to be verified theoretically and experimentally for varying speed of the motor.

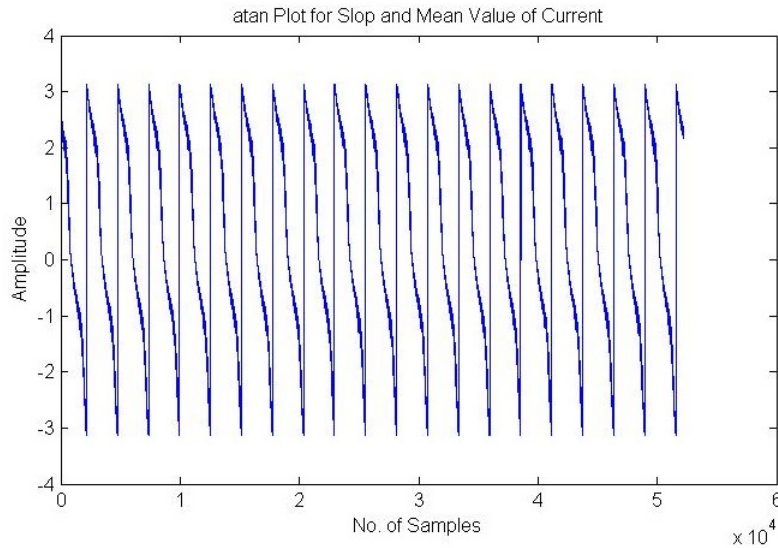


Figure 5.1: tan Inverse of Slop and Mean values of Current

- A new per phase electrical model is required for modeling the impedance of the motor phase instead of modeling it with only a resistor in series with an inductor.

- Testing the same approach for other available motors in market with different number of pole pairs to verify the inductance variation.
- New motor design is also one of the alternate solutions for BLDC sensorless operations. As the BLDC motor design is not standardized till date, a new design is desirable for BLDC motors to get the maximum efficiency and reduces the overall cost of BLDC motor system.

Bibliography

- [1] T. Jahns, “Motion control with permanent magnet AC machines,” *Proceedings of the IEEE*, vol. 82, pp. 1241–1252, August 1994.
- [2] T. J. E. Miller, *Switched Reluctance Motors and their Control*. Magna Physics Publishing and Oxford University Press, Hillsboro, OH and New York, 1993.
- [3] N. F. W.R. Ray. P.J. Lawrenson, RM. Davis. LM. Stephenson and R. Blake, “High performance switched reluctance brushless drives,” *IEEE IAS Annual Meeting Conference Record*, pp. 1769–1985, 1985.
- [4] R. D. W. Ray and R. Bkke, “Inverter drive for switched reluctance motor: Circuits and component ratings,” *IEEE Proceedings*, vol. 128, pp. 126–136, March 1981.
- [5] M. K. J.F. Gieras, R-J Wang, ed., *Axial Flux Permanent Magnet Brushless Machines*. Boston:Kluwer, 2004.
- [6] <http://www.nmbtc.com/brushless-dc-motors/engineering/BLDC-motor-rotor-design.jpg>.
- [7] D. Hanselman, ed., *Brushless Permanent Magnet Motor Design*. Ohio:Magna Physics Publishing, 2006.
- [8] <http://m.eet.com/media/1178412/bldcfg3.jpgg>.
- [9] <http://www.edn.com/design/sensors/4406682/Brushless-DC-Motors---Part-I--Construction-and-Operating-Principles>.

- [10] J. M. M.R. Harris, J.W. Finch and T. Miller, "A review of the integral horsepower switched reluctance drive," *IEEE Transactions on Industry Applications*, vol. 22, pp. 716–721, July/August 1986.
- [11] C. V. M. Lajoie-Mazenc and J. Hector, "Study and implementation of a hysteresis controlled inverter on a permanent magnet motor," *IEEE Transactions on Industry Applications*, vol. 2, March/April 1985.
- [12] R. Krishnan and A. J. Beutler, "Performance and design of an axial field permanent magnet synchronous motor servo drive," *Proceedings of IEEE IAS Annual Meeting*, pp. 630–640, 1985.
- [13] H. K. M. E. T. M. K. Iizuka, K. Uzuhashi, "Microcomputer control for sensorless brushless motor," *IEEE Transactions*, vol. 21, pp. 595–601, April 1985.
- [14] S. J. Nadolski R., Gawcki Z. and L. K., "Gearless drive of light electric vehicles on the example of the bicycle driven with brushless dc motor with threephase winding," *4th International Workshop on Research and Education in Mechatronics*, October 2003.
- [15] http://en.wikipedia.org/wiki/Amp%C3%A8re's_circuital_law.
- [16] <http://www.pmdcorp.com/images/applicationNotes/3phaseBrushless.gif>.
- [17] http://www.pmdcorp.com/news/articles/html/motion_control_amplifier_deep_dive.cfm.
- [18] K. S. S. John, J. P. and B. Jaya, "Space vector modulation based field oriented control scheme for brushless dc motors," *IEEE*, pp. 346–351, July 2011.
- [19] http://www.pmdcorp.com/news/articles/html/Field_Oriented_Control_Deep_Dive.cfm.
- [20] J. Zambada and D. Deb, "Sensorless field oriented control of a pmsm," *Microchip*, 2011.

- [21] S. Dan, "Clarke's and park's transformations," *College of Electrical Engineering, Zhejiang University*, 2008.
- [22] <http://dev.emcelettronica.com/sensorless-pmsm-drive-dishwasher-pump-using-freescale-mc56f8006-device-12>.
- [23] M. Depenbrock, "Direct self-control of inverter-fed induction machine," *IEEE Transactions on Power Electron*, vol. 3, pp. 420–429, October 1988.
- [24] I. Takahashi and T. Noguchi, "A new quick-response and high-efficiency control strategies of an induction motor," *IEEE Transactions Applications*, vol. 22, pp. 820–827, September 1986.
- [25] I. Boldea and S. A. Nasar, "Torque vector control a class of fast and robust torque-speed and position digital controllers for electric drives," *Electrical and Mechanical Power Systems*, vol. 15, pp. 135–147, 1988.
- [26] W. Y. H. L. Zhong, M. F. Rahman and K. W. Lim, "Analysis of direct torque control in permanent magnet synchronous motor drives," *IEEE Transactions on Power Electronics*, vol. 12, pp. 528–536, May 1997.
- [27] C. M. Paturca, S. V. and L. Melcescu, "Direct torque control of permanent magnet synchronous motor (pmsm) an approach by using space vector modulation (svm)," *Conference on Electric Power Systems, High Voltages, Electric Machines*, vol. 6, pp. 111–116, 2006.
- [28] P. F. S. G. Cassadei, D. and A. Tani, "Foc and dtc: Two viable schemes for induction motors torque control," *IEEE Transactions On Power Electronics*, vol. 17, no. 5, pp. 779–787, 2002.
- [29] <http://www.elmomc.com/capabilities/10.Servo%20Advanced%20Feedback%20Technology/12%20Digital%20Halls/picture/10-12-1.png>.

- [30] E. G.-G. J. Gamazo-Real, J.C.; Vzquez-Snchez, "Position and speed control of brushless dc motors using sensorless techniques and application trends," *Sensors*, July 2010.
- [31] I. Bucak, "Position error compensation via a variable reluctance sensor applied to a hybrid vehicle electric machine," *Sensors*, pp. 1918–1934, February.
- [32] W. Hernandez, "Robust multivariable estimation of the relevant information coming from a wheel speed sensor and an accelerometer embedded in a car under performance tests," *Sensors*, pp. 488–508, May 2005.
- [33] http://ab.rockwellautomation.com/resources/images/allenbradley/gl/medlrgprod/844D_HollowShaftOpticalEncoder_right1-large_312w255h.jpg.
- [34] <http://www.automationdirect.com/static/press/encoder-white-paper.pdf>.
- [35] H. Y. S. D. M. Tomita, M. Satoh and S. Okuma, "Sensorless estimation of rotor position of cylindrical brushless dc motors using eddy current," *IEEE International Workshop on Advanced Motion Control*, pp. 24–28, August 1996.
- [36] S. Ogasawara and H. Akagi, "An approach to position sensorless drive for brushless dc motors," *IEEE Transactions on Industry Applications*, vol. 27, pp. 928–933, October 1991.
- [37] M. Lu and Y. Li, "New design for sensorless bldc motor using half-bridge driver circuit," *Proceedings of 2010 International Conference on E-Product, E-Service and E-Entertainment, Hanan*, pp. 1–4, November 2010.
- [38] T.-H. Kim and M. Ehsani, "Sensorless control of the bldc motors from near-zero to high speeds," *IEEE Transactions on Power Electronics*, vol. 19, November 2004.

- [39] C.-S. V. B. I. Ungurean, A., "Sensorless control of a bldc pm motor based on i-f starting and back-emf zero-crossing detection," *International Conference on Optimization of Electrical and Electronic Equipment*, vol. 12, pp. 377–382.
- [40] T. Becerra, R.C. Jahns and M. Ehsani, "Four-quadrant sensorless brushless ecm drive," *Proceedings of the Sixth Annual Applied Power Electronics Conference and Exposition (APEC 1991)*, pp. 202–209, March 1991.
- [41] L. H. Kim, T. and Ehsani, "Position sensorless brushless dc motor/generator drives: Review and future trends," *IET Electronics Power Applications*, vol. 1, pp. 557–564, July 2007.
- [42] N. D. Shao, J. and T. Hopkins, "A novel direct back emf detection for sensorless brushless dc (blcdc) motor drives," *Proceedings of the Seventeenth Annual IEEE Applied Power Electronics Conference and Exposition (APEC 2002), Dallas*, vol. 1, pp. 33–37, March 2002.
- [43] P. Damodharan and K. Vasudevan, "Indirect back-emf zero crossing detection for sensorless blcdc rotor operation," *Proceedings of the International Conference on Power Electronics and Drives Systems (PEDS 2005), Kuala Lumpur, Malaysia*, pp. 1107–1111, November 2008.
- [44] J. H. P. G. H. Jang and J. H. Chang, "Position detection and start-up algorithm of a rotor in a sensorless blcdc motor utilising inductance variation," *IEEE Proceedings Electronics and Power Applications*, vol. 149, pp. 137–142, December 2002.
- [45] A. CASSAT and L. CARDOLETTI, "closed-loop control of a brushless dc motor from standstill to medium speed," *US patent 51 17465*, 1992.
- [46] A. S. S. Jacob, J. and A. E. Daniel, "Speed control of brushless dc motor implementing extended kalman filter," *International Journal of Engineering and Innovative Technology (IJEIT)*, vol. 3, no. 1, pp. 305–308, 2013.

- [47] B. Terzic and M. Jadric, "Design and implementation of the extended kalman filter for the speed and rotor position estimation of brushless dc motor," *IEEE Transactions On Industrial Electronics*, vol. 48, no. 6, pp. 1065–1073, 2001.
- [48] M. N. Dhaouadi, R. and L. Norum, "Design and implementation of an extended kalman filter for the state estimation of a permanent magnet synchronous motor," *IEEE Transactions on Power Electron*, vol. 6, pp. 491–497, 1991.
- [49] P. S. Vinatha, U. and K. Vittal, "Recent developments in control schemes of bldc motors," *Proceedings of the IEEE International Conference on Industrial Technology (ICIT 2006), Mumbai, India*, pp. 477–482, December 2006.
- [50] S. Spurgeon, "Sliding mode observers: A survey," *International Journal of Systems Science*, vol. 39, no. 8, pp. 751–764, 2008.
- [51] A. J. Koshkouei and A. S. I. Zinober, "Sliding mode controller-observer design for multivariable linear systems with unmatched uncertainty," *International Journal of Systems Science*, vol. 36, no. 1, pp. 95–115, 2000.
- [52] H. Lee and J. Lee, "Design of iterative sliding mode observer for sensorless pmsm control," *IEEE Transactions On Control Systems Technology*, vol. 21, no. 4, pp. 1394–1399, 2013.
- [53] C. B. F. Filicori and A. Tonielli, "Modeling and control strategies for variable reluctance directrive motor," *IEEE Transactions on Industrial Electronics*, vol. 40, pp. 105–115, February 1993.
- [54] R. Wallace and D. Taylor, "Torque-ripple switched reluctance motors for direct-drive robotics," *IEEE Transactions on Robotics and Automation*, vol. 7, pp. 733–742, December 1991.
- [55] M. E. R.C. Becerra and T. Miller, "Commutation of sr motors," *IEEE Transactions on Power Electronics*, vol. 8, pp. 257–262, July 1993.

- [56] . H. M. Ehsani and A. Kubmi, "Elimination of discrete position sensor and current sensor in switched reluctance motor drive," *IEEE Transactions on Industry Applications*, vol. 28, pp. 128–135, January/February 1992.
- [57] A. Lurnsdaine and J. Lang, "State observer for variable reluctance motors," *IEEE Transactions on Industrial Electronics*, pp. 133–142, April 1990.
- [58] J. Cai and Z. Deng, "Sensorless control of switched reluctance motor based on dynamic thresholds of phase inductance," *Electric Power Components and Systems*, vol. 40, no. 8, pp. 915–934, 2012.
- [59] J. A.E. Fitzgerald, Charles Kingsley, ed., *Electric Machinery*. New York: McGraw-Hill, 2006.
- [60] J. R. Mevey, "Sensorless field oriented control of brushless permanent magnet synchronous motors," 2009.
- [61] M. E. A. Tashakori and N. Hosseinzadeh, "Modeling of BLDC motor with ideal back-EMF for automotive applications," *Proceedings of the World Congress on Engineering*, vol. 2, pp. 978–983, July 2011.

Appendix A

Torque for Multiple Pole-Pairs

Total energy stored in air gap of motor is given as:

$$W = lr \int_0^{2\pi} \frac{B^2(\theta)}{2\mu} g(\theta) d\theta \quad (\text{A.1})$$

Torque can be found by integrating the energy over the rotor position:

$$T = \frac{dW}{d\alpha} \quad (\text{A.2})$$

Suppose P is number of poles of magnet and q is number of poles of stator, then rotor and stator fields are given as:

$$B_s(\theta) = B_s \cos\left(\frac{P}{2}\theta\right) \quad (\text{A.3})$$

$$B_r(\theta) = B_r \cos\left(\frac{q}{2}(\theta - \alpha)\right) \quad (\text{A.4})$$

When p=q

$$T = -\frac{d}{d\alpha} \left[\frac{Rlg}{2\mu_0} \int_0^{2\pi} 2B_s B_r \cos\left(\frac{P}{2}\theta\right) \cos\left(\frac{P}{2}(\theta - \alpha)\right) + B_s^2 + B_r^2 d\theta \right] \quad (\text{A.5})$$

$$T = -\frac{d}{d\alpha} \left[\frac{Rlg}{2\mu_0} \int_0^{2\pi} 2B_s B_r \cos\left(\frac{P}{2}\theta\right) \cos\left(\frac{P}{2}(\theta - \alpha)\right) d\theta \right] \quad (\text{A.6})$$

$$T = -\frac{d}{d\alpha} \left[\frac{Rlg}{2\mu_0} \int_0^{2\pi} 2B_s B_r \left[\frac{1}{2} \cos\left(\frac{p\alpha}{2}\right) + \frac{1}{2} \cos(p\theta - \frac{p\alpha}{2}) \right] d\theta \right] \quad (\text{A.7})$$

$$T = -\frac{d}{d\alpha} \left[\frac{Rlg}{2\mu_0} B_s B_r \int_0^{2\pi} \cos\left(\frac{p\alpha}{2}\right) \cos\left(p\theta - \frac{p\alpha}{2}\right) d\theta \right] \quad (\text{A.8})$$

$$T = -\frac{d}{d\alpha} \left[\frac{Rlg}{2\mu_0} B_r B_s \int_0^{2\pi} \left[\cos\left(\frac{p\alpha}{2}\right) + \cos(p\theta) \cos\left(\frac{p\alpha}{2}\right) - \sin(p\theta) \sin\left(\frac{p\alpha}{2}\right) \right] d\theta \right] \quad (\text{A.9})$$

$$T = -\frac{d}{d\alpha} \left[\frac{Rlg}{2\mu_0} B_r B_s \int_0^{2\pi} (1 + \cos(p\theta)) \cos\left(\frac{p\alpha}{2}\right) - \sin(p\theta) \sin\left(\frac{p\alpha}{2}\right) d\theta \right] \quad (\text{A.10})$$

$$T = -\frac{d}{d\alpha} \left[\frac{Rlg}{2\mu_0} B_r B_s * 2\pi \cos\left(\frac{p\alpha}{2}\right) \right] d\theta \quad (\text{A.11})$$

$$T = -\frac{d}{d\alpha} \left[\frac{Rlg}{\mu_0} B_r B_s * \cos\left(\frac{p\alpha}{2}\right) \right] d\theta \quad (\text{A.12})$$

As

$$-\frac{d}{d\alpha} \cos\left(\frac{p}{2}\alpha\right) = \frac{p}{2} \sin\left(\frac{p}{2}\alpha\right) \quad (\text{A.13})$$

Total torque in case of equal number of poles is:

$$T = \frac{\pi Rlgp}{2\mu_0} B_r B_s \sin\left(\frac{p}{2}\alpha\right) \quad (\text{A.14})$$

When $p \neq q$

$$T = -\frac{d}{d\alpha} \left[\frac{Rlg}{2\mu_0} \int_0^{2\pi} 2B_s B_r \cos\left(\frac{p}{2}\theta\right) \cos\left(\frac{q}{2}(\theta - \alpha) + B_s^2 + B_r^2\right) d\theta \right] \quad (\text{A.15})$$

$$T = -\frac{d}{d\alpha} \left[\frac{Rlg}{2\mu_0} \int_0^{2\pi} 2B_s B_r \left[\frac{1}{2} \cos\left(\frac{p\theta - q\theta - q\alpha}{2}\right) + \frac{1}{2} \cos\left(\frac{p\theta - q\theta + q\alpha}{2}\right) \right] d\theta \right] \quad (\text{A.16})$$

$$T = -\frac{d}{d\alpha} \left[\frac{Rlg}{2\mu_0} B_s B_r \int_0^{2\pi} \cos\left(\frac{p\theta - q\theta - q\alpha}{2}\right) + \cos\left(\frac{p\theta - q\theta + q\alpha}{2}\right) d\theta \right] \quad (\text{A.17})$$

Now solving the underline portion only in above equation:

$$\int_0^{2\pi} \cos\left(\frac{p\theta - q\theta - q\alpha}{2}\right) d\theta = \int_0^{2\pi} \left[\cos\left(\frac{p\theta - q\theta}{2}\right) \cos\left(\frac{q\alpha}{2}\right) + \sin\left(\frac{p\theta - q\theta}{2}\right) \sin\left(\frac{q\alpha}{2}\right) \right] d\theta \quad (\text{A.18})$$

$$= \left[\cos\left(\frac{q\alpha}{2}\right) \int_0^{2\pi} \cos\left(\frac{p\theta - q\theta}{2}\right) d\theta \right] + \left[\sin\left(\frac{q\alpha}{2}\right) \int_0^{2\pi} \sin\left(\frac{p\theta - q\theta}{2}\right) d\theta \right] \quad (\text{A.19})$$

$$= \left[\cos\left(\frac{q\alpha}{2}\right) \left[\int_0^{2\pi} \cos\left(\frac{p\theta}{2}\right) \cos\left(\frac{q\theta}{2}\right) - \sin\left(\frac{p\theta}{2}\right) \sin\left(\frac{q\theta}{2}\right) \right] d\theta \right] - \quad (\text{A.20})$$

$$\dots \left[\sin\left(\frac{q\alpha}{2}\right) \left[\int_0^{2\pi} \sin\left(\frac{p\theta}{2}\right) \cos\left(\frac{q\theta}{2}\right) - \sin\left(\frac{q\theta}{2}\right) \cos\left(\frac{p\theta}{2}\right) \right] d\theta \right]$$

Now taking the integral and putting the values of the integral gives zero as:

$$\sin(n\pi) = 0 \quad (\text{A.21})$$

So the underline portion in Equation A.17 becomes zero after solving the integral:

$$\int_0^{2\pi} \cos\left(\frac{p\theta - q\theta - q\alpha}{2}\right) d\theta = 0 \quad (\text{A.22})$$

Similarly, it can be shown easily that the second portion of equation A.17 concludes to zero as well. Hence the total torque of the motor becomes zero when the number of rotor poles (p) is not equal to number of stator poles (q).

$$T = 0 \quad (\text{A.23})$$

Appendix B

Inductance Variation of BLDC motor

Phase A		Phase B		Phase C	
L_s (μH)	R_s (R)	L_s (μH)	R_s (R)	L_s (μH)	R_s (R)
938	248.333	786.666	194.666	844.666	214.666
915.666	238.333	839.333	213.333	804.333	198.333
853	214.666	907.666	237.333	800	198.333
800	196.666	927	242.333	836	210
787	193.333	890.333	229	893	232.333
803.333	200.333	823	204	942.666	249.666
853	219	776.333	189	932	246.333
920.333	242.666	770.666	188.333	877	224
936.333	246.333	799	199.666	821.333	203.666
893	229	867.333	223.666	800	197.666
829.666	206	919.333	241	805.666	201.333
791	193.333	917.666	239	849.666	217.333
788.333	194	861.333	218.333	911.333	240
820	206.666	798.333	195.333	949.666	251.666
879.666	228.666	771.333	187.666	915	237.666
934.666	246.333	776.666	191	843.666	215
927	242	824	208.666	811.333	200.333
871	220.333	893	233	800.333	199
807.666	198.666	924.333	242	823.333	207.666
785.666	192.333	899	232.333	878	226.666
792.333	196	836.333	209.333	936.333	247.333
839	214	783.666	191.333	945.666	248.666
907.666	238	769	188.333	893.333	230
940.666	247.666	791.666	197	834	208.333
902.666	235.333	851.666	219	803	198.666
842	209.666	915.666	240.333	803.333	200.333
795.666	194.333	924.333	242.666	840.333	213.666
783.666	191.666	880	224.333	905.333	236.666
806	201	816.666	201.666	949.666	251.333
862	222	775	188.333	932	244.333
925.333	243.666	773.666	190.333	868.333	220.666
934.333	244.666	812.666	204.333	816.666	202.666
885.333	226.333	877.666	228	801	198
821	203.333	926.666	243.666	810.666	203.666
787	192.333	912.666	237	861	220.666
788.666	195	854.333	215.666	926	243.666
824	208.333	798.333	195	949.666	251
888.333	231.666	771.333	188.333	909	235.666
938.666	247	784	194.333	842.666	212
922	240	834.333	212	807.333	199.333
856.333	216.333	904.666	237	800	198.333
800.666	196.666	930	244	825.333	208.333
784.333	192	894.333	230.666	887.333	230
798.666	198.666	827.666	206	940	248
851.666	218.666	781.666	190.666	936.333	246.333
912	239.666	770.666	189.333	881	225.666
941.333	248	799.666	199.666	826.666	205.666
900.666	232.666	864.666	223	800.666	198.333
835	206.333	919.333	241.333	803	200.333
795	194.333	923.666	241.333	843	214.333
786	193.333	870.333	221	910	238
813	204.666	808.333	199	945.666	249.666
874.333	227.333	774.333	189	916.666	239
933.666	246.333	777	191.333	854.666	215.666
932.333	244.666	819.333	206.666	809.333	200.666
876.666	223	886.66	231	797.333	197.666

Phase A		Phase B		Phase C	
L_s (μH)	R_s (R)	L_s (μH)	R_s (R)	L_s (μH)	R_s (R)
814	200	927.666	244.333	813	203.666
788.33	192.66	906	234.66	868	223
791	196.333	843	211.666	930.333	245.666
832.666	211.666	790.666	193.333	941.666	248.666
878.333	233.333	770.666	188.333	897.333	231.333
941.666	248.333	789.333	195.666	831.666	209
919.666	239.666	843.666	215.333	802	198
852	213.666	907.333	237.333	799.666	198.666
802.333	196.333	926.333	242.666	829.666	209.666
786.666	193	884.333	227	890.666	231
803.666	200.333	813.666	201.333	944.333	249.666
856	220.333	777.333	189.666	930	244
921.666	242.333	771	188.666	869.333	221.666
939	247	803.333	201.333	820.666	203
891.666	228.666	870.666	225.333	798.666	197
825.333	204.333	921	241.666	807.666	201.333
790.666	193.333	912	237.666	854	218.333
787.333	193.666	853.333	215.333	920	241.666
819	206	799.333	196	947.666	250.333
878.333	228.333	769	187.666	911.333	237.333
937.333	247	776.666	191.333	842.333	212
925	241	823	208.333	806.333	198.666
869.333	220	894	233	799	198.333
808	199	928	243	821	206.666
784.666	191.666	895.333	231.333	881.333	227.333
796.333	197.333	831.333	208.333	938.33	248.333
840	213.666	783.666	191.66	939.333	247.333
911	239	769	187.666	889.333	228.666
941.666	247.33	790	196.333	830.333	207.333
907.66	233.333	852.666	219	802.666	198.333
839.333	208	914	239.66	804.333	200.666
796	194	923	242	841.333	213.66
783	191.333	868.333	221.666	909	238
805.333	200	812.66	200	948.666	251
866.333	223.666	773.666	188.333	923	241.66
929.333	244.333	773	189.66	862.33	218.666
933.333	243.666	813.666	204.666	816.666	202
881.666	224.333	881.666	228.666	800	198
816	200.333	926.333	239.666	813	203.666
784.666	191	908.333	235.666	873.333	224.666
786.666	193.333	843.666	211.666	930	245
823.666	208	789.333	193	947.333	250
892.333	233	769	188	900.333	232.333
939.333	247.333	786.333	195	841	210.666
916.666	238	847.333	216.333	807.666	200.666
845	211.666	907.666	237.333	799.666	198
794.333	194.333	923.666	243.666	830.333	209.333
782	191	889	229	892.333	232
799.333	198.666	827.666	205.333	944.666	249.666
849.666	218.333	781.666	190	935	245.666
918.333	241	772.666	189.666	878.333	224.666
938.666	246.333	805.666	201.666	821.666	204.666
891.333	228	871.666	225	800.333	197.666
817.666	203.333	921	239	804	199.666
788.666	191.666	917	239	849.66	217
784	192.333	861.666	218.333	918	240.66
816	205	801.333	196.333	949	251
882.666	229.666	773	188.666	907.666	236
933.666	245.666	782.333	193.666	850.666	215
928	242.333	831.333	210.666	809.333	199.666
859.666	217	897	234	796	197.333
805.666	197.666	929.333	243.333	815.666	204.666
784.333	191	894.666	230.666	879	227.333
794.666	196.666	836.333	208.333	932	246
838.333	213.333	786.666	192.333	940.333	247.666
907.666	238	772.666	189.33	882.333	226.333
940.333	247.333	797	198.666	825.666	206
903	232.333	857.333	223.666	798.333	196.666
840	209	915	240.333	799.333	198.666
793	193.666	924.333	242	837.333	212.333
785.333	192.666	873.666	223.333	903	236.333
813	204	810.666	200	946.666	250.666
871.666	226	778	189.666	923	241.333
928.666	244.666	778.666	192	861.333	220.333
933.666	244.666	813.33	204.66	812.666	200.66
878.333	223.666	883.333	229.666	795.666	196.333
816.666	200.666	927.666	244	807	202
789	193	909.666	236.333	862.666	222.333
791.333	195.666	849	213.333	930	242.666
828.333	210	795	194.333	944.333	249
896.666	235	771.666	188.333	900.333	232.666
940	248	789	195.333	833.666	209
917.666	238.666	840.666	214	801.333	197.333

Phase A		Phase B		Phase C	
L_s (μH)	R_s (R)	L_s (μH)	R_s (R)	L_s (μH)	R_s (R)
852.333	213.666	902.333	236	795	198
802.666	196.666	928.666	243.333	826.666	209
786.333	192.333	889	228.333	894	232.666
801.333	199.333	824.333	204.333	944.333	250
855	219.666	778.666	189.666	931.333	244.333
919.666	241.666	770	188.666	874	223
941.333	247	804	201.333	820	203
897	230	870.333	225.333	798	197
829.333	205.333	923	242	805.666	201.666
791.666	193	916.666	239	851.666	218
787	193.333	861	218.333	919	241.333
817	205.333	801.666	196.666	947.666	251
882.333	229.333	771	188.333	911	237
934.666	246	777.666	192	847.666	213
929.666	242	824.666	209	808.666	199.333
869.666	219.666	892.666	233.333	797.333	197.666
809.333	198.333	929.333	243.666	816.666	205.666
786.666	192.333	900	233	878.333	227.333
794.666	196.333	830.333	208.666	939	248
840	213	785	191.666	940.333	248
906.333	237.333	768.666	188	893	229.666
940	247.333	793.333	197.333	831	207
909	234.333	853.333	219.333	802	198
841.666	210	915.666	240.333	801	199.33
796	194	923.666	241.666	833.666	209
784	192.333	873.666	224	905.666	236.666
803.333	200	812.333	200.333	948.666	251
864.666	223.333	774.666	188.666	921.333	241
925.333	243.666	776	191	861.666	218
935.333	244.666	816.333	206.333	814.66	201.333
880.333	223.666	883.333	229.666	797.666	197.666
820.333	201.666	927	244	810	202.666
787.333	191.666	910.333	236.666	865.666	222
786	193.666	848.333	214	928	244.666
827	209	789.666	193.666	944.666	250
891.333	231.666	771	188.666	904.666	234.333
937	246.666	787.666	196	841	211
918.666	237.666	842.666	215.333	805.333	198.666
854.666	214.666	906.333	238	798.66	198
797.333	195	929.333	245	827	208.333
783.666	191.333	891.666	230	887.333	230.333
798.333	198.666	826	205.333	941	248
850.666	218.333	780.333	190.333	934.333	245.333
916	240.666	774.666	190.333	877.666	224.333
934.666	246.666	807.333	202.666	819	204
897	230.333	870	225	799	197.333
828.333	206	923	242.666	803	200
789.666	192.333	919.333	239.666	848.666	216.333
784	192.666	865.666	219.666	912.333	238.666
815	205	806	199	946.666	250
873.666	227	774.666	189.333	912.333	237
931	245.666	779.666	192.666	849	213.666
927	241.333	824.333	209	806.333	199.333
864	218.333	890.333	232.333	794.666	196.666
807.333	198	931	244.666	816.666	205
785.666	192	904.333	234.333	874.333	225
793.666	196.666	840.6666	211	934.666	246.333
839.333	214	786.666	192.666	941	248.666
904.333	236.666	773	189	891	229
941	247.666	796.333	198.666	830.333	207.333
912	236.333	851.666	218.333	800.666	198
846.666	212.333	914.666	240	799.33	199
797	194.333	926.666	242.666	836.666	212
786	192.666	882	226.333	897.666	233.666
807.666	202	818.333	202.666	945.333	250
864.666	223.333	779	190.333	922.333	242
923	242.666	774	190.333	863.333	220
939	245.333	811.333	203.666	815.666	201.333
887	225.666	878	227.666	796.333	196.333
826	203.333	926.333	243	807	201.666
789.666	193	915.666	238.333	857.666	220
789.333	194.666	852	215	926	243.333
828.333	209.666	795	195	947.66	251
890.666	232.666	771	188.333	907	235
937	246.666	784.666	194	843.666	211.333
924.666	239.666	842	214.666	804.333	198
865.666	217.666	900.666	235.333	797.666	197.666
806	197.333	928.666	243.333	825.666	208.666
787	192.333	890.666	229	890.666	231.333
798	198	826	205.666	943	249.333
848.333	217.333	784.666	190.333	933.333	245.666
915.666	240.333	771	188.666	881.666	225.666

Phase A		Phase B		Phase C	
$L_s (\mu H)$	$R_s (R)$	$L_s (\mu H)$	$R_s (R)$	$L_s (\mu H)$	$R_s (R)$
941	247.666	804	201.333	819.666	203
897	230.333	864	222.333	799.666	197.666
838.666	208.333	919.333	241	804.333	201
795	193.666	917.333	240	846.333	215.333
787.333	193.333	865.333	219.666	916.666	240.333
814.33	204	804.666	198	947.666	250.333
872	225.666	773.333	188.333	920.333	240
933	245.333	780.333	192	851	214.666
929.666	242.333	824.666	208	811	200.666
873.333	221.333	891.333	232.333	798.666	198
811.333	199.333	928.666	244.666	816.333	205
787	192	902.333	234.666	872.333	224.666
791	195.333	840.333	211.333	937	247.333
834	211.666	788.333	192.666	944	249.333
896.666	234.666	771.666	189	895.333	232
939	247	794.666	198	833	206.333
911	235	847.333	217	802.666	198.333
844.666	210.666	910.666	238.666	802.666	199.666
800.333	195	927.333	243.666	837	212
784	191.666	882.333	226	905	236
801.333	199.333	819.333	202	948.666	251.333
857.33	220.333	778.666	189.666	928.333	243.333
922	242.333	775.333	190.333	871.666	221.666
937.333	245.333	810.333	204	819.333	203.333
884.333	225.666	875.666	226.666	799	197.666
821.333	203	927.666	244.666	811.666	202.666
788.666	192.333	916	239.333	856.666	219.666
787.666	193.666	858	217.666	925.333	243.33
821.333	207.333	802.666	197	948.333	251.333
884.333	230.333	775.333	190	905	236.333
937.66	247	788.333	195.333	842	212.333
921	239	836	212.666	804	198.333
859	215.666	901.666	235.666	798.666	198.333
804.333	197	931.333	244	827	209
785	191.33	898	231.333	887.33	230
794.333	196.333	836.666	208	942	249.333
844	218.333	788	193	939.333	247.333
912.333	238	774.666	190	878	225
940.666	247	802.66	200.333	823.666	204.666
902.333	232.333	861.333	221.666	798.333	197
836	207.66	920.666	241.666	801	199.333
791.666	193	924	240.333	842.333	214
786.666	193.33	870	222	911.333	239
815	204.666	812	200.333	949	251.333
872.666	226.333	777.333	190	912	238.66
933.333	245.666	779	191.666	848	214.666
930	242.666	819.333	206.333	806.666	200.333
877.666	222	887.666	231.333	796	197
813.666	200.333	929.333	244.333	818	205.666
789.333	192.666	910	236.333	871.333	225
793.666	196.666	848	212.666	936	247
833.333	211.333	793.333	194	940	248.666
898.666	235	772.333	189.666	894.666	231.333
940.666	247.333	791	196	832	208.66
911	237	842.666	215	801.666	197.333
849.666	212	911.666	238.333	798.666	198
802.333	196	925.333	242.666	830	210
788	193.333	886.333	227.333	904.666	236.333
799.666	198.666	820.333	203.333	947.666	251.333
858	220.666	779	190	930	245.333
923.33	243	772	189.333	866.333	220.666
938.333	246	805	201.666	818	202
888	226.333	869.666	225	797.333	197
827	204	925.666	242.333	809	202.666
794	194	914.666	238	861.333	221
789.666	195.333	856.333	217	924.333	243.666
824	207.333	796.666	197	947.666	251.333
883.66	230	770.666	188.333	902.666	234.666
937	246.666	779	192.333	844.66	212.666
927.333	241.666	824	208.333	804.66	199
867.333	219.333	896	234	800	199.333
813.333	199.666	928.333	243.333	824.666	208
788.666	192.666	897	232	887	230
796.666	198	834.333	209.333	944	250
841.666	214.33	784	192	940.333	249.333
910.333	236.666	770	188	883	227.666
940.666	247	794.333	197.666	826.666	206
901	232	857	220.666	802	198.66
840.333	208.666	916.666	241	804.333	200.666
796.666	194.33	922.333	241.666	850.333	216.66
785.333	193	867.333	222	915.333	240
807	201.666	805	198.333	949.333	251.333

Phase A		Phase B		Phase C	
L_s (μH)	R_s (R)	L_s (μH)	R_s (R)	L_s (μH)	R_s (R)
867	224.333	773.333	189	919	240.333
928.333	244	775.666	191	861	217.666
932.333	243.333	816.66	206.333	814	201.33
878.666	222.666	889	230.666	799.666	198.333
819.333	201	929.333	244.333	818	205.333
785.333	192.33	904	234.333	878.666	226.666
786.666	193.333	844.333	212.66	931.333	245.666
828	209	790	193	947	250
892.66	233.333	771	188.66	899.33	233
937	243.66	790.666	196.666	834.666	209
917.333	237.333	846.333	216.666	804.666	198.666
852	214.33	909.33	238.333	803.66	200
799.66	196	927	243.666	836.666	212
783.66	191.666	882.666	227.333	899	234
799.666	199	822	203.333	947	251.333
833.333	218.666	782	191	931	244.333
917	240.666	774.666	190.666	873	222.333
938	246	808.333	203	819	203.666
894	230.333	877	227.333	799.66	198
827.666	205.666	925.666	243	811.333	203
789.666	192	914.333	238	857.66	219.333
785.333	193	862	218.666	923.666	242
815.333	204.333	805.333	198	947.666	250.66
880	229	774.666	189	910.6667	236.666
935.333	246.333	782	193.333	844	212
923.666	240	831.666	211	807	199.666
866.666	218	896.666	233.666	799	198.666
806.666	197.333	930	244.333	823.666	207.333
784.666	192.333	901.333	233	883.333	229
793.666	197	838.666	209.333	938.666	247.666
837.333	213.333	788.666	192.666	940.333	247.333
903	236	772.666	189	886	228
940.666	247.666	800.666	200	828.666	208.333
908	233.666	860.333	220.333	799.333	197.333
843.333	210	918.666	241.333	803	200
795.333	193.666	924.666	241	846	215.666
785.666	192.666	874.333	223.666	909	237.666
808.333	202.333	813.66	201	948	251.333
866.333	223.33	778	190	919.333	240
930.333	244.333	778	191	853	217.333
935	244.333	816.666	206	812	200.333
881.333	224.666	879.333	228	797.333	197.333
822.333	202.333	926.333	243	814	204
789.66	193	911.333	236	869.666	224
791	195	854.333	215	934.333	246
823.333	207.666	797.666	194.666	946.333	249.666
889.66	231.66	772	188.666	904	234.666

Curriculum Vitae

Name: Muhammad Ikhlas

Post-Secondary The Western University

Education and London, ON, Canada

Degree: 2012 - 2014 M.Sc.

University of Computer and Emerging Sciences

Islamabad, Pakistan

2005 - 2009 BS (TE).

Internship: Accelerated Systems Inc.

March - April 2014

Related Work Teaching Assistant

Experience: The Western University

2013 - 2014

Teaching Assistant

University of Computer and Emerging Sciences

2008 - 2009